HDAC6 controls the development and progression of cardiac mal-adaptive hypertrophy

Inaugural-Dissertation
to obtain the academic degree
Doctor rerum naturalium (Dr. rer. nat.)

submitted to the Department of Biology, Chemistry and Pharmacy
of Freie Universität Berlin

by

Sarah Brix

from Witzenhausen

2017

First Evaluater: Prof. Dr. med Ulrich Kintscher

Second Evaluater: Prof. Dr. Gerhard Wolber

Date of Defense: 12.10.2017

Acknowledgement

An dieser Stelle folgt mein Dank all denen Menschen, die mich auf diesem teilweise holprigen, nicht leichten Weg begleitet haben und in irgendeiner Weise mir dabei geholfen haben diese Arbeit anzufertigen.

Mein Dank gilt vor allem Prof. Kintscher, der mir vor etwa 4 Jahren als ich in seiner Arbeitsgruppe anfing, überhaupt die Möglichkeit gab diese Arbeit anzufertigen. Dr. Anna Foryst-Ludwig danke ich ebenfalls von Herzen für die stetige Betreuung und Hilfestellung bei Labortätigkeiten sowie beim Zusammenschreiben der Arbeit. Ein großes Dankeschön gilt Prof. Wolber, der mir als „Doktorvater“ ebenfalls die Möglichkeit für das Erstellen dieser Arbeit an der FU Berlin gab.

Die Zeit im Doktorandenraum, Labor, Tierstall sowie die unternommenen gemeinsamen Aktivitäten waren einmalig. Ich werde die Zeit vermissen. Ob es nun darum ging, meine Arbeit voran zu bringen oder um Abwechslung jeglicher Art: DANKE. Zu diesen Menschen gehören Beata Höft, Frau Sprang, Miranda Nastula, Jana Grune, Zofia Ban, Annelie Blumrich, Janek Salatzki, Ela Januszewicz, Niklas Beyhoff, Elia Smeir, Iris Betz, Sarah Julia Qaiyumi, Patrick Schmerler, Melanie Briese, Manuela Sommerfeld, Dr. Elena Kaschina, Prof. Robert Klopfleisch und Prof. Franz Theuring.

Weiterhin danke ich Bruno & Tanja und den LeMoMos (Anna, Biggi, Sandy, Verena, Maria, Petra, Janna, Eva und Judith), da sie immer für mich da sind. Des Weiteren danke ich Birgit und Annalisa für das Korrekturlesen dieses Werkes.

Ein riesengroßes DANKESCHÖN gilt meiner ganzen Familie. Besonders danke ich meiner Mutter, Uli und meinem Vater. Denn sie haben mich zu dem gemacht, was ich heute bin. Ich bin sehr glücklich darüber eine so tolle Familie zu haben.

Table of content

List of abbreviations

ACSL	acyl-CoA synthetase-1
ANP	atrial natriuretic peptide
Ang II	angiotensin II
ANOVA	analysis of variance
AR	adrenergic receptors
BNP	brain natriuretic peptide
bp	base pair
BW	body weight
CD36	Cluster of Differentiation 36/fatty acid translocase
CD68	Cluster of Differentiation 68
cDNA	complementary deoxyribonucleic acid
CF	cardiac fibroblast
CO_2	carbon dioxide
Col1	collagen1
Col3	collagen3
CTP1-beta	carnitine palmitoyltransferase 1 beta
Bec-1	Beclin 1
DAPI	4′,6-Diamidin-2-phenylindol
DMSO	dimethylsulfoxide
DNA	deoxyribonucleic acid
dNTPs	deoxynucleoside triphosphates
ECM	extracellular matrix
EDTA	ethylenediaminetetraacetate
EF	ejection fraction
ESC	embryonic stem cells
ET-1	endothelin-1
FBS	fetal bovine serum
FS	fractional shortening
Gαq	G protein α q subunit
Glut1	glucose transporter1
Glut4	glucose transporter4
GPCR	G protein-coupled receptors
GTT	glucose tolerance test
h	hour
HAT	histone acetyltransferase
HDAC	histone deacetylase
HDAC6	histone deacetylase 6
HDACi	histone deacetylase inhibitor
HDAC6i	histone deacetylase 6 inhibitor
H&E	hematoxylin and eosin

HF	heart failure
HFmrEF	heart failure with midrange ejection fraction
HFpEF	heart failure with preserved ejection fraction
HFrEF	heart failure with reduced ejection fraction
HR	heart rate
HSP 90	heat shock protein 90
IP	intraperitoneal injection
iPSC	induced pluripotent stem cell
Iso	isoproterenol
IVS	intraventricular septum
l	length
KO	knock out
LS	global longitudinal strain
LV	left ventricular
LVID	left ventricular internal diameter
LVM	left ventricular mass
LVPW	left ventricular posterior wall
MAPK	mitogen activated protein kinases
Mef2	myocyte enhancer factor-2
MHC	myosin heavy chain
Min	minute
MLC-1	megalencephalic leukoencephalopathy with subcortical cysts 1
M-MLV RT	moloney murine leukemia virus reverse transcriptase
MMP	matrix metalloproteinase
MTOC	microtubule organizing center
NaCl	sodium chloride
NE	norepinephrine
NMR	nuclear magnetic resonance
NP	natriuretic peptides
n.s.	not significant
p62	ubiquitin-binding protein p62
PBS	phosphate buffered saline
PCM	primary cardiomyocytes
PSC	pluripotent stem cell
PKC	protein kinase C
RASSF1A	Ras association domain-containing protein 1
qRT-PCR	quantitative real time polymerase chain reaction
RQ	respiratory quotient
S	strain
SR	strain rate
Sec	seconds
STE	speckle tracking echocardiographic analysis

t	time
TAC	Transverse Aortic Constriction
TSA	Trichostatin A
Tuba	Tubacin
UPS	ubiquitin-proteasome system
β-MHCH	beta myosin heavy chain

List of figures

List of tables

1 Introduction

1.1 Cardiac hypertrophy and heart failure

The heart consists of different cell types: cardiomyocytes, non-myocytes and surrounding extracellular matrix. Cardiomyocytes are muscle cells. The structure of cardiac myocytes is formed by myofibrils containing myofilaments with sarcomeres which are responsible for the contraction in the heart (Bernardo et al., 2010). Other cell types present in the heart are non-myocytes such as fibroblasts, vascular smooth muscle cells, endothelial cells and mast cells (Bernardo et al., 2010).

In the mammalian heart differentiated cardiomyocytes do not proliferate (Shimizu and Minamino, 2016). Therefore, heart growth is only accomplished by an increase of cardiomyocyte size which is determined by hemodynamic load (Jonker et al., 2010). As a response to several physiological or pathological alterations cells can become hypertrophic, atrophic or apoptotic (Shimizu and Minamino, 2016).

There are two different forms of cardiac hypertrophy: physiological and pathological hypertrophy which differ at cellular, molecular and functional levels (Cacciapuoti, 2011) (Figure 1-1). Physiological hypertrophy is induced by exercise or pregnancy and is characterized by a normal or enhanced cardiac function (Weeks and McMullen, 2011).

In pathological hypertrophy, cardiac remodeling is taking place, which includes processes such as cell death, fibrosis, an upregulation of fetal genes and a metabolic switch which are explained in chapter 1.5 (Bernardo et al., 2010; Shimizu and Minamino, 2016). Pathological hypertrophy occurs in various diseases with chronic pressure or volume overload, for example by cause of hypertension or aortic stenosis (Bernardo et al., 2010; Shimizu and Minamino, 2016).

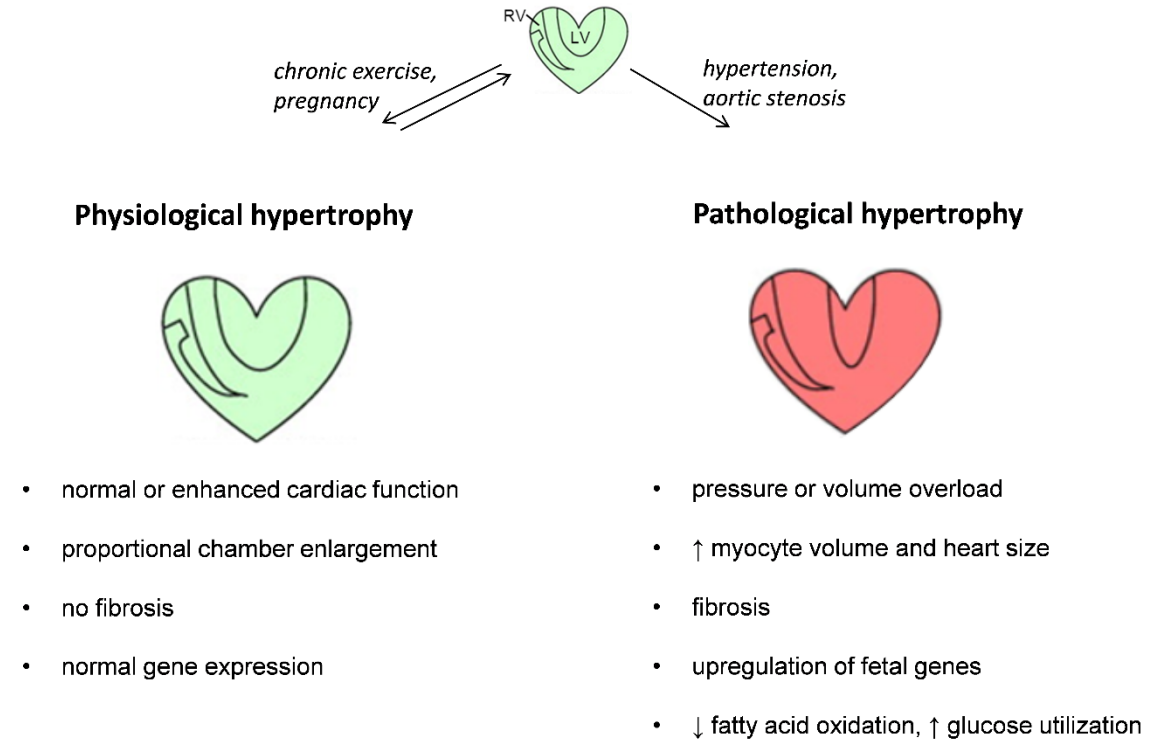

Figure 1-1: The two different forms of cardiac hypertrophy: physiological and pathological hypertrophy and their characteristic morphology (adapted from Bernardo et al., 2010). RV: right ventricle; LV: left ventricle.

The early state of cardiac hypertrophy is described as an adaptive "compensatory" phase and this state can switch to a maladaptive phase characterized by LV dilatation and heart failure (HF) (Figure 1-2) (Shimizu and Minamino, 2016). Compensatory pathological cardiac hypertrophy is defined as an increase in heart mass and increased pumping ability to counterbalance the increased chronic pressure overload (Bernardo et al., 2010; Cacciapuoti, 2011; Cooper, 1987). Left ventricular (LV) wall thickness increases to normalize wall stress (Lai et al., 2013).

HF is one of the main reasons of cardiovascular mortality and morbidity (Lai et al., 2013; Nabeebaccus et al., 2016; Ponikowski et al., 2016a; Reddy and Borlaug, 2016).

In decompensated HF, the heart loses the ability to pump enough blood to provide sufficient apply of nutrients and oxygen to the body (Levy et al., 1990; Shimizu and Minamino, 2016) (Figure 1-2).

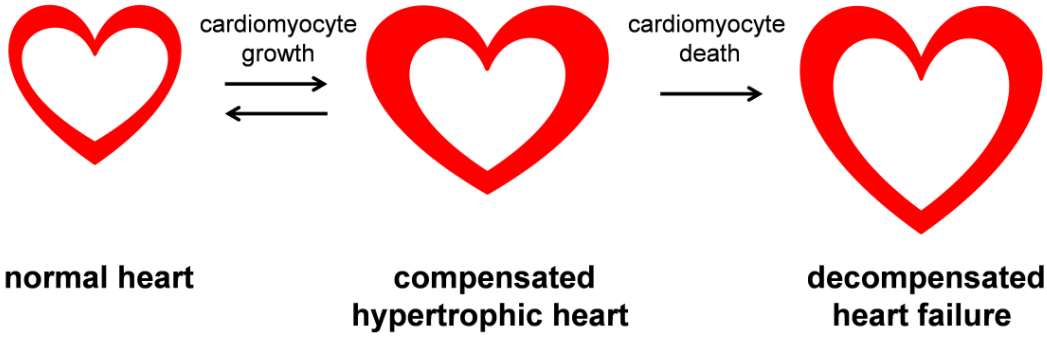

Figure 1-2: Development of compensated cardiac hypertrophy and irreversible decompensated heart failure (adapted from Diwan and Dorn, 2007).

HF is a progressive disorder and is divided into three forms: heart failure with reduced ejection fraction (HFrEF or systolic heart failure), HF with preserved ejection fraction (HFpEF or diastolic heart failure) and HF with midrange ejection fraction (HFmrEF). As described in the European Society of Cardiology (ESC) guidelines the different forms of HF are distinguished based on measurements of the Ejection fraction (EF) (Ponikowski et al., 2016b; Yancy et al., 2013).

EF is a relative measure of the ejected blood volume in relation to the end-diastolic blood volume. It is an important parameter to determine cardiac function (Shimizu and Minamino, 2016) (Figure 1-3). A reduced EF indicates systolic cardiac dysfunction.

$$\text{EJECTION FRACTION} = \frac{\text{amount of blood pumped out}}{\text{amount of blood in chamber}}$$

Figure 1-3: Definition of ejection fraction (EF).

EF can be determined using different cardiac imaging techniques and its values depend on the imaging technique, the performing investigator and the method of analysis (Hayley and Burwash, 2012; Yancy et al., 2013). The gold standard to measure the EF in out-off hospital settings is echocardiography (Ponikowski et al., 2016b).

Half of patients with HF suffer from HFpEF with normal or almost normal values of EF (≥ 50 %), non-dilated LV and concentric remodeling induced by cardiomyocyte hypertrophy (Miljkovik and Spiroska, 2015; Nabeebaccus et al., 2016; Ponikowski et al., 2016b; Reddy and Borlaug, 2016; Shimizu and Minamino, 2016). Concentric remodeling is determined by an increase in wall thickness and cardiac mass but no changes in chamber volume. In eccentric remodeling both, chamber volume and cardiac mass are increased (Bernardo et al., 2010).

Patients with HFrEF have reduced LVEF (< 40 %) and dilated LV (Ponikowski et al., 2016b). In HFrEF eccentric remodeling is induced by cardiomyocyte death and increased LV stiffness (Reddy and Borlaug, 2016; Shimizu and Minamino, 2016; Yancy et al., 2013). The ESC Guidelines for the diagnosis and treatment of acute and chronic heart failure from 2016 determined a new form termed as HFmrEF for HF patients with EF values between 40-49 % (Ponikowski et al., 2016b). Typical characteristics, treatment and pathophysiology of this type of HF have to be investigated.

1.2 Cardiac Function and Histone Deacetylases

Histone deacetylases (HDACs) and Histone acetyltransferases (HATs) are enzymes responsible to keep the balance of reversible acetylation of core histones by introducing or removing acetyl groups (McKinsey, 2012a) (Figure 1-4). In chapter 1.3 the process of histone acetylation will be explained more in detail.

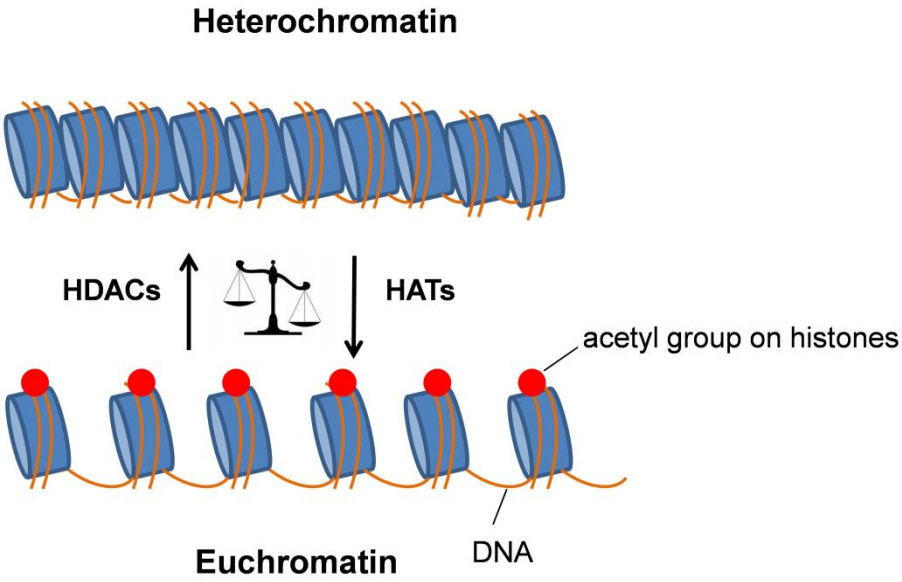

Figure 1-4: Histone deacetylases (HDACs) and histone acetyltransferases (HATs) keeping the balance of reversible acetylation modifications at core histones (blue) by introducing or removing acetyl groups at histone tails (adapted from http://cancergrace.org).

HDACs play important roles in transcriptional regulation in every cell. A majority of the investigations about HDACs take place in the heart, kidney and brain (Kameshima et al., 2016; McKinsey, 2012a). Previous animal models of heart failure and cardiac hypertrophy showed that HDAC inhibitors (HDACi) have protective effects on the development of heart failure. However, the exact mechanism is not clear (Ferguson and McKinsey, 2015; Kee et al., 2006; Kook et al., 2003; Lemon et al., 2011). One of the first studies on HDACs and cardiac hypertrophy demonstrated that HDACs interact with the transcription factor myocyte enhancer factor-2 family (MEF2). MEF2 is involved in the process of cardiac hypertrophy because of calcium-dependent signaling pathways (McKinsey et al., 2002).

Cao and colleagues showed that a non-selective HDACi Trichostatin A (TSA) reverses preexisting cardiac hypertrophy in a Transverse Aortic Constriction (TAC)

mouse model (Cao et al., 2011). This protective effect of TSA on the development of cardiac hypertrophy was also shown in another *in vivo* model where cardiac hypertrophy was induced by angiotensin II (Ang II) infusion (Kee et al., 2006). A study from Kong et al. 2006 showed the cardio-protective effect of TSA after 3 weeks of treatment in a pressure-overload mouse model (Kong et al., 2006).

Most HDACi investigated in pre-clinical studies are non-selective HDACi (Lemon et al., 2011; McKinsey, 2012a). An increasing number of isoform-selective HDACi are tested to treat cardiac hypertrophy and heart failure to avoid severe systemic side effects (McKinsey, 2012a).

Lemon and colleagues found out that the catalytic activity of HDAC6 is elevated in the myocardium upon hypertensive stimuli but not under physiological conditions. They concluded that HDAC6 has a pivotal role in the heart resulting from an increased HDAC6 catalytic activity in pathological cardiac hypertrophy (Lemon et al., 2011). The induction of HDAC6 catalytic activity is linked with elevated HDAC6 expression.

Furthermore, a study from Demis-Davies and colleagues showed that HDAC6 inhibition by a specific HDAC6 inhibitor (HDAC6i) Tubastatin A in mice and in HDAC6 null mice seem to regulate the systolic function of the heart (Demos-Davies et al., 2014). Also in the progression of atrial fibrillation, HDAC6 plays an important role in the microtubule structure reorganization due to α-tubulin proteostasis (Zhang et al., 2014). In the study from Zhang and colleagues, they identify that HDAC6i protects against atrial fibrillation. Moreover, they demonstrated that HDAC6 activation can lead to a derailment of α-tubulin proteostasis, which change the microtubule structure. α-tubulin is an important component in the stability and function of the cytoskeleton which is described more in detail in chapter 1.3.1. HDAC6 deacetylate α-tubulin (Hubbert et al., 2002). It was shown that in atrial fibrillation, HDAC6 inhibition in HL-1 cardiomyocytes and *Drosophila* pupae hearts by using Tubacin, a specific HDAC6i, preserved the microtubule structure and prevented depolymerized α-tubulin from degradation. In another study cardiac fibroblasts were treated with Tubacin, leading to reduced fibroblast activation and thereby attenuated fibrosis (Tao et al., 2016).

Taken together previous studies showed that specific HDAC6i prevents against cardiac remodeling. In our study for the first time, the effect of a specific HDAC6i

Tubacin was investigated on the development and progression of cardiac hypertrophy and cardiac fibrosis.

1.3 Histones and HDACs

Histones are large proteins that are crucial for the structural integrity of eukaryotic chromatin. DNA is wound up around histones, allowing the whole genome to be tightly packed and condensed (Khorasanizadeh, 2004) (Figure 1-4). Histones and DNA are termed as nucleosomes. Units of nucleosome are highly dynamic structures and can be folded into higher-order chromatin fibers (Kornberg, 1977). A single nucleosome DNA contains 147 base pairs (bp) and DNA forms a left-handed double superhelix (Khorasanizadeh, 2004; Luger and Richmond, 1998; Luger et al., 1997).

In total, there are five families of histone proteins. Dimers of highly conserved core histones H2A, H2B, H3 and H4 are organized into an octamer in one nucleosome (Khorasanizadeh, 2004; Luger et al., 1997). Core histones contain histone-fold regions and flexible histone tails with amino termini that stick out of the nucleosome (Jenuwein and Allis, 2001; Luger and Richmond, 1998; Luger et al., 1997). The fifth histone family are “linker” histones which connect and compact repeating nucleosomes and therefore have a function for the stabilization of the DNA (Luger and Richmond, 1998; Luger et al., 1997).

Histone tails are making up about 28 % of the core histone mass and are accountable for histone-histone and histone-DNA interactions (Dorigo et al., 2003; Luger et al., 1997). The amino acid side chains from histone tails are regulated by different post-translational modifications, for example acetylation, phosphorylation, methylation, ubiquitination and ADP-ribosylation. These alterations can affect transcription, replication, recombination and repair of DNA (Jenuwein and Allis, 2001; Luger, 2003). On one or more histone tails may have distinct modifications. The combination of histone modifications affects chromatin structure and interaction of histones with other proteins (Berger, 2002).

Histone acetylation is the most studied post-translational modification of histones and was first described in 1964 by Allfrey and colleagues (Allfrey et al., 1964; Haberland et al., 2009). Histone acetylation and deacetylation can occur at the lysine residues on the amino-terminal tails of histones. Histone deacetylases (HDACs) remove acetyl

groups at histone tails, so the DNA is in a heterochromatin order and is not that accessible for the transcription than in the euchromatin structure. Histone acetylation introduces an acetyl group to lysine residues resulting in a relaxed euchromatin order (Haberland et al., 2009; Hong et al., 1993; Kuo and Allis, 1998; Norton et al., 1989; Struhl, 1998) (Figure 1-4). Consequently, the possibility for transcription factors to bind on their target genes increases (Haberland et al., 2009). Furthermore, it is known that acetylation is associated with an activation of transcriptional co-activators such as p300 (Han et al., 2009) and also non-histone nuclear transcription factors e.g. p53 and Rb (Hubbert et al., 2002; Roche and Bertrand, 2016). In summary, the modification of histones by acetylation/deacetylation can change nucleosomal structure and result in gene regulation by suppressing or enhancing transcription (Gregoretti et al., 2004; Hong et al., 1993; Lundby et al., 2012; Norton et al., 1989; Struhl, 1998).

The catalytic core of histone deacetylases (HDACs) was first described in a bacteria named *Aquifex aeolicus* which shares 35.2 % sequence identity with the human HDAC1 (Finnin et al., 1999). It is known that HDACs also deacetylase other proteins such as tubulin, heat shock protein 90 (HSP90) and cortactin (Haggarty et al., 2003; Kovacs et al., 2005; Li et al., 2011; Zhang et al., 2007).

Based on similarity to transcriptional repressors of yeast the 18 known mammalian HDACs are divided into four classes (Table 1-1) (Ferguson and McKinsey, 2015; Haberland et al., 2009; Kao et al., 2002; Roche and Bertrand, 2016).

Table 1-1: Overview of all well-known HDAC classes.

class	mammalian	yeast	catalytic domain	localization	length
I	HDAC 1, 2, 3 and 8	RPD3	zinc ion	ubiquitously, predominantly in the nucleus	400-500 amino acids
II a	HDAC 4, 5, 7 and 9	HDA1	zinc ion	shuttle between nucleus and cytoplasm	~ 1000 amino acids
II b	**HDAC 6**	**HDA1**	**zinc ion**	**primarily in the cytoplasm**	**1215 amino acids**
II b	HDAC 10	HDA1	zinc ion	nucleus and cytoplasm	~ 1000 amino acids
III	Sirtuine 1–7	Sir2	NAD+	Nucleus: SIRT 1,6 and 7	310-757 amino acids
IV	HDAC 11		zinc ion	nucleus	347 amino acids

HDACs are dysregulated in different cardiovascular or metabolic diseases and in tumor formation (Van Dyke, 2014). They are involved in many cellular processes because of their ability to affect transcription by deacetylation of histones. For the expression of various genes which are involved in DNA repair and synthesis HDACs activities are crucial (Zwergel et al., 2016).

In the heart HDACs control hypertrophy, autophagy, fibrosis and energy metabolism and therefore, HDACs are intensively studied in cardiovascular disease (Cao et al., 2011; Iyer et al., 2010; McKinsey, 2012a; Montgomery et al., 2008).

1.3.1 HDAC6

HDAC6 is expressed in the heart and there it has an essential role. As described in chapter 1.2, HDAC6 is involved in various processes such as cytoskeletal dynamics and autophagy (Figure 1-5). In many cell types, including cardiomyocytes, autophagy occurs and functions as an important regulator of protein quality control. Hence, dysregulated protein degradation in the heart is linked with cardiac dysfunction (Zheng and Wang, 2010).

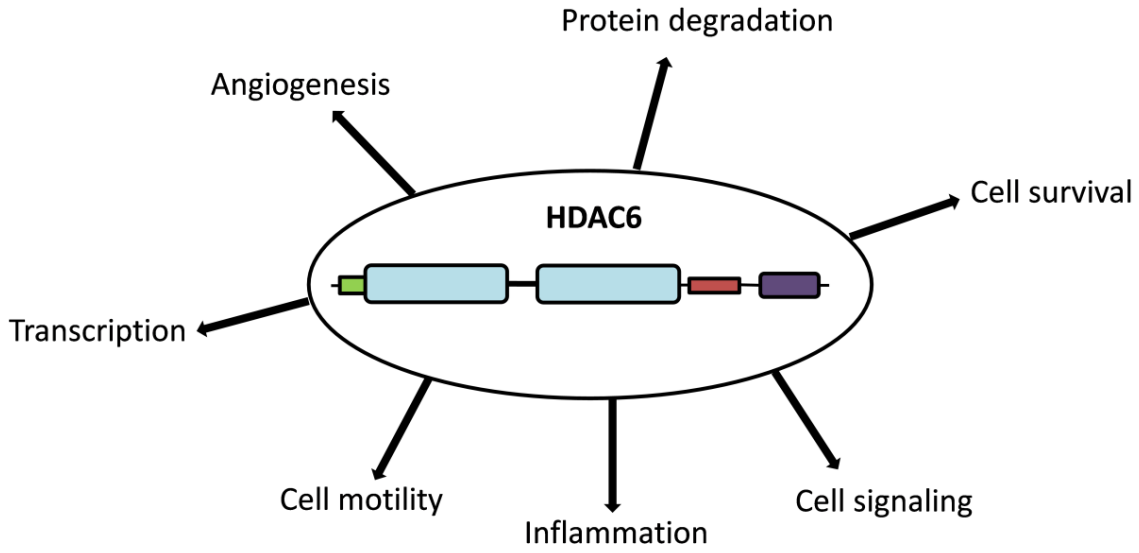

Figure 1-5: Involvement of HDAC6 in different biological processes.

HDAC6 was discovered in 1999 (Li et al., 2011; Verdel et al., 2000). HDAC10 and HDAC6 represent the class IIb families of the HDACs (Table 1-1).

In humans the HDAC6 gene is located on the X-chromosome in the chromosome region Xp11-23 (Mahlknecht et al., 2001). Predominantly, mammalian HDAC6 is localized in the cytoplasm but it also controls core functions by regulating the transcription. HDAC6 deacetylases several non-histones target proteins such as tubulin, heat shock protein 90 (HSP90) and the F-actin binding protein cortactin (Li et al., 2013). This results in degradation of structural proteins (Ferguson and McKinsey, 2015; Valenzuela-Fernández et al., 2008; Verdel et al., 2000; Zhang et al., 2006). Human HDAC6 has 1255 amino acid residues, including a conserved leucine-rich motif, which is also known as nuclear export signal or NES. NES is CRM1/exportin1-dependent and important for the transport of proteins from the nucleus to the cytoplasm (Li et al., 2011; Verdel et al., 2000). HDAC6 is characterized by two

catalytic domains and an ubiquitin binding domain termed as ZnF-UBP domain or BUZ (Ferguson and McKinsey, 2015; Haberland et al., 2009; Valenzuela-Fernández et al., 2008) (Figure 1-6). HDAC6 is the only HDAC with two catalytic deacetylase domains (Grozinger et al., 1999; Li et al., 2013). Between the second deacetylase domain and ZnF-UBP is a domain which is a tetradecapeptide repeating Ser-Glu (SE14) (Bertos et al., 2004; Valenzuela-Fernández et al., 2008). This domain allows a stable cytoplasmic localization of HDAC6 (Bertos et al., 2004; Valenzuela-Fernández et al., 2008).

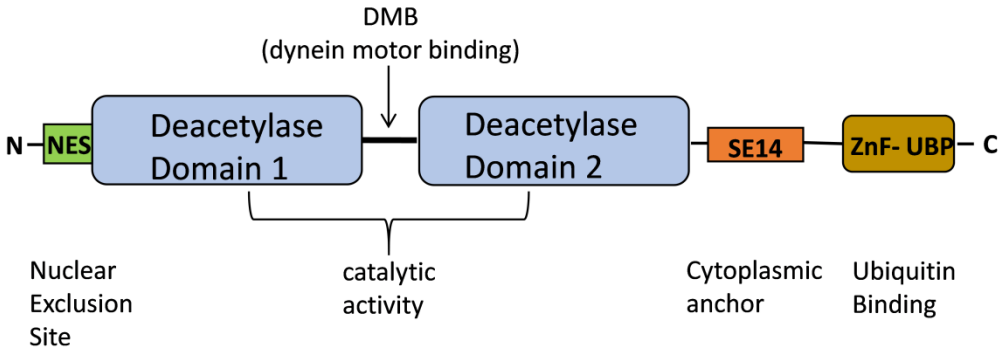

Figure 1-6: Domain structure of HDAC6. Blue boxes show the deacetylase domain 1 and 2. SE14, SerGlu-containing tetradecapeptide repeats. ZnF-UBP, ubiquitin binding domain (adapted from Valenzuela-Fernández et al., 2008).

The ubiquitin-proteasome system (UPS) and autophagy are the main protein degradation pathways in the cell, needed for the clearance of tremendous amount of misfolded proteins (Li et al., 2011). If the degradation of proteins in the heart is impaired, this can lead to cardiac dysfunction including cardiac hypertrophy. HDAC6 seem to play an important role in intracellular protein degradation pathways (Pandey et al., 2007).

Autophagy is induced by different stimuli like starvation or stress mainly to ensure regular cell function. Alterations of the autophagy-activity can end in pathological processes such as cancer and neurodegenerative disorders (Cao et al., 2011). During autophagy misfolded proteins aggregate and are carried along the microtubules towards the microtubule organizing center (MTOC) (Kawaguchi et al., 2003; Ouyang et al., 2012). Then they build a large aggregate called aggresome at the MTOC. The formation of aggresomes prevents the accumulation of protein

aggregates (Li et al., 2011). Within the aggresome misfolded proteins are cleared. Autophagy is a lysosomal degradation process where formation of double-membrane vesicles known as autophagosomes take place (Kawaguchi et al., 2003; Ouyang et al., 2012; Yan, 2014).

HDAC6 is known as a microtubule-associated deacetylase which interacts with polyubiquitinated proteins (Hubbert et al., 2002; Kawaguchi et al., 2003). It can bind to ubiquitinated proteins with the ZnF-UBP domain and HDAC6 interacts with dynein motors by the dynein motor binding domain (DMB) (Boyault et al., 2006; Hook et al., 2002; Li et al., 2011; Ouyang et al., 2012). Binding of HDAC6 to dynein support the transport of the misfolded proteins along microtubules (Batchu et al., 2016). Both, ubiquitinated proteins and dynein motors are components of the degradation machinery that eliminates misfolded proteins produced during different cellular processes.

α-tubulin was the first identified non-histone protein which is deacetylated by HDAC6 (Hubbert et al., 2002). α-tubulin polymerizes into microtubules and regulates microtubule stability and function and therefore, it is important for the habitus of the cell (Hubbert et al., 2002; Piperno et al., 1987). Microtubules are cylindrical components of the cytoskeleton in eukaryotic cells and consist of α- and β-tubulin which form a stable structure named tubulin-heterodimer (Chakraborti et al., 2016; Zhang et al., 2003). α-tubulin have three structural different domains: N-terminal, intermediate and C-terminal domain (Chakraborti et al., 2016). HDAC6 reversible acetylates α-tubulin on a lysine residue (Lys40) close to the N-terminus (Matsuyama et al., 2002). Accordantly, HDAC6 has an influence on cell motility.

In summary, HDAC6 seems to be a promising molecule in the development of new therapeutic regimes because of its essential role of the transport of misfolded protein aggregates to the dynein motor and aggresome formation (Kawaguchi et al., 2003; Valenzuela-Fernández et al., 2008).

1.3.2 HDAC inhibitors

HDACi were used and investigated as therapeutic targets especially in cancer research because of its major influence in oncogenic cell transformation (Aldana-Masangkay and Sakamoto, 2011; Roche and Bertrand, 2016). Nowadays, increasing number of investigations focus on HDACi also in the context of other diseases such as neurodegenerative and cardiovascular diseases (Batchu et al., 2016). Inhibiting HDACs by HDACi leads to an accumulation of acetylated histones and other proteins which results in various cell responses such as proliferation, differentiation and cell death (Wang and Dymock, 2009).

The general HDACi structure consist of three primary domains: a zinc binding group (ZBG) chelating the zinc ion and masking it thereby, a chain imitating the lysine side chain named linker chain and a functional cap group binding to the substrate-binding region of the enzyme (Batchu et al., 2016) (Figure 1-7). Variations of the cap group seem to be most important for isoform selectivity (Batchu et al., 2016; Dallavalle et al., 2012).

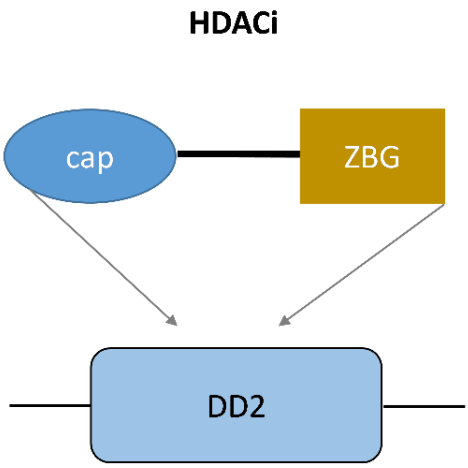

Figure 1-7: HDAC inhibitors (HDACi) comprise a characteristic domain structure: a cap, a linker chain and a zinc-binding group (ZBG). The catalytic domain (DD2) with the cap and ZBG where it binds to the deacetylase domain 2 (DD2) of HDAC6 (adapted from Batchu et al., 2016).

There are four main classes of HDACi: hydroxamic acid, benzamides, short-chain fatty acids and cyclic peptides according to the chemical structure of the ZBG (Li et al., 2011; McKinsey, 2012a; Wang and Dymock, 2009). In this study an unspecific HDACi Trichostatin A (TSA) and a specific HDACi6 Tubacin were investigated and both belonging to the class of hydroxamic acids. Most of the HDACi like TSA are broad-spectrum inhibitors, which mean that they inhibit several HDACs, leading to undesirable side effects such as diarrhea, thrombocytopenia, nausea and fatigue. In order to provide therapy with less side effects selective HDACi such as Tubacin are investigated. The specific inhibition result in a decreased cytotoxicity potency (Dallavalle et al., 2012).

Two HDACi are FDA-approved (Food and Drug Administration): HDACi, Vorinostat (SAHA, Zolinza, Merck&Co., White House Station, NJ, USA) and Romidepsin (Istodax, FK228) a depsipeptide HDAC inhibitor (HDACi). Both are approved for anticancer therapy (Dallavalle et al., 2012; Wang and Dymock, 2009).

Vorinostat is a naturally-occurring hydroxamic acid and was in 2006 the first approved HDACi for the treatment of cutaneous T-cell lymphoma (Wang and Dymock, 2009). Trichostatin A (TSA) inhibits class I and II HDACs at nanomolar concentrations and was the first identified natural product of the hydroxamic acid class (Kelly and Marks, 2005).

Furthermore, there are several HDACi in clinical trials, for example Belinostat and Panobinostat which are investigated in the treatment of cancer (Agarwal et al., 2016; Thomas et al., 2016). Until now, there are just a few selective HDAC6 inhibitors (HDAC6i) described (Haggarty et al., 2003).

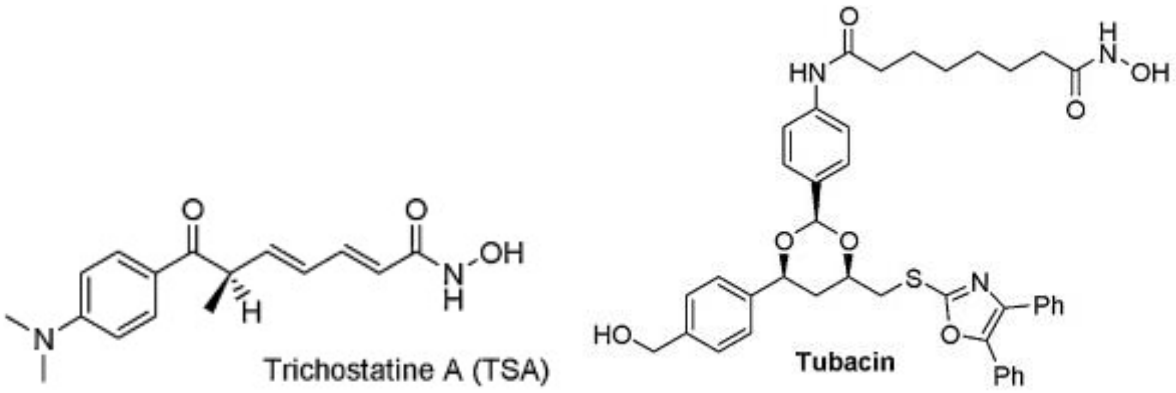

Figure 1-8: Chemical structure of the unspecific HDAC inhibitor Trichostatin A (TSA) and of the specific HDAC6 inhibitor Tubacin.

In 2003, Tubacin (**tu**bulin **ac**etylation **in**ducer) was the first identified selective HDAC6i (Haggarty et al., 2003). It inhibits α-tubulin deacetylation but does not affect histone acetylation, gene expression profiling or cell-cycle progression in mammalian cells. Like TSA, Tubacin inhibits HDAC6 deacetylase activity by chelating a Zn^{++} cation resulting in hyperacetylation (Simms-Waldrip et al., 2008).

Other specific HDAC6i are Tubastatin A, Rocilinostat (ACY-1215) and ACY-241, which also increase α-tubulin acetylation and not global histone acetylation.

1.4 Cellular signaling networks in pathological cardiac hypertrophy

As mentioned in chapter 1.1, in this study we focused on the development of pathological cardiac hypertrophy using Transverse Aortic Constriction (TAC). In this form of cardiac hypertrophy, induced by pressure overload, several vasoactive, autocrine and humoral factors such as endothelin 1 (ET-1), angiotensin II (Ang II) and noradrenaline (norepinephrine, NE) are released and subsequently trigger cardiac growth by activating intracellular signaling pathways. These autocrine factors bind to their G protein-coupled receptors (GPCR) which are present on the surface of cardiomyocytes: endothelin receptors (ET_A and ET_b), Ang type I receptor (AT_1 receptor), α- and β-adrenergic receptors (ARs) (Arai et al., 1995; Bernardo et al., 2010). Figure 1-9 shows a simplified model of one of the best described signaling cascades responsible for mediating pathological cardiac hypertrophy. Activation of the G protein α q subunit (Gαq) pathway induced by various diseases increase the expression of mitogen activated protein kinases (MAPKs), protein kinase C (PKC), calmodulin and calcineurin, which are calcium-dependent signaling molecules (Bernardo et al., 2010; Berry et al., 2008). It is known that alterations in calcium homeostasis in the cardiomyocytes trigger hypertrophy (Zhang et al., 2003).

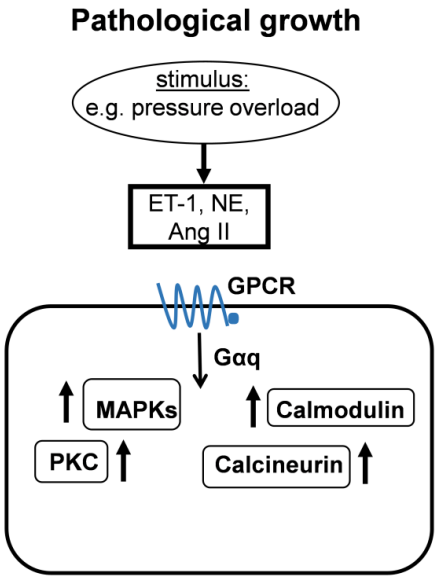

Figure 1-9: Signaling cascade implicated in mediating pathological cardiac hypertrophy in cardiomyocytes. Ang II (angiotensin II), ET-1 (endothelin-1), GPCR (G protein-coupled receptor), MAPK (mitogen-activated protein kinase), NE (norepinephrine) and PKC (protein kinase C); (adapted from Bernardo et al., 2010).

1.5 Mechanisms implicated in pathological cardiac remodeling

Pathological cardiac remodeling affects cardiomyocytes and other cells in the heart on electrophysiological, transcriptional and signaling levels. These functional and structural events are maladaptive. The mechanisms which are implicated in the process of pathological cardiac hypertrophy such as metabolic remodeling, fibrosis, inflammation and the upregulation of fetal genes are described in the following chapters (Burchfield et al., 2013) (Figure 1-10). To investigate if HDAC6 is involved in the development of cardiac remodeling, these mechanisms are examined.

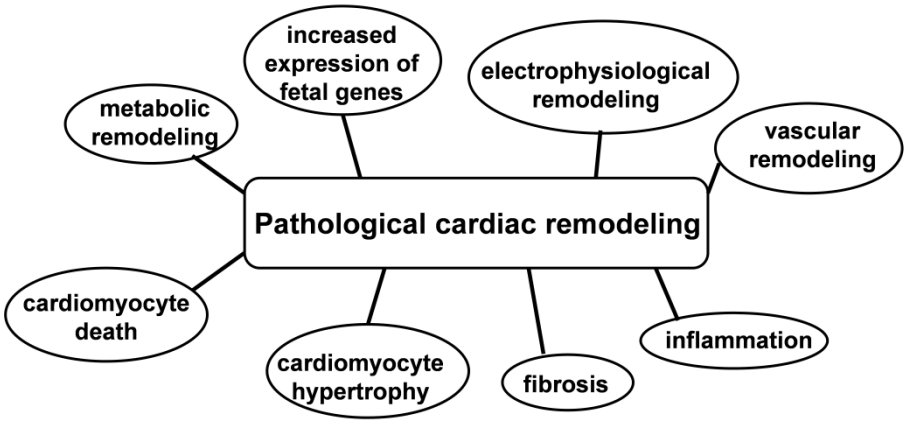

Figure 1-10: Overview of mechanisms implicated in pathological cardiac hypertrophy.

1.5.1 Metabolic remodeling

ATP is the energy source crucial for the contractile function of cardiomyocytes, necessary for blood circulation in the organism (Doenst et al., 2013). Under physiological conditions adenosine triphosphate (ATP) is derived from various carbon-based substrates such as fatty acids, carbohydrates, amino acids and ketones (Aerni-Flessner et al., 2012). The main metabolic pathway providing energy for the adult heart is fatty acid oxidation that produces 70-90 % of cardiac ATP. Only 10-30 % of ATP is produced by glucose and lactate metabolism (Aerni-Flessner et al., 2012; Bernardo et al., 2010). The heart has the ability to alter substrate utilization depending on their availability, which is known as the metabolic switch (Aerni-Flessner et al., 2012). In both, physiological and pathological hypertrophy ATP utilization differs according to the stimulus (Allard, 2004).

Under pathological conditions such as pressure overload less fatty acid oxidation takes place. Hence, metabolic switch from fatty acids to glucose utilization is induced. This metabolic switch to predominantly glucose utilization depends on workload and allows a continuous supply with ATP. The process is comparable to fetal hearts where fatty acid utilization is very low and glucose is predominantly used (Bernardo et al., 2010; Stanley et al., 2005). In contrast, in physiological cardiac hypertrophy fatty acid oxidation increases and glucose utilization decreases (Figure 1-11). Parallel to glucose oxidation cellular glucose transport is increased in pathological hypertrophy. Members of the glucose transporter (GLUT) family are responsible for glucose transport into the cardiomyocytes. GLUT1 and GLUT4 are the most studied GLUTs in mammalian tissue (Aerni-Flessner et al., 2012). GLUT4 is insulin-responsive and the main transporter in the adult heart (Studelska et al., 1992). In fetal and pathological hearts predominantly GLUT1 is present (Aerni-Flessner et al., 2012; Razeghi et al., 2001).

Several genes allowing fatty acid transport and metabolism are expressed in the heart. Cluster of Differentiation 36/fatty acid translocase (CD36) facilitates cellular uptake of fatty acids from the extracellular space, Acyl-CoA synthetase (ACSL) generates fatty acyl-CoA. Carnitine palmitoyltransferase 1 beta (CPT1b), enables acyl-CoA uptake into the mitochondria, where ß-oxidation generates reducing equivalents.

In this study, we wanted to know if Tubacin and TSA have an effect on the energy consumption in pathological cardiac hypertrophy.

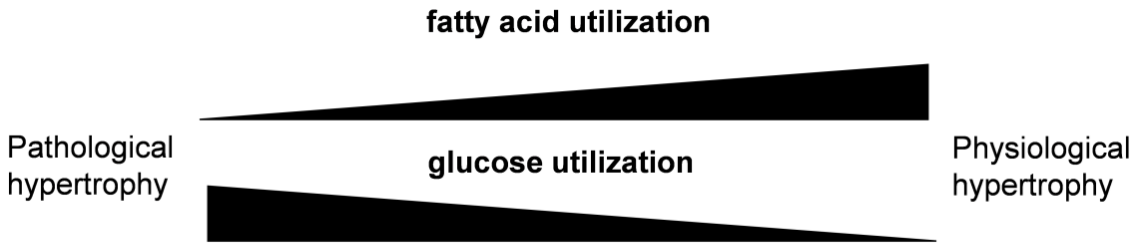

Figure 1-11: Differences in energy utilization between physiological and pathological hypertrophy in adult mammalian hearts (adapted from Bernardo et al., 2010).

1.5.2 Inflammation and fibrosis

Inflammation and fibrosis are not isolated processes. Chronic inflammation regarding to volume or pressure overload induces the development of cardiac fibrosis (Dobaczewski and Frangogiannis, 2009). Chronic inflammation is a persistent immune response accompanying repair processes and tissue remodeling (Wynn, 2008). Repair processes are induced by stimuli which trigger the production of inflammatory cytokines (TGF-β), tumor necrosis factor (TNFα), interleukin 1 β (IL-1β), interleukin 6 (IL-6)) and activation of proteases which further facilitate cardiac hypertrophy. These signaling molecules support the remodeling process, which destroys the tissue architecture and integrates connective tissue (Dobaczewski and Frangogiannis, 2009; Shimizu and Minamino, 2016; Wynn, 2008). Inflammatory cells such as monocyte-derived macrophages are produced due to stress or cardiac injury and infiltrate cardiac tissue (Shimizu and Minamino, 2016).

Cardiac injury also induces cardiomyocyte death, which in turn activates leukocytes leading to protease activation and matrix degradation.

Then, phagocytes facilitate the reparative process by clearing damaged cell components. Accumulated myofibroblasts produce more extracellular matrix (ECM) proteins (Dobaczewski et al., 2010). Under physiological conditions, ECM serve as a frame for the cellular component, enclose the cardiomyocytes and are responsible for the transfer of the contractile force (Bernardo et al., 2010; Kong et al., 2014; Travers et al., 2016).

Pathological cardiac fibrotic remodeling is induced by cardiac diseases such as hypertension or aortic stenosis to maintain the structural integrity and the capacity of the heart to preserve adequate blood circulation (Travers et al., 2016). The development of pathological cardiac hypertrophy is characterized by an increased rate of cardiomyocyte death and development of interstitial fibrosis. This leads to increased stiffness, which can result in diastolic and systolic impairment. Cardiac fibrosis is characterized by an accumulation of extracellular matrix (ECM) produced by cardiac fibroblasts (CF). Alterations of the ECM composition induced by cardiac diseases transform CFs to myofibroblasts producing and releasing higher levels of ECM proteins such as collagen, growth factors and cytokines. It mediates an activation of matrix metalloproteinases (MMPs). MMPs control the turn-over of ECM

and therefore, they are important in fibrogenic process (Robert et al., 2016). There are MMPs which have anti-fibrotic as well as profibrotic functions (Giannandrea and Parks, 2014; Robert et al., 2016).

Collagen type I and collagen type III are present in the myocardium: type I about 85 % and type III about 11 %. Collagen type I is organized in thick fibers, while collagen type III forms thin fibers (Kong et al., 2014). The major physiological function of collagen fibrils is structural support. But focussing on pathological conditions, an increasing accumulation of collagen is a hallmark of cardiac fibrosis (Jugdutt, 2003; Kong et al., 2014). Besides collagen, gylcosaminoglycans, glycoproteins and proteoglycans are the other main components of the ECM (Kong et al., 2014).

There are several studies, which investigate cardiac fibrosis and inflammation combined with HDACs. Among those, Kang and colleagues identified that inhibition of HDACs diminished cardiac hypertrophy and fibrosis in spontaneously hypertensive rats (Kang et al., 2015).

In our study, we were interested if the specific HDAC6 inhibitor Tubacin modulates the development of cardiac fibrosis.

1.5.3 Biomarker for pathological cardiac hypertrophy

Atrial natriuretic peptide or atrial natriuretic factor (ANP, ANF) and B-type natriuretic peptide (BNP) belong to the natriuretic peptides (NPs). They are predominantly expressed in the cardiomyocytes and are released from myocytes into the circulation (Nemer et al., 1986; Volpe et al., 2014; Woods, 2004). NPs are hormones that regulate the balance of cardio-renal homeostasis by reducing preload in failing hearts to inhibit the renin-angiotensin/endothelin systems, thereby enabling renal elimination of water and salt (Woods, 2004). Circulating ANP and BNP have vasodilating effects and several other cardiovascular effects, which are shown in Figure 1-12. ANP and BNP are so called pathological markers in cardiac hypertrophy, since the degree of their release and plasma levels are linked with the heart´s dysfunction. They are also known as fetal marker genes because their gene expression levels are highly expressed during fetal development (Taegtmeyer et al., 2010; Volpe et al., 2014).

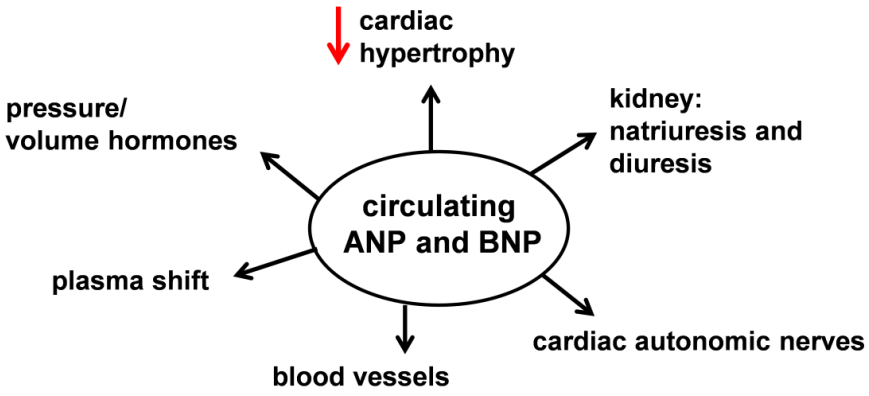

Figure 1-12: Cardioprotective effects of circulating atrial natriuretic peptide (ANP) and B-type natriuretic peptide (BNP) (adapted from Woods, 2004).

Besides ANP and BNP, beta myosin heavy chain (β-MHC), α-skeletal actin and atrial Megalencephalic Leukoencephalopathy with Subcortical Cysts 1 (MLC-1) are part of the fetal gene setup. An upregulation of these genes is an established indicator for pathological cardiac hypertrophy and heart failure (Bernardo et al., 2010).

Two isoforms of MHC are expressed in the mammalian heart: α- and β-MHC. They are part of myosin, which is an ATPase motor protein driving contractility in muscle cells. In several cardiovascular studies it was shown that HDACi diminish the expression of those pathological markers (ß-MHCH, ANP and BNP) meaning HDACi have a protective role in the heart (Kee et al., 2006; Mathiyalagan et al., 2014) (Figure 1-13).

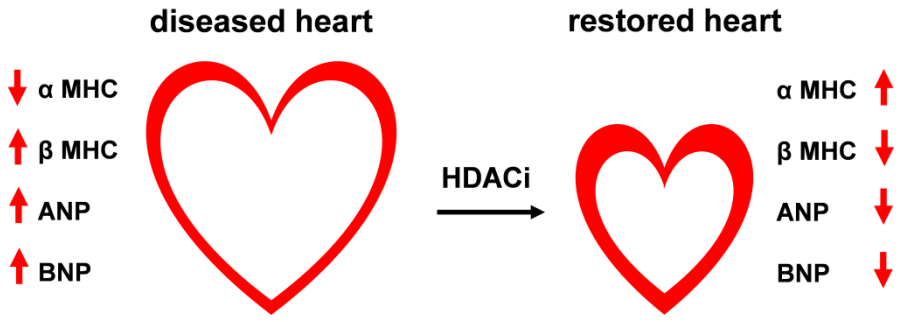

Figure 1-13: Gene expression levels of pathological markers. In cardiac diseases pathological markers beta myosin heavy chain (ß-MHCH), atrial natriuretic peptide (ANP) and B-type natriuretic peptide (BNP) are elevated and by treatment with HDACi these pathological markers are diminished (adapted from Mathiyalagan et al., 2014).

2 Aim of study

The main focus of this study was to characterize the role of HDAC6 activation in the development of cardiac hypertrophy, fibrosis and inflammation in a pressure overload model in mice and in an Isoproterenol-induced cardiomyopathy model.
Additionally, the animal studies were complemented by *in vitro* experiments, performed in HL-1 cells to identify HDAC6-inhibitors as potential compounds for the treatment of cardiac dysorders.
We aimed to:

1. analyse the effect of the general HDAC inhibitor (HDACi) Trichostatin A (TSA) and the specific HDAC6 inhibitor (HDAC6i) Tubacin upon hypertrophic stimulation *in vitro*. The question was if the HDACi exerts anti-hypertrophic effects in HL-1 cells.

2. identify the functional importance of HDAC6 in the development of cardiac hypertrophy by using the HDAC6 specific inhibitor Tubacin, and an unspecific HDACs inhibitor Trichostatin A (TSA) in a pressure overload-induced cardiac hypertrophy model *in vivo*.

3. characterize the metabolic phenotype of Tubacin-treated mice.

4. investigate the functional importance of HDAC6 in the development of cardiac fibrosis and inflammation in an Isoproterenol-induced cardiomyopathy model.

5. identify the molecular mechanism beneficial for anti-hypertrophic effect of Tubacin.

3 Material

3.1 Laboratory equipment

Table 3-1 Laboratory equipment

Name	**Manufacturer**
Accu-jet® *pro* Pipette Controller	BrandTech Scientific (Essex, USA)
Bioruptor, Tissue ruptor	Diagenode (Liège, B)
Camera CFI60	Nikon
Centrifuge 5810R	Eppendorf (Hamburg, D)
Centrifuges	Eppendorf (Hamburg, D)
Curix 60 Processor	AGFA (Köln, D)
Heracell™ 150	Thermo Scientific (Hamburg, D)
Laminar Airflow Clean Bench (Holten)	Thermo Scientific (Hamburg, D)
Microscope	Olympus (Hamburg, D)
Mikro 20 and 22R Centrifuge	Hettich (Hanau, D)
Microscope	Keyence Deutschland GmbH (Neu-Isenburg, D)
Multipipette® Stream	Eppendorf (Hamburg, D)
Nanodrop® ND-1000 spectrophotometer	PeqLab (Erlangen, D)
pH-Meter pH211	Hanna Instruments (Kehl am Rhein, D)
Neubauer-Zählkammer	Marienfeld GmbH (Lauda-Königshofen, D)
Real-time PCR-System Mx3000P	Stratagene (La Jolla, USA)
Scale BL 150 S	Sartorius AG (Göttingen, D)
Sonopuls (sonication device)	Bandelin (Berlin, D)
Thermomixer comfort	Eppendorf (Hamburg, D)
Vortex-Genie® 2T	Scientiis (Baltimore, US)
Waage BL 1500S	Sartorius AG (Göttingen, D)
Water bath	Memmert GmbH (Schwabach, D)
Western blot equipment (Electrophoresis, blot chamber)	Bio-Rad (München, D)
Mark™ Microplate Absorbance Spectrophotometer	Bio-Rad (München, D)

3.2 Laboratory material

Table 3-2 Laboratory material

Name	Manufacturer
96-well multiply PCR plates	Sarstedt AG (Nümbrecht, D)
Amersham hybond PVDF (0.45 µm)	GE Healthcare (Solingen, D)
Amersham hyperfilm ECL	GE Healthcare (Solingen, D)
Cell culture flasks and plates	BD Bioscience (Heidelberg, D)
Cell scraper	Sarstedt AG (Nürmbrecht, D)
Cryo tubes	Nunc (Roskilde, DK)
Descosept®	Dr. Schumacher (Malsfeld, D)
Falcons, pipetts, tips	BD, Sarstedt, VWR, Eppendorf
Glass covers,12mm	neoLab Migge Laborbedarf-Vertriebs GmbH
Mr. Frosty™ Freezing Container	Thermo Fisher Scientific (Hamburg, D)
Omnifix syringes, different sizes	Braun Melsungen (Melsungen, D)
Parafilm® M Barrier Film	SPI supplies (Glasgow, UK)
RNaseZap™	Sigma-Aldrich GmbH (Steinheim, D)
Rotilabo® Spritzenfilter (syringe filter)	Carl Roth GmbH (Karlsruhe, D)
Sealing tape, optically clear	Sarstedt (Nümbrecht, D)
Sterican cannulas, different sizes	Braun Melsungen (Melsungen, D)
Whatmanpaper	Whatman plc (München, D)

3.3 Animal facility equipment and material

Table 3-3 Animal facility equipment and material

Name	Manufacturer
26-G needle	Beckton Dickinson (Heidelberg, D)
Animal cages type 2 IVC	Ehret Labor- und Pharmatechnik (Schönwalde, D)
Animal scale PK2000	Mettler-Toledo (Giessen, D)
Aquasonic 100 Ultrasound Transmission Gel	Parker Laboratories, Inc.
Baby-Mixter Hemostat - Curved 14 cm	Fine Science Tools (Heidelberg, D)
BD Microlance 3	Beckton Dickinson (Heidelberg, D)
Bepanthen	Bayer Vital GmbH
Blood glucose test stripes “Contour next”	Bayer Vital GmbH

Braunol	Braun Melsungen (Melsungen, D)
Castroviejo Micro Needle Holder - Curved w/Lock 9 cm	Fine Science Tools (Heidelberg, D)
ETHIBOND EXCEL green braided, USP 6/0	Medionex (Győr, H)
Graefe Forceps - 0.8 mm Tips Curved	Fine Science Tools (Heidelberg, D)
Glucosteril	Fresenius Kabi Deutschland GmbH (Bad Homburg, D)
Heated pad	Sanitas (Uttenweiler, D)
Iris Scissors - ToughCut Straight 9cm	Fine Science Tools (Heidelberg, D)
Iris Scissors - ToughCut Tungsten Carbide Straight 11.5 cm	Fine Science Tools (Heidelberg, D)
Microscope MZ12.5	Leica (Biberach, D)
Mouse Ventilator minivent Typ 845	Hugo Sachs Elektronik - Havard Apparatus GmbH (March-Hugstetten, D)
NaCl	Fresenius Kabi Deutschland GmbH (Bad Homburg, D)
NMR (Echo MRI mouse) “Minispec mq series”	Bruker Corporation
Non-Sterile Suture Thread - 6/0	Fine Science Tools (Heidelberg, D)
PERMA-HAND silk black braided, USP 6/0	Medionex (Győr, H)
Spectra 360 Electrode Gel	Parker Laboratories, Inc.
Spinal Cord Hook – 12 cm	Fine Science Tools (Heidelberg, D)
TSE Labmaster	TSE Systems GmbH (Bad Homburg, D)
Veet hair removal crème with Aloe vera for sensitive skin	Reckitt Benckiser (Slough, E)
Vevo 770 high-resolution imaging system with a RMV 707 scan head	VisualSonics (Toronto, Ontario, CA)
Vevo 3100 Imaging Platform	VisualSonics (Toronto, Ontario, CA)

3.4 Solutions and buffers

Table 3-4 Solutions and buffers

Solutions	**Manufacturer**
BCA protein assay reagent	Thermo Scientific (Langenselbold, D)
Claycomb medium	Sigma-Aldrich GmbH (Steinheim, D)
Dimethyl sulfoxide (DMSO)	Sigma-Aldrich GmbH (Steinheim, D)
Fetal bovine serum (FBS) (#12J1001)	Sigma-Aldrich GmbH (Steinheim, D)
G153A+B Developer	AGFA (Köln, D)
G354 Rapid Fixer	AGFA (Köln, D)

M-MLV RT 5x Buffer	Promega (Mannheim, D)
Penicillin/streptomycin (P/S)	Biochrom AG (Berlin, D)
Phosphate buffered saline (PBS)	Gibco by Life technologies (Karlsruhe, D)
Qiazol	Qiagen (Hilden, D)
Restore™ Western Blot Stripping Buffer	Thermo Scientific (Langenselbold, D)

Buffers	**Components**
0.5 M stacking buffer	Tris 6.05 g *Add H20; set pH to 6.8 with HCl*
1.5 M separating buffer	Tris 18.15 g *Add H20 and set pH to 8.8 with HCl*
6 x probe buffer for Western blot	Tris 1 M (pH 6.8) SDS 1 g glycerol 1 ml dithiothreitol 0.93 g bromphenol blue (2%) 60 µl
10 x electrophoresis buffer	Tris-Base 0.25 M Glycin 19.92 M SDS 10 % *Add H2O.*
RIPA Buffer	Tris pH 7.5 50 mM NaCl 150 mM MgCl2 5 mM Nonidet P-40 1 % Glycerol 2.5 % EDTA 1 mM Na3VO4 1 mM NaF 50 mM Na4P2O7 10 mM Phenylmethylsulfonylfluorid 100 µM Protease inhibitor «Com. Mini» 1 tablet in 50

	ml PhosStop 1 tablet in 10 ml
10 x TBS	Tris 0.2 M NaCl 1.4 M *pH was set to 7.6 with HCl, and ddH2O added.*
TBST	10 x TBS 100 ml Tween 20 1 ml ddH2O 900 ml
Towbin buffer	Tris 25 mM Glycin 192 mM SDS 0.05 % Methanol 20 % *Add ddH2O.*

3.5 Chemicals and compounds

Table 3-5 Chemicals and compounds

Name	**Manufacturer**
Acrylamid/bis (30%)	Serva Electrophoresis (Heidelberg, D)
Ammoniumpersulfat (APS)	Sigma-Aldrich GmbH (Steinheim, D)
Bromphenol blue	VWR (Darmstadt, D)
2-Mercaptoethanol	Sigma-Aldrich GmbH (Steinheim, D)
Chloroform	Merck (Darmstadt, D)
Deoxynucleotide triphosphates (dNTPs)	Promega (Mannheim, D)
Dimethylsulfoxid (DMSO)	Sigma-Aldrich GmbH (Steinheim, D)
Endothelin-1 (powder)	Sigma-Aldrich GmbH (Steinheim, D)
Ethanol 96 %	Merck (Darmstadt, D)
Fibronectin	Sigma-Aldrich GmbH (Steinheim, D)
Fluorescent Mounting Medium	Dako
Forene 100 % (isoflurane)	Abbott GmbH (Wiesbaden, D)

Formaldehyde	Merck (Darmstadt, D)
Gelatin from bovine skin	Sigma-Aldrich GmbH (Steinheim, D)
Goat serum	Sigma-Aldrich GmbH (Steinheim, D)
Hydrochloride acid (HCl)	Merck (Darmstadt, D)
Isoproterenol hydrochloride	Sigma-Aldrich GmbH (Steinheim, D)
Ketamine hydrochloride	Sigma-Aldrich GmbH (Steinheim, D)
Collagenase Type II	Worthington Biochemical Corporation
L-Ascorbic acid, Sodium salt	Sigma-Aldrich GmbH (Steinheim, D)
L-Glutamine	Sigma-Aldrich GmbH (Steinheim, D)
Methanol	Merck (Darmstadt, D)
NaCl	Merck (Darmstadt, D)
NaOH	Merck (Darmstadt, D)
Norepinephrine [(±)arterenol]	Sigma-Aldrich GmbH (Steinheim, D)
Novaminsulfon-ratiopharm (metamizole)	Ratiopharm GmbH (Ulm, D)
PageRuler™ Prestained Protein Ladder	Thermo Fisher Scientific
PhosSTOP Inhibitor Tablets	Roche Diagnostics (Mannheim, D)
Power SYBR Green PCR Mastermix	Applied Biosystems (Darmstadt, D)
Random Primers	Promega (Mannheim, D)
Rimadyl (carprofen)	Pfizer GmbH (Berlin, D)
RNAsin	Promega (Mannheim, D)
Sodiumdodecylsulfat (SDS)	SERVA Electrophoresis (Heidelberg, D)
Tetramethylethylenediamine (TEMED)	Sigma-Aldrich GmbH (Steinheim, D)
Tris-Base	Merck (Darmstadt, D)
Triton-X	Sigma-Aldrich GmbH (Steinheim, D)
Trichostatin A	Sigma-Aldrich GmbH (Steinheim, D), Hölzel Diagnostika
Tubacin	Sigma-Aldrich GmbH (Steinheim, D), Hölzel Diagnostika
Trypsin inhibitor Type I-S, Soybean	Sigma-Aldrich GmbH (Steinheim, D)
Trypsin-EDTA	Sigma-Aldrich GmbH (Steinheim, D)
Tween 20®	Carl Roth GmbH (Karlsruhe, D)
Ultra Pure Water (UP-H_2O)	Biochrom AG (Berlin, D)
Xylazine hydrochloride	Sigma-Aldrich GmbH (Steinheim, D)

3.6 Kits and markers

Table 3-6 Kits and markers

Name	**Manufacturer**
Pikro-Siriusred for Kollagen I & II	Morphisto (Frankfurt am Main, D)
RNeasy® Micro Kit	Qiagen (Hilden, D)
RNeasy® Mini Kit	Qiagen (Hilden, D)
RT^2 SYBR Green ROX qPCR Mastermix	Qiagen (Hilden, D)

3.7 qRT-PCR primer sequences

Table 3-7 qRT-PCR primer sequences

Gene (mouse)	**Forward primer 5'-3'**	**Reverse Primer 5'-3'**
18s	TTAATGAGCCATTCGCAGTTTTC	ACCTGGTTGATCCTGCCAGTAG
ACSL-1	CTCACCACCTTCTGGTATGC	AGCCATCGTACATGGTTCTG
ANF	AGGAGAAGATGCCGGTAG AAG A	GCTTCCTCAGTCTGCTCACTCA
B2M	CTGCTACGTAACACAGTTCCACCC	CATGATGCTTGATCACATGTCTCG
BNP	CACCGCTGGGAGGTCACT	GTGAGGCCTTGGTCCTTCAA
CD36	GATTAATGGCACAGACGCAGC	TCCGAACACAGCGTAGATAGACC
CD68	AATGTGTCCTTCCCACAGGCAG	AGAGCAGGTCAAGGTGAACAGC
Col1	CTGACGCATGGCCAAGAAGA	ATACCTGGGTTTCCACGTC
Col3	CTGGTCCTGCTGGAAAGGAT	TCCATTGCGTCCATCAAAGC
CPT1b	CCCATGTGCTCCTACCAGAT	CCTTGAAGAAGCGACCTTTG
Glut1	TGTGGTGTCGCTGTTTGTTGTAG	CAATGAAGTTTGAGGTCCAGTTGG
Glut4	GCTTTGTGGCCTTCTTTGAG	CAGGAGGACGGCAAATAGAA
HDAC6	ACCGGTATGACCGTGGCACT	TCCAGGGCACATTGACAGTGA
ß-Actin	GACAGGATGCAGAAGGAGATTACTG	GCTGATCCACATCTGCTGGAA
ß-MHCH	TTCCTTACTTGCTACCCTC	CTTCTCAGACTTCCGCAG

3.8 Antibodies

Table 3-8 Antibodies

primary antibodies	**origin**	**dilution**	**Company**
anti-acetylated Tubulin	mouse	1:16 000	Santa Cruz Biotechnology, Inc.
anti-Actinin alfa	mouse	1:400	Sigma-Aldrich GmbH (Steinheim, D)
α-Tubulin	mouse	1:200	Santa Cruz Biotechnology, Inc.
ß-Actin	mouse	1:500	Santa Cruz Biotechnology, Inc.
secondary antibodies	**origin**	**dilution**	**Company**
anti-rabbit	donkey	1:10000	Jackson ImmunoResearch
anti-mouse	donkey	1:10000	Jackson ImmunoResearch
AlexaFluor 488 dye	donkey	1:400	Thermo Fisher Scientific
DAPI		1:1000	Thermo Fisher Scientific, blue

3.9 Animals

Male C57BL/6J wildtype mice and male 129/SV were purchased from Janvier:

Janvier S.A.S.
Rout edes Chenes Secs
C.S. 4105 Le Genest-St-Isue
53941 St Berthevin Cedex
France

3.10 Software and online tools

Table 3.10.9 Software and online tools

Software	Function
BZ-II Analyzer software	Cell size analysis
Dynamic Cell Count Tool	Cell size analysis
Graphpad Prism 6	Statistical analysis, Figures
Primer Blast NCBI	Primer design for qRT-PCR
PubMed	Literature research
Stratagene MxPro	qRT-PCR analysis
Biorad CFX Connect	qRT-PCR analysis
Vevo 770 3.0.0	Echocardiography analysis
Vevo 3100	Echocardiography analysis
Word, Excel, Powerpoint	Data analysis
Zotero	Citation manager

4 Methods

4.1 Cell culture experiments

In vitro experiments were performed with HL-1 cardiomyocytes, which are derived from AT-1 mouse atrial cardiomyocyte tumor lineage, kindly provided by W.C. Claycomb (Louisiana State University, LA) and cultivated in Claycomb Medium, supplemented with 10 % FBS, 1 % P/S, Norepinephrine (0.1 mM) and L-glutamine (2 mM) until 70-80 % confluency.

4.1.1 Stimulation experiments with HL-1 cells

HL-1 cardiomyocytes were seeded into 6-well plates in triplicates. After an overnight starvation with reduced FBS content (0.5 %) to stop proliferation, cells were stimulated with 100 nM Endothelin1 (ET-1), TSA and Tubacin for 6 h. Afterwards cells were collected and frozen at -80° C until RNA isolation, or used immediately for immunostaining (Figure 4-1).

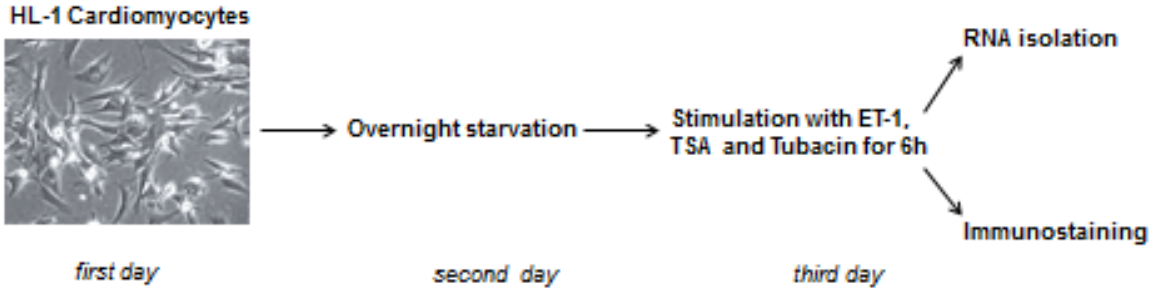

Figure 4-1: *in vitro* stimulation experiment set up

4.1.2 Immunostaining with HL-1 cells

After 6 h stimulation (Figure 4-1), HL-1 cells were fixed with formaldehyde (3.7 %) in phosphate–buffered saline (PBS) on cover slides. Permeabilization of the cell membrane was performed with 0.5 % Triton X-100 in PBS for 5 min. Afterwards cells were blocked with 10 % goat serum (in PBS containing 0.1 % Triton X-100) for at least 1 h or overnight and incubated with primary antibody for sarcomeric alpha-actinin, diluted in blocking solution for 1 h (1:400, Sigma-Aldrich GmbH). Then the cells were washed three times with PBS for 10 min and light sensitive secondary antibody (AlexaFluor 488-conjugated, 1:400, Thermo Fisher Scientific) was applied for 1 h and washed again three times with PBS for 10 min. Nuclei staining was performed with light sensitive 4′,6-Diamidin-2-phenylindol (DAPI) (dilution 1:1000, Thermo Fisher Scientific) for 7 min and washed three times with PBS. Finally, mounting step was performed with Dako Fluorescent Mounting Medium (S3023).
Cell images were taken with an inverted fluorescence phase-contrast microscope at x20 and x40 magnification. Pictures were taken using a digital camera CFI60 (Nikon) and cell size was analyzed using BZ-II Analyzer software and Dynamic Cell Count Tool (Keyence).

4.2 Animal experiments

4.2.1 Ethical approval

All animal procedures were permitted by the Landesamt für Gesundheit und Soziales (LaGeSo, G 0091/13, Berlin, Germany) for the use of laboratory animals and followed the latest version of the German Law for the Protection of Animals. All animal procedures were carried out in accordance with the guidelines of the Charité Medical University Berlin.

4.2.2 Transverse Aortic Constriction model set-up and treatment

In the Transverse Aortic Constriction (TAC) model and in the Isoproterenol (Iso)-induced cardiomyopathy model (see chapter 4.2.3), male C57BL/6J and 129/SV were housed with a 12 h light-dark cycle in a temperature-controlled facility (25 C) (Fliegner et al., 2010; Samuel et al., 2014). Mice were fed at libitum with a standard diet. Body weight (BW) development was observed throughout the experiments.

In the cardiac hypertrophic model eight week old mice were randomized into six treatment subgroups existing of TAC and SHAM-operated groups. In SHAM-operated mice the thorax was opened and then closed again but ligation of the aortic branch was not performed. After one week of pre-treatment and a baseline echocardiography mice were subjected to TAC- or SHAM surgery:

1) SHAM-operated and Vehicle-treated (n = 7),
2) TAC-operated and Vehicle-treated (n = 9),
3) SHAM-operated and TSA-treated (n = 8),
4) TAC-operated and TSA-treated (n = 10),
5) SHAM-operated and Tubacin-treated (n = 8),
6) TAC-operated and Tubacin-treated (n = 10).

Vehicle, TSA and Tubacin were applied every day by intraperitoneal injection (i.p.) (1mg/kg/d, (Cao et al., 2011)) through the whole experiment with a short recovering period of three days after the surgery. Six weeks after OP-intervention, the mice underwent a final echocardiography and a metabolic phenotyping. For this, mice were placed for 24 h in metabolic cages (TSE-Labmaster system) with integrated indirect calorimetry to determined energy expenditure, physical activity and drinking/feeding monitoring system. Furthermore glucose tolerance testing (GTT) and analysis of body composition (NMR) were performed. At the end of the study animals were sacrificed and tissue from different organs was removed for histological-, gene expression- and protein analysis (Figure 4-2).

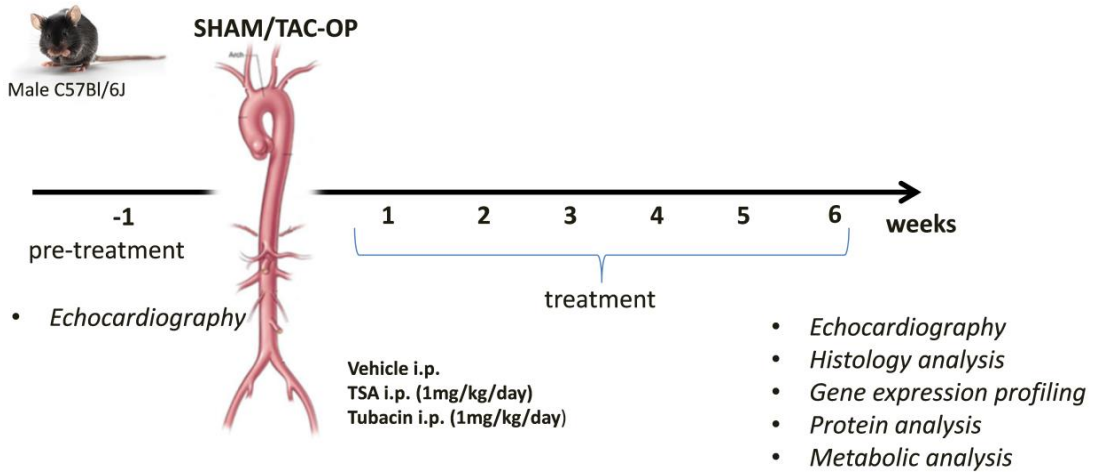

Figure 4-2: Pressure overload induced cardiac hypertrophy model-Transverse Aortic Constriction (TAC) animal set-up.

The TAC model is a pressure overload induced cardiac hypertrophy model (Figure 4-2). The method was established by Fliegner and colleagues (Fliegner et al., 2010). According to the published protocol, mice were sedated by intraperitoneal injection (i.p.) of 1 mg/ml per kg body weight (BW) Ketamine/Xylazin (100 mg/ml; 20 mg/ml per kg BW). The fur was removed with depilatory crème and mice were placed in a supine position on a heating pad under a dissecting stereoscope. Then the animals were intubated and ventilated. Next, a partial thoracotomy to the second rib was performed, the thymus was softly parted and adipose tissue was removed from the aortic arch. Using a 6.0 silk suture positioned around a 26.6 gauge needle the aorta was ligated between the innominate and left carotid arteries to minimize the cross-section. After this procedure, the needle was removed. With the SHAM-operated group of mice, the same intervention was performed without the final aortic ligation. The thorax was closed using a 6.0 prolene suture. The animals received Rimadyl (5.0 mg/kg BW; s. c.) after surgery and for the following 7 days Metamizol as analgeticum, dissolved in the drinking water.

To demonstrate standardized TAC conditions of the different treated groups, six weeks after surgery a trans-constriction pressure gradient was determined. In all TAC-operated mice, trans-constriction pressure gradient were similar indicating comparable TAC conditions (Figure 4-3).

Gradient P was measured using following formula:

$$\boldsymbol{P = 4 * ((AoVmax\ desc[mm/s]/1000)\text{^}2 - (AoVmax\ ascend\ [mm/s]/1000)\text{^}2)}$$

Calculated according to the manufacturer´s instruction, P (pressure gradient), A_0V_{max} desc. (blood flow speed in the descending aorta) and A_0V_{max} ascend. (blood flow speed in the ascending aorta) (Vevo 770, Standard measurements and calculations).

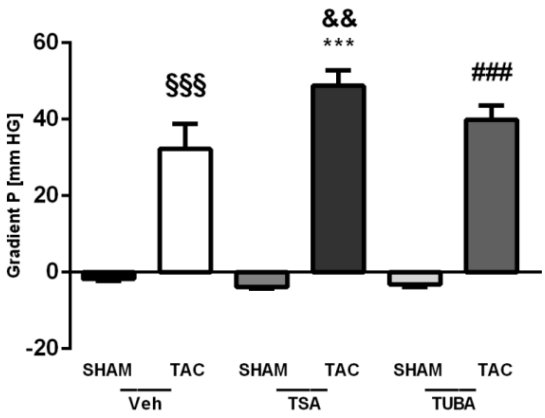

Figure 4-3: Pressure gradient P after SHAM or TAC surgery from all different treated operated animals. §§§ p<0.001 vs. SHAM Vehicle, *** p<0.001 vs. SHAM TSA, ### p<0.001 vs. SHAM Tubacin, && p<0.01 vs. TAC Vehicle; 2-way ANOVA (Bonferroni posttest).

4.2.3 Isoproterenol-induced cardiomyopathy model

To investigate the impact of HDAC6-inhibition on cardiac fibrosis and cardiac inflammation, an experimental model for myocardial injury was carried out (Benjamin et al., 1989). Therefore, male 129/SV mice (5-6 weeks old; Janvier, France) were injected s.c. with Iso (25 mg/kg/d) or saline (Samuel et al., 2014). Tubacin (i.p.; 1 mg/kg/d) or Vehicle was administered by intraperitoneal injection.

The animals were randomized into four treatment groups:

1) Saline-Vehicle-treated (n = 10),
2) Saline-Tubacin-treated (n = 10),
3) Iso-Vehicle-treated (n = 10),
4) Iso-Tubacin-treated (n = 10).

At the beginning of the experiment, animals underwent a baseline echocardiographic examination. After three days of pretreatment with Tubacin/Vehicle, mice were injected with Iso/saline for four consecutive days to induce myocardial injury.

Application of Tubacin/Vehicle was repeated once daily until the end of the experiment. After 20 days, mice underwent a final echocardiography. Then animals were sacrificed and tissue from different organs was removed for histological-, gene expression- and protein analysis (Figure 4-4).

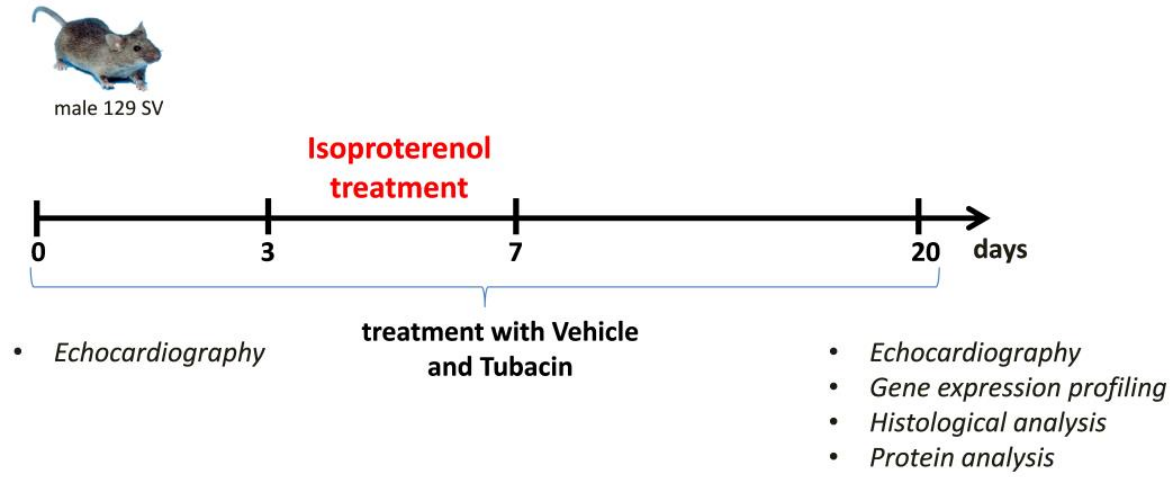

Figure 4-4: Isoproterenol (Iso)-induced cardiomyopathy animal set up.

4.2.4 Echocardiography

4.2.4.1 TAC model

In the TAC model, echocardiography was performed using Vevo 770 high-resolution imaging system (VisualSonics, Canada) with a RMV 707 transducer (centre frequency: 30 MHz, axial resolution: 55 µm; VisualSonics, Canada) to analyze hypertrophy-linked cardiac parameters. Animals received inhalational anesthesia (3 % isoflurane) and were fixed on a heated pad (37 °C) to stabilize body temperature. During examination, Isoflurane was adjusted to values about 1.5 %.

M-mode images of the LV mid-papillary region in short axis view were analyzed for diastolic and systolic wall thicknesses and -dimensions (left ventricular posterior wall [LVPW], left ventricular internal diameter [LVID] and interventricular septum [IVS]) (Figure 4-5). The gradient across the aortic banding (“gradient P”) was assessed using Doppler mode.

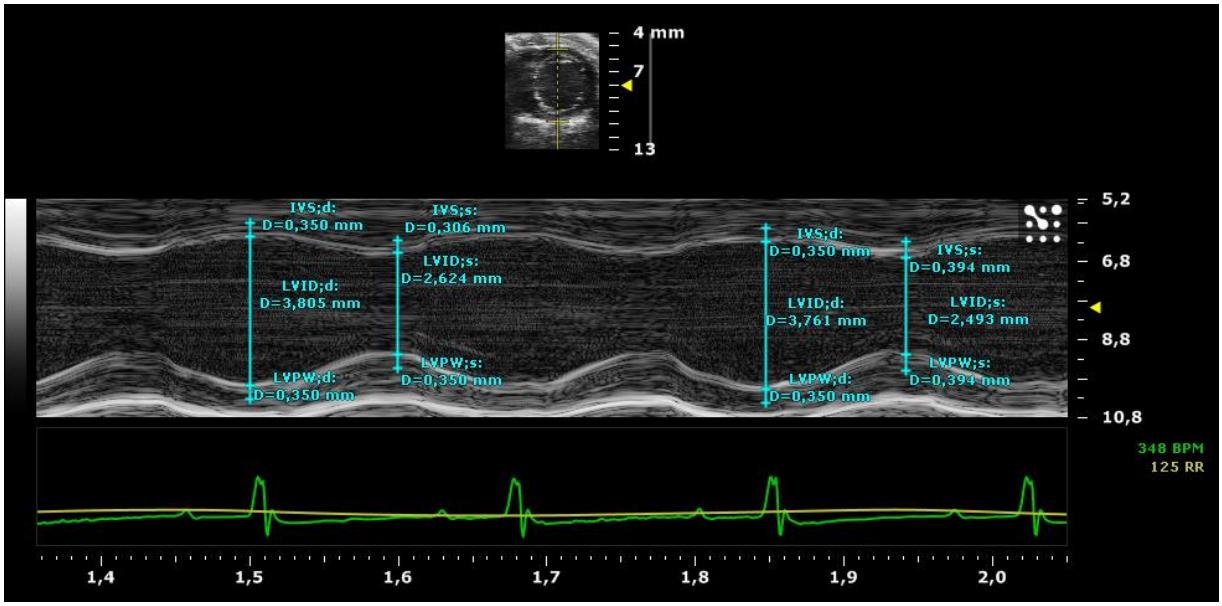

Figure 4-5: Analysis of an M-mode image of the LV mid-papillary region in short axis view. Determination of left ventricular posterior wall (LVPW), left ventricular end-diastolic diameter (LVID) and intra ventricular septum (IVS) during two different heart cycles. Yellow line: respiration control; green line: ECG-recording.

Left ventricular mass (LVM) was calculated according to the Penn cube formula (Collins et al., 2003):

$$\boldsymbol{LVM = 1.05 \times ((IVS, d\,[mm] + LVID, d\,[mm] + LVPW, d\,[mm])^3 - (LVID, d\,[mm])^3)}$$

Ejection fraction (EF) is a parameter of systolic function and was calculated using the following formula:

$$\boldsymbol{EF = \frac{LV_{VOl,d} - LV_{Vol,s}}{LV_{Vol,d}} \times 100}$$

Vol,d (end-diastolic left ventricular volume) and Vol,s (end-systolic left ventricular volume) (Vevo 770, Standard Measurements and Calculations). Volumina were calculated from the M-Mode with the Teichholz method (Vevo 770, Standard Measurements and Calculations, http://www.echobasics.de/systole.html).

Fractional Shortening (FS), also a relative measure, indicate the shortening of the left ventricle during the systole in percentage. It was determined for the left ventricle using the following formula:

$$\boldsymbol{FS = \frac{LVID,d - LVID,s}{LVID,d} \times 100}$$

LVID,d (end-diastolic left ventricular internal diameter) and LVID,s (end-systolic left ventricular internal diameter) (Vevo 770, Standard Measurements and Calculations).

4.2.4.2 Isoproterenol-induced cardiomyopathy model

In the Iso-induced cardiomyopathy model, echocardiographic examination was performed using a MX400 ultra-high frequency linear array transducer (18-38 MHz, center transmit: 30 MHz, axial resolution: 50 µm) coupled to a Vevo3100 device (both VisualSonics, Canada). Wall thicknesses were assessed using the formulas described in chapter 4.2.4.1. Since no alterations of global systolic function were expected in this model, speckle tracking echocardiography (STE) was carried out additionally in order to detect early and minor changes in ventricular function. STE allows analyzing the deformation of the myocardium (“strain”) during the cardiac cycle. Myocardial strain and strain rate can be assessed in the three principal planes of deformation: longitudinal, circumferential and radial. Longitudinal and circumferential shortening are expressed in negative strain values, radial thickening results in a positive strain values, received by subtracting systole from diastole (Shah and Solomon, 2012).

For the analysis, advanced cardiac analysis software was used (VevoStrain, VisualSonics, Canada). The STE is based on the distance measurement between two stable patterns (speckles) in the left ventricle in one heart cycle (Figure 4-6). Speckle tracking images and analysis of the left ventricle were performed in the long axis. Strain (S), strain rate (SR) and myocardial function parameters like EF were determined using Vevo Lab software.

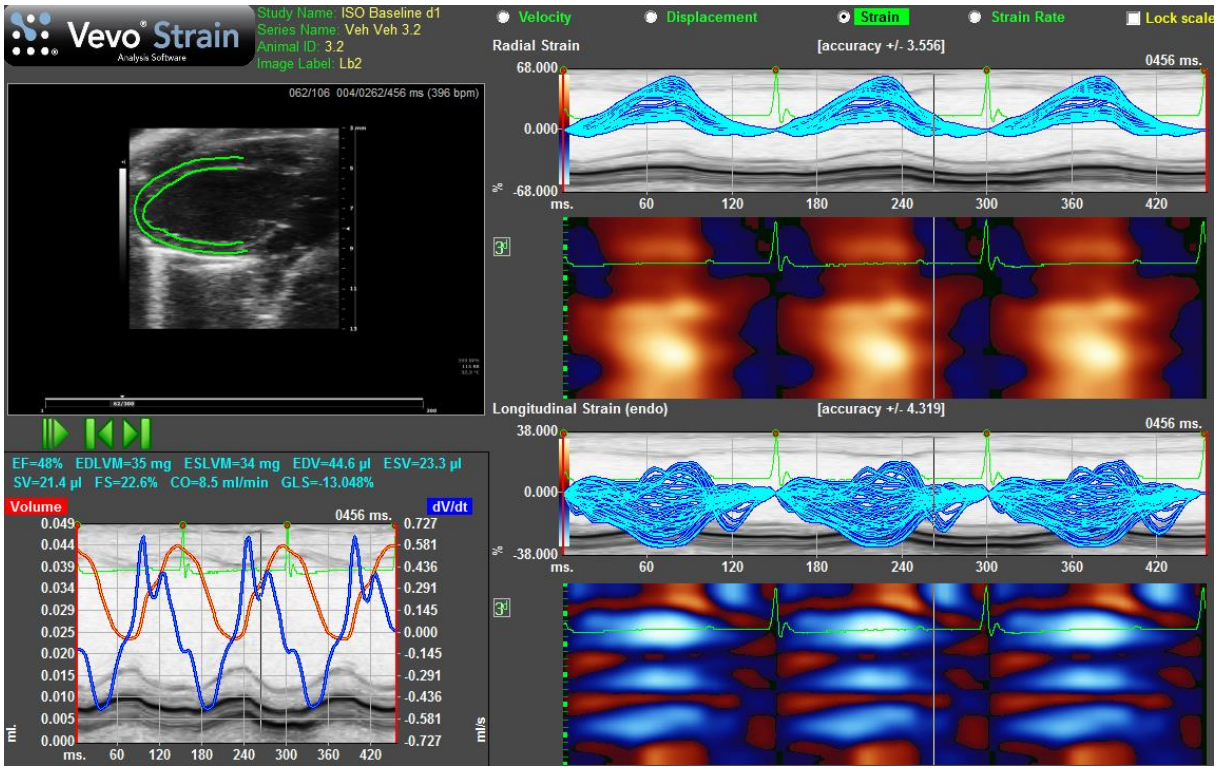

Figure 4-6: Long axis image of the left ventricle from a Vehicle Vehicle-treated mouse (upper left side) and three heart cycles with radial and longitudinal strain parameters (right side).

Strain analysis offers a more sensitive approach for early detection of cardiac dysfunction than conventional echocardiography and enables to analyze changes of the specific tissue sections of the heart (An et al., 2016; Barbosa et al., 2013; Ponikowski et al., 2016b). Generally speaking, strain defines how much the myocardial tissue has been deformed (Voigt et al., 2015):

$$\boldsymbol{S = \Delta L/L0 = (L1 - L0)/L0}$$

S (longitudinal strain); ΔL (absolute change in length) and L_0 (baseline length) (Vevo 3100, Standard Measurements and Calculations).

SR is the local rate of deformation or strain per unit time (Voigt et al., 2015):

$$\boldsymbol{SR = S/\Delta t = \Delta L/L0/\Delta t}$$

SR (strain rate); S (longitudinal strain); ΔL (absolute change in length), L_0 (baseline length) and Δt (absolute change per unit time) (Vevo 3100, Standard Measurements and Calculations).

4.2.5 NMR

Metabolic phenotyping was performed based on body composition measurements of mice, determined by nuclear magnetic resonance (NMR) at the end of the model of pressure overload induced cardiac hypertrophy.

4.2.6 Metabolic cage system

Physical activity, energy expenditure and drinking/feeding monitoring were recorded by using TSE-Labmaster (a combined indirect calorimetry system).
First, animals were adapted for 24 h to the system. The following 24 h the TSE-labmaster recording was performed. The physical activity was recorded using a multi-dimensional infrared light beam system.
The respiratory quotient (RQ) was defined as ratio between produced carbon dioxid (CO_2) and consumed oxygen (O_2):

$$RQ = \frac{CO2produced}{O2consumed}$$

To avoid possible confusing effects from variant body weight and fat mass the energy expenditure was normalized to the lean body mass.

4.2.7 Glucose tolerance test

Animals were fasted overnight and received glucose injection i.p. (1g/kg body weight). The baseline blood glucose level was estimated prior injection.
After glucose injection in the intervals of 15, 30, 60, 90, 120 and 150 min blood glucose were measured from tail vain using blood glucose test stripes (“Contour next”).

4.2.8 General molecular methods

RNA isolation and quantification

Qiazol and RNeasy Mini Kit were used according to manufacturer´s protocol to isolate RNA from the cell culture experiments.
Left ventricular tissue was lysed in Lysis tubes containing RLT-ß-mercapto-ethanol buffer (RNeasy Micro Kit) in the speed mill (30 sec, 13000 rpm) according to the manufacturer´s protocol. Afterwards the total RNA was isolated with the RNeasy Micro Kit.
In both procedures DNA was digested with DNAse (DNase Set, Qiazol) by incubation the RNA-samples for 15 min at room temperature. The final RNA concentration was measured with a spectrophotometer (NanoDrop). Samples were stored at -80 ° C.

cDNA transcription

Using reverse transcriptase (RT), RNAsin, MLV-Buffer and dNTPs RNA samples were reverse transcribed for quantitative real-time PCR analyses according to manufacturer´s protocol. The reaction was carried out for 5min at 70 °C. 1 µg of the total RNA and 1 µl random primers (1:5) were used.
Afterwards master mix or RT- mix (negative control, lacking reverse transcriptase) was added and samples were incubated at 37 ° C for 1 h. cDNA in the final concentration of 5 ng/µl (diluted 1:4, with UP-H_2O) were stored at -20 °C.

Table 4-1: Protocol of reverse transcription

RNA amount in total volume	37.5 µl	37.5 µl
Random Primers	1 µl	1 µl
+	**RT(+)-Mastermix**	**RT(-)-Mastermix**
	50 µl	50 µl
UP-H_2O	-	0.5 µl
M-MLV reverse transcriptase	0.5 µl	-
RNAsin	0.5 µl	0.5 µl
M-MLV Buffer (5x)	10 µl	10 µl
dNTPs (10 mM)	1 µl	1 µl

Gene expression analysis with quantitative Real-time PCR (qRTPCR)

The fluorescent dye SYBRgreen cDNA was used in qRT-PCR reactions to determine gene expression levels. Generally after normalization to murine 18S or ß-Actin the relative amount of mRNA was calculated with the 2^{-ddct} method (Livak and Schmittgen, 2001). The measurements were performed in technical triplicates. Non-template controls (NTC) were measured every time. Sequences of the primers which were used for the analysis are listed in the material list (Table 3-7).

Protein isolation and concentration

Cells were washed with ice-cold PBS and then RIPA buffer including protease and phosphatase inhibitors (Complete mini/PhosStop, Roche) was added. The cells were lysed and the samples were sonicated to shear DNA (30 sec, 50 %) and centrifuged to pellet DNA and membrane components (4 ° C, 14000 rpm, 30 min). For the Western Blot the cytosolic protein containing supernatant was used. The concentration of proteins was measured in the samples using BCA assay kit (manufacturer´s protocol from Thermo Scientific). Animal tissue was lysed in Lysis-tubes with ice-cold Ripa-buffer and was homogenized in the speed mill for 30 sec,

then incubated for 60 min on ice and centrifuged (4 ° C, 13000 rpm, 30 min). Samples were stored at -20 ° C

SDS-Polyacrylamid gel electrophoresis (SDS-Page) and Western blot

For Western blot analysis the samples with the same concentration of protein were mixed with 6x probe buffer and incubated for 5 min at 95 ° C. Next, the samples were spotted on an acrylamide-gel and subjected to SDS-PAGE electrophoresis at 120 V for at least 1 h (depending on protein size) by using Bio-Rad equipment and electrophoresis buffer. Prior to transfer of the proteins on a PVDF membrane, the membrane was activated in methanol for 1 min. Blotting was performed in a tank blotting chamber with cold Towbin buffer at 100 V for 60 min. Afterwards, membranes were blocked in 5 % BSA (dissolved in TBST) at room temperature under constant shaking. After 2 h the primary antibody dissolved in 5 % BSA was added to the membrane. The membrane with the primary antibody was incubated over night at 4 ° C as described above. Next day the membrane was washed 3 times in 1x TBST and then incubated with the secondary antibody, dissolved in 1.5 % BSA for 1 h at room temperature. Protein expression was visualized using enhanced chemiluminescence kit (Amersham hyperfilm ECL, GE Healthcare). For further analysis the membrane was stripped for 15 min with 16 ml Restore™ Western Blot Stripping Buffer (Restore™Western Blot Stripping Buffer, Thermo Scientific) and another primary and secondary antibody were used. As loading control the abundance GAPDH or ß-Actin was analyzed.

4.2.9 Histological analysis of cardiac tissue

Histological analysis of heart tissue sections from all animal experiments was performed together with Prof. Robert Klopfleisch from the Department of Veterinary Pathology, Freie Universität Berlin.
The cardiac tissue was fixed and embedded in paraffin (FFPE). The specific staining of hematoxylin and eosin (H&E) and Picrosirius red were performed in the laboratory of Prof. Klopfleisch (Klopfleisch et al., 2011).

The size of the cardiomyocytes in the LV was determined. Randomly selected cells were evaluated and cross sectional area was measured using Analysis Software (Olympus).
Additionally, Picrosirius red staining was performed to visualize collagen accumulation in the cardiac tissue. It was performed according to the manufacturer´s instruction (Morphisto, Germany) with two additional incubation times of the cardiac sections in 6 % acetic acid for 20 min.
The fibrotic content was calculated from microscopic images and was determined as percent fraction of collagen regions from the total tissue area.

4.3 Statistical analysis

Mean values comparisons among the different groups were evaluated by two-way ANOVA or ANOVA and Bonferroni posthoc-test. When appropriate, two-way ANOVA with repeated measurements was performed. For the comparison of two groups with normal distribution an unpaired t-test was used. In every figure the statistical analysis is stated. Statistical analysis was performed with GraphPad Prism 6 Software. Statistical significance was considered with the $p<0.05$. Vertical lines in the histograms indicate ± SEM.

5 Results

Main focus of this study was to characterize the role of HDAC6 in cardiac function.
In vitro experiments were performed in HL-1 cardiomyocytes to investigate the effect of a specific HDAC6i Tubacin in direct comparison to a general HDACi Trichostatin A (TSA) on hypertrophic responses induced by ET-1. Previously, it was shown that general HDACi improved cardiac function (Cao et al., 2011; Kao et al., 2013; Majumdar et al., 2011).
The effect of the HDACi, especially of the HDAC6 inhibitor Tubacin, on the development of cardiac hypertrophy was investigated in a murine model of pressure overload-induced cardiac hypertrophy by TAC intervention. In an additional *in vivo* experiment cardiac fibrosis was induced by systemic Iso application and the influence of Tubacin on the development of cardiac fibrosis and inflammation was analyzed. This study investigated for the first time the effect of the specific HDAC6 inhibitor Tubacin on the development of cardiac hypertrophy.

5.1 HDAC inhibition reduced endothelin 1-mediated cardiac hypertrophy in HL-1 cardiomyocytes

5.1.1 Determination of the effective dose from Tubacin which reduced hypertrophic response induced by ET-1 in HL-1 cells

In a previous study in our laboratory ET-1, a potent vasoconstrictor, was established as an effective factor inducing cellular hypertrophy in HL-1 cells (Foryst-Ludwig et al., 2015a). Treatment of the HL-1 cells with ET-1 led to a hypertrophic response, enlarged volume of the cells and induction of fetal gene expression profiles of pathological markers such as ANF, BNP and ß-MHCH (Foryst-Ludwig et al., 2015b). These pathological markers are key indicators specific for a hypertrophic response.
First, to find out which Tubacin dosage is able to reduce ET-1-mediated hypertrophic effect, three different concentrations of Tubacin were tested in HL-1 cardiomyocytes (Figure 5-1). Concentrations of 0.05 µM, 0.5 µM and 5 µM of Tubacin were used in conjunction with 100 nM ET-1. The cells were incubated with DMSO, ET-1 or ET-1 combined Tubacin for 6 h, as indicated. All three different concentrations of Tubacin

reduced the hypertrophic response from ET-1 significantly. ANF gene expression level was significantly diminished in cells treated with Tubacin combined with ET-1, when compared to ET-1 treated cells (Figure 5-1).

For further experiments the dosage of 5 µM Tubacin was taken similar to the study published by Winkler et al (Winkler et al., 2012).

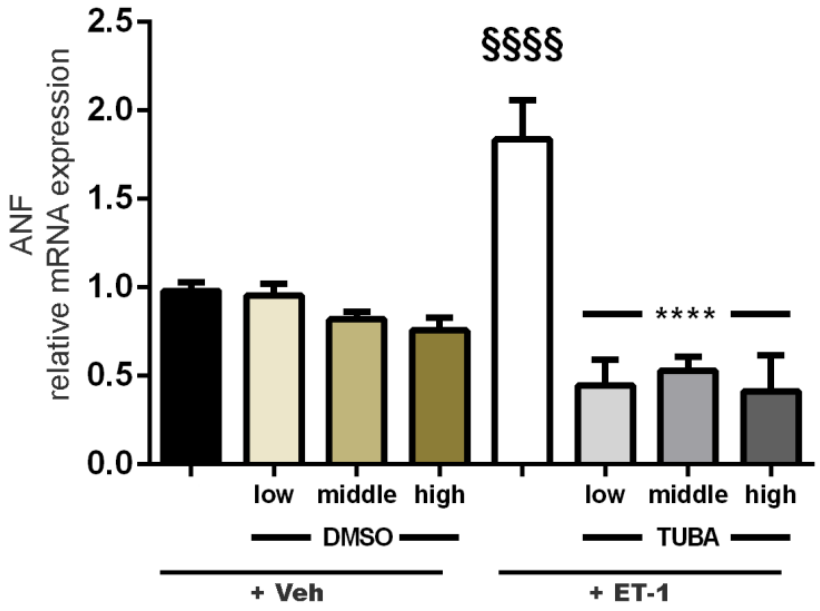

Figure 5-1: ANF gene expression level was measured using qRT-PCR; HL-1 cardiomyocytes were treated with ET-1 (100nM) and different concentrations of Tubacin (low: 0.05 µM, middle: 0.5 µM and high: 5 µM) for 6 h. ANF: atrial naturetic factor, Veh: Vehicle, Tuba: Tubacin, ET-1: endothelin 1. §§§§ $p<0.0001$ vs. control; **** $p<0.0001$ vs. Et-1, ($n = 3$; 1-way ANOVA (Bonferroni posttest)).

5.1.2 HDACi TSA and Tubacin showed anti-hypertrophic effects in HL-1 cells

HL-1 cells were stimulated with ET-1, TSA and Tubacin for 6 h as described in Figure 5-1. TSA, a general HDACi, was used and compared to the specific HDAC6i Tubacin.

Treatment of the HL-1 cells with ET-1 significantly increased the gene expression levels of ANF and ß-MHCH after 6 h, when compared to vehicle-treated control cells. Both Tubacin and TSA significantly reduced the hypertrophic responses of ET-1 similar powerful (Figure 5-2).

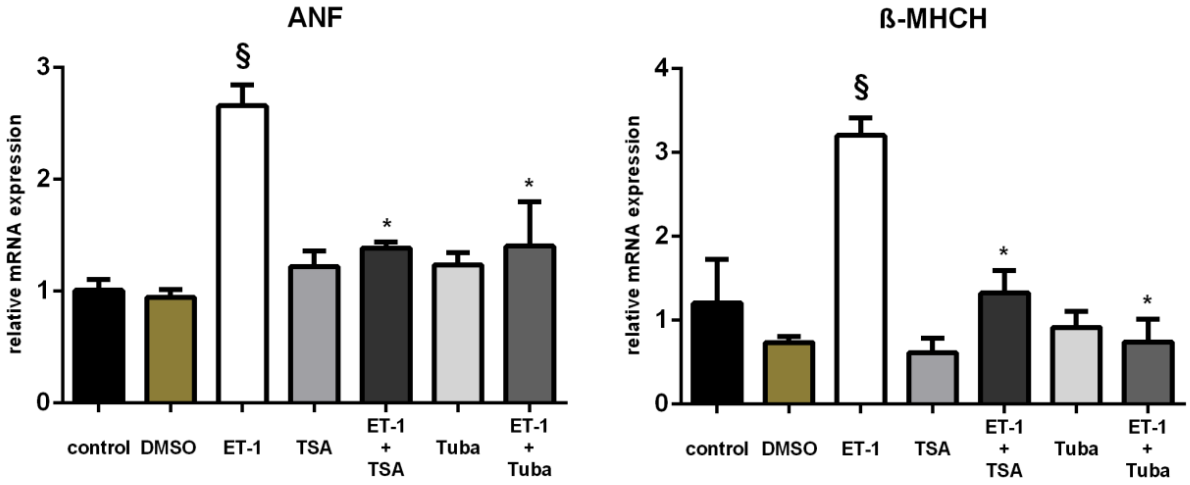

Figure 5-2: Gene expression levels of ANF and ß-MHCH were measured using qRT-PCR; HL-1 cells were treated with 100 nM ET-1 alone or together with TSA (1 µM) or Tubacin (5 µM) for 6 h. ANF: atrial naturetic factor, ß-MHCH: beta-cardiac myosin heavy chain isogene, ET-1: endothelin 1, Tuba: Tubacin, TSA: Trichostatin A. § $p<0.05$ vs. control; * $p<0.05$ vs. Et-1, (n = 3; 1-way ANOVA (Bonferroni posttest)).

5.1.3 Immunostaining experiments showed reduction of the cell size from hypertrophic HL-1 cells after treatment with HDACi

Immunostaining experiments were performed with HL-1 cells to examine the effect of TSA and Tubacin regarding cell size regulation. The anti-hypertrophic effect of TSA and Tubacin was confirmed (Figure 5-2). HDAC6 inhibition reduced ET-1-mediated increases in cardiomyocyte size. Cell sizes of ET-1 treated cells were significantly reduced after 6 h incubation with TSA or Tubacin compared to cells treated with ET-1 alone.

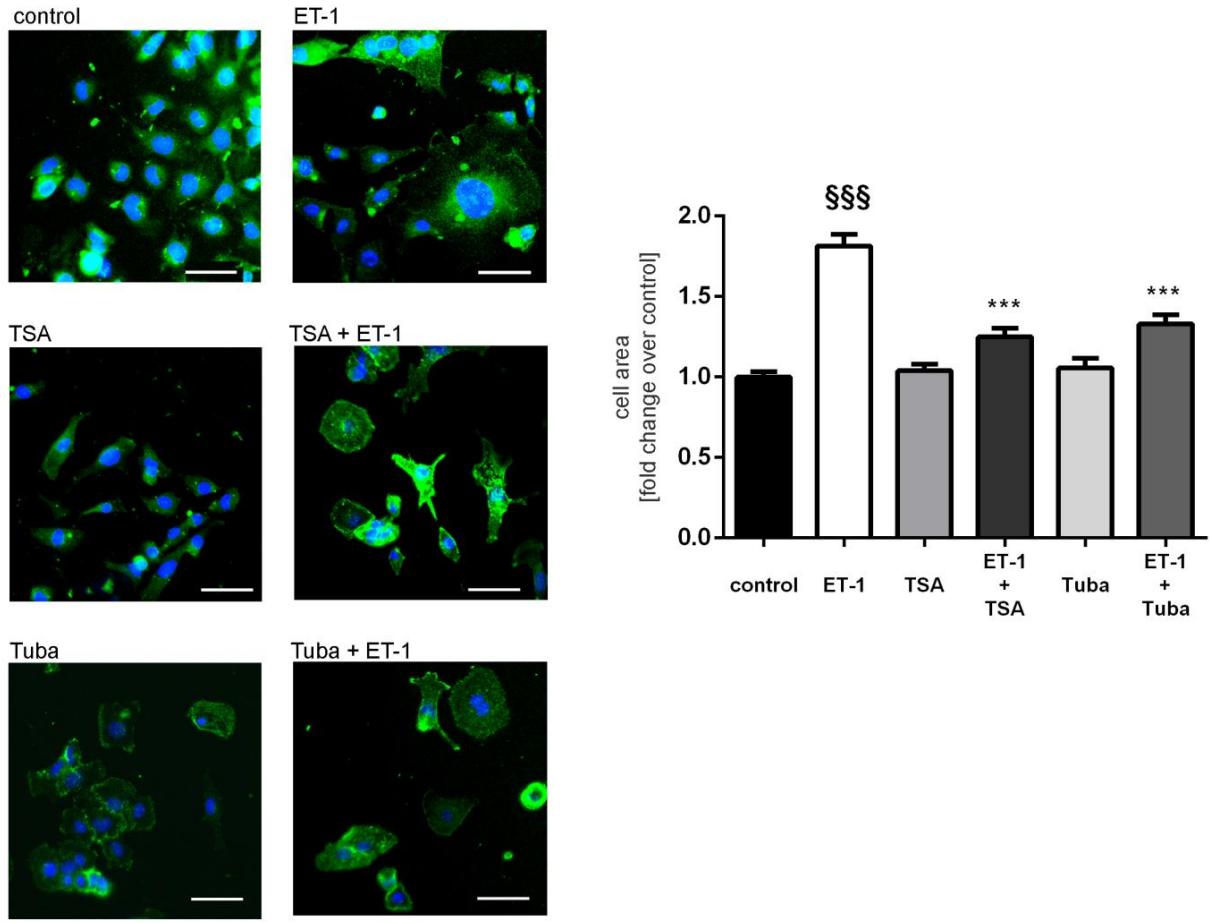

Figure 5-3: Analysis of the HL-1 cell surface area calculated from immunofluorescence images; HL-1 cells were treated with 100 nM ET-1 alone or together with TSA (1 µM) or Tubacin (5 µM) for 6 h. ET-1: endothelin 1, Tuba: Tubacin, TSA: Trichostatin A. Data are presented as x-fold over control; cell area was quantified with the BZ-II Analyzer software. §§§ $p<0.001$ vs. control; *** $p<0.001$ vs. Et-1, (n = 3; 1-way ANOVA (Bonferroni posttest)).

5.2 HDACi Tubacin and TSA attenuate cardiac hypertrophy *in vivo*

An established TAC model was applied on eight weeks old C57/Bl6 male mice to induce pressure overload cardiac hypertrophy (described in chapter 4.2.2, Fliegner et al., 2010). The effect of Tubacin and TSA was investigated on the development of cardiac hypertrophy (Figure 4-2).

Cardiac phenotyping was performed using final echocardiographic analysis. Left ventricular mass (LVM) from each animal was calculated and are represented relative to tibia length (TL).

TAC-operated Vehicle-treated mice showed significant higher LVM/TL compared to SHAM-operated Vehicle-treated animals. TSA and Tubacin-treated TAC-operated mice showed significant lower LVM/TL compared to the Vehicle-TAC-operated mice (SHAM Veh 4.72 ± 0.51 mg/mm, TAC Veh 7.51 ± 1.65 mg/mm, SHAM TSA 4.31 ± 0.32 mg/mm, TAC TSA 5.78 ± 1.33 mg/mm, SHAM TUBA 4.64 ± 0.31 mg/mm, TAC TUBA 5.60 ± 0.90 mg/mm) (Figure 5-4).

Additionally, other cardiac parameters like intraventricular septum (IVS) thickness and left posterior wall (LVPW) thickness were analyzed. Analysis of the IVS and LVPW thickness using M-mode images showed that TAC-operated Vehicle-treated mice had significantly higher values of IVS and LVPW in comparison to the SHAM-operated Vehicle-treated animals (Figure 5-4). Both, TSA and Tubacin-treated TAC-operated mice showed significantly lower IVS and LVPW values after six weeks of treatment (Figure 5-4).

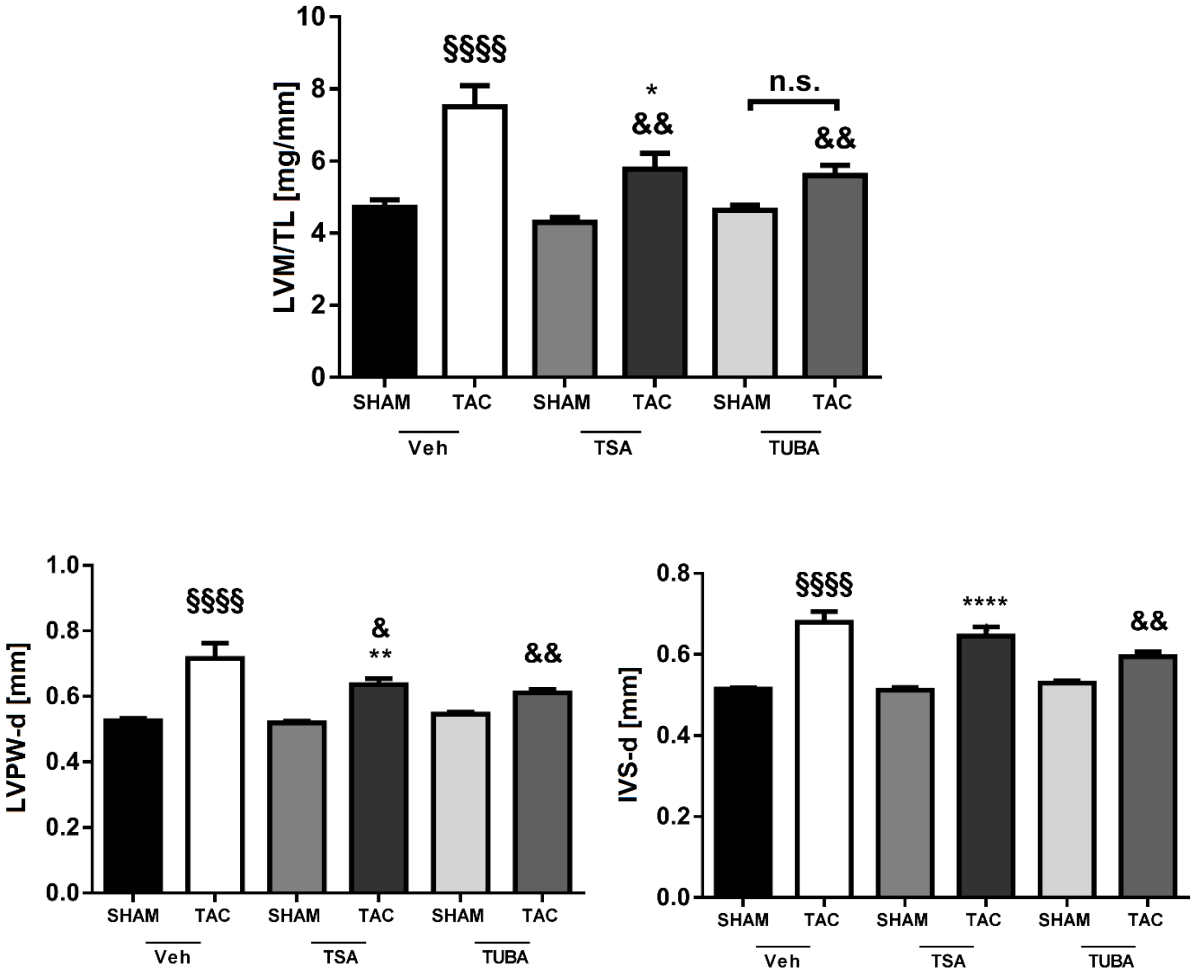

Figure 5-4: Echocardiographic analysis of TAC- or SHAM-operated mice treated with TSA, Tubacin or Vehicle; LVM: left ventricular mass, IVS: left ventricular inter-septum, LVPW: left ventricular posterior wall; TL: Tibia length, Veh: Vehicle, TSA: Trichostatin A, Tuba: Tubacin. Values are means ± SEM.
§ p<0.05 vs. SHAM Vehicle, §§ p<0.01 vs. SHAM Vehicle, §§§§ p<0.0001 vs. SHAM Vehicle * p<0.05 vs. SHAM TSA, ** p<0.01 vs. SHAM TSA, **** p<0.0001 vs. SHAM TSA, & p<0.05 vs. TAC Vehicle, && p<0.01 vs. TAC Vehicle; 2-way ANOVA (Bonferroni posttest).

In the macroscopic photographs and echocardiographic M-Mode pictures, TAC-operated Vehicle-treated mice showed increased wall thickness and increased heart size compared to SHAM-operated Vehicle-treated mice six weeks after surgery. Treatment with both HDACi TSA and Tubacin prevented increased wall thickness and reduced the heart size (Figure 5-5).

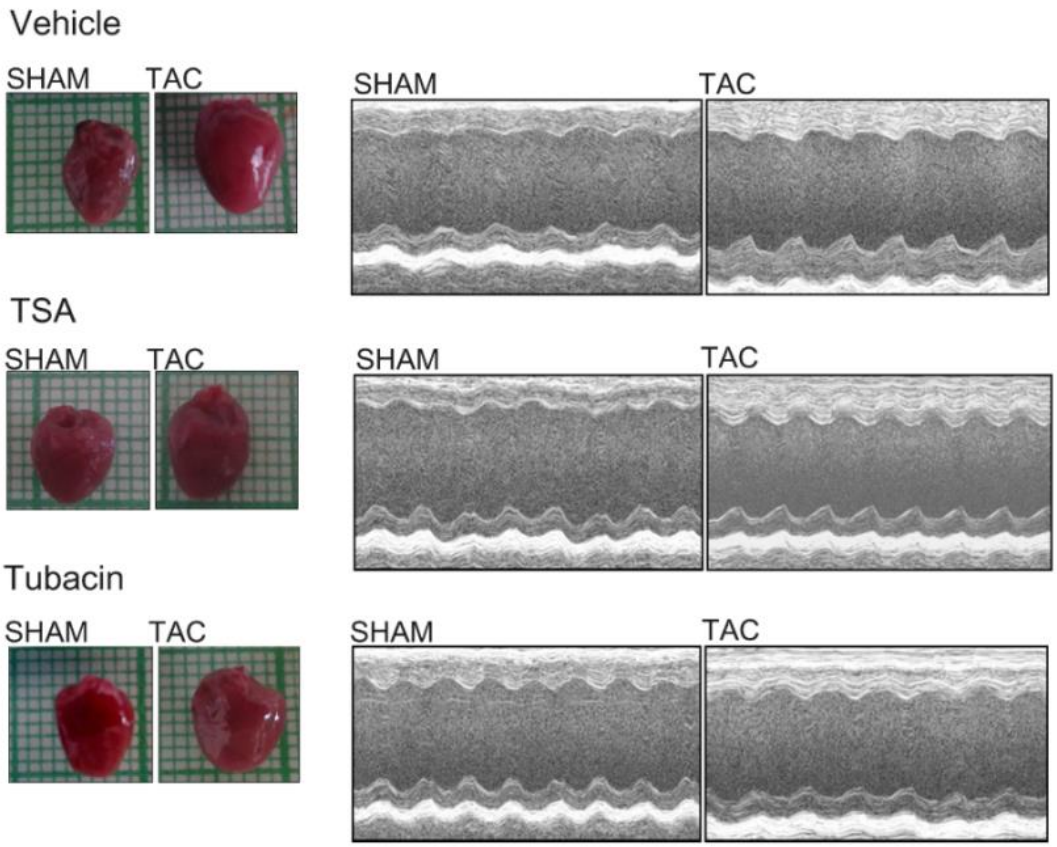

Figure 5-5: Representative heart and M-mode images from TAC/SHAM operated mice treated with Tubacin, TSA or Vehicle.

Accordingly, cardiac cross sectional H/E images were analyzed. Cross sections were taken in the mid papillary section of the heart from each mouse. The results from this analysis indicated that the TAC-Vehicle animals were characterized by increased cardiac cross-section area compared to the SHAM-Vehicle group. TAC-TSA and TAC-Tubacin mice had smaller cross sectional H/E areas, compared to the TAC-Vehicle ones (Figure 5-6). Cardiomyocytes from the TAC-operated mice were in general larger than cardiomyocytes from SHAM animals. More importantly, cardiomyocytes from TAC-Vehicle-treated mice were bigger in size than those

measured in both TAC-TSA and TAC-Tubacin-treated groups indicating that TSA and Tubacin had anti-hypertrophic effects (Figure 5-6, right panel side).

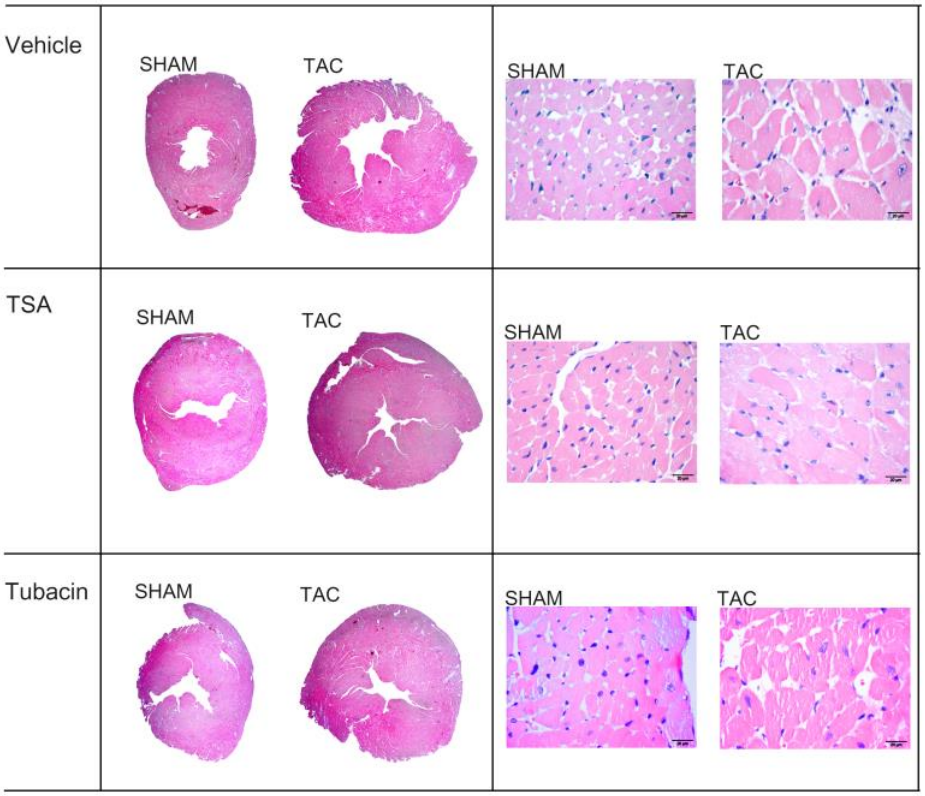

Figure 5-6: H/E staining from the cross sectional heart and cardiac tissue section images of the different treated mice after TAC or SHAM operation.

EF and FS are markers for cardiac function and systolic heart failure (chapter 4.2.4.1). In systolic heart failure EF and FS values are lower than under physiological conditions in healthy hearts. In our experiments, TAC-operated mice did not show significant differences in EF or FS, when compared to SHAM-operated animals meaning that the animals had no systolic dysfunction. In summary, key echocardiographic parameters are presented in Table 5-1.

Table 5-1: Cardiac phenotyping of mice 6 weeks post TAC/SHAM intervention. N = 5-10

	Vehicle SHAM	**Vehicle TAC**	**TSA SHAM**	**TSA TAC**	**Tuba SHAM**	**Tuba TAC**
LVM/Tibia [mg/mm]	4.72 ± 0.51	7.51 ± 1.65§§§§	4.31 ± 0.32	5.78 ± 1.33$^{*\&\&}$	4.64 ± 0.31	5.60 ± 0.9$^{\&\&}$
LVM/BW [mg/g]	2.11 ± 0.18	3.31 ± 0.72	2.06 ± 0.21	2.51 ± 0.53	2.02 ± 0.11	2.43 ± 0.37
LVM/HW [mg/g]	411.40 ± 20.64	524.16 ± 71.98§	446.48 ± 58.98	442.25 ± 98.69	455.87 ± 27.15	419.85 ± 82.29$^{\&}$
IVSd [mm]	0.52 ± 0.01	0.68 ± 0.08§§§§	0.51 ± 0.02	0.65 ± 0.07****	0.53 ± 0.01	0.60 ± 0.04$^{\&\&}$
LVIDd [mm]	3.99 ± 0.27	4.25 ± 0.24	3.98 ± 0.23	3.84 ± 0.41	4.01 ± 0.12	4.08 ± 0.37
LVPWd [mm]	0.53 ± 0.01	0.72 ± 0.13§§§§	0.52 ± 0.01	0.64 ± 0.05$^{**\&}$	0.55 ± 0.02	0.61 ± 0.03$^{\&\&}$
FS [%]	23.95 ± 4.22	20.69 ± 4.90	28.34 ± 4.26	26.89 ± 7.74	23.33 ± 2.08	25.93 ± 5.43
EF [%]	47.85 ± 6,69	42.11 ± 8.16	53.35 ± 9.03	52.16 ± 11.83	47.08 ± 3.50	50.88 ± 8.53
HR [bpm]	392 ± 22.59	411 ± 24.64	414 ± 12.38	403 ± 15.60	393 ± 23.67	393 ± 9.50
Gradient P	-1.8 ± 0.5	32.3 ± 6.5 §§§	3.8 ± 0.4	48.8 ± 4.1 $^{***\&\&}$	3.2 ± 0.7	39.9 ± 3.8$^{\#\#\#}$

LVM: left ventricular mass, IVSd: left ventricular inter-septum during diastole, LVPWd: left ventricular posterior wall during diastole, BW: body weight, HW: heart weight, FS: fractioning shortening, EF: ejection fraction, HR: heart rate, § p<0.05 vs. SHAM Vehicle, §§ p<0.01 vs. SHAM Vehicle, §§§ p<0.001 vs. SHAM Vehicle, §§§§ p<0.0001 vs. SHAM Vehicle, & p<0.05 vs. TAC Vehicle, && p<0.01 vs. TAC Vehicle, &&& p<0.001 vs. TAC Vehicle, * p<0.05 vs. SHAM TSA, ** p<0.01 vs. SHAM TSA, *** p<0.001 vs. SHAM TSA, **** p<0.0001 vs. SHAM TSA; 2-way ANOVA (Bonferroni posttest).

5.2.1 Systemic application of HDAC6i Tubacin and TSA led to reduced HDAC6 activity in the cardiac tissue

To confirm pharmacological inhibitory HDAC activity of TSA and Tubacin in the mouse hearts, HDAC6 activity was determined. The acetylation status of α-tubulin, a known target of HDAC6, was analyzed in left ventricle samples of TAC- and SHAM-operated mice after six weeks of treatment. Importantly, cardiac gene expression of HDAC6 was not significantly regulated by the TAC-intervention and/or treatment with both HDACi (Figure 5-7).

α-Tubulin is the first identified substrate of HDAC6 and HDAC6 activity can be estimated by the acetylation status of this protein (Li et al., 2011). In the TAC animals the acetylation-status of α-Tubulin was slightly reduced, when compared to SHAM-operated controls. Tubacin, when applied to mice, induced hyperacetylation of α-tubulin in murine cardiac tissue. Meaning, that Tubacin displays specific activity in the heart and inhibits HDAC6 activity when applied systemically (Figure 5-7). In addition, cardiac gene expression level of HDAC6 was estimated. Regarding the impact of TSA on α-tubulin acetylation status, TSA did not induce hyperacetylation such as Tubacin.

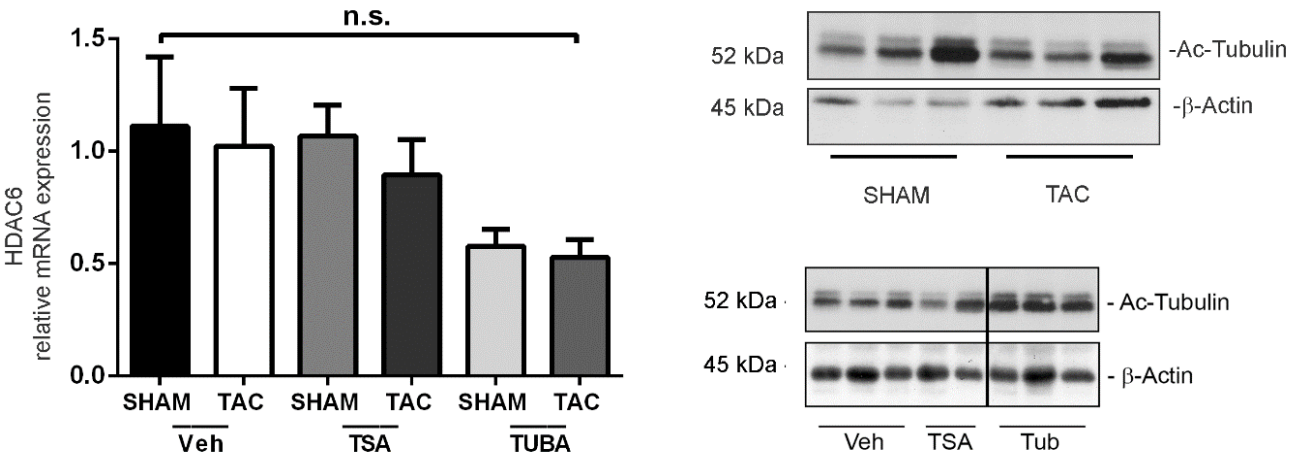

Figure 5-7: Cardiac gene expression levels of HDAC6 in the different treated and operated animals six weeks after treatment; Western Blot analysis of tubulin acetylation status and ß-Actin in left ventricle samples isolated from TAC-operated Vehicle-, TSA or Tubacin-treated mice. Veh: Vehicle, TSA: Trichostatin A, Tuba: Tubacin; 2-way ANOVA (Bonferroni posttest).

5.2.2 HDACi prevented induction of pathological marker expression after TAC

Besides echocardiography, gene expression profiles of pathological markers were examined in the six treatment groups. ANF and BNP were significantly increased in TAC-operated animals treated with Vehicle, when compared to SHAM-operated Vehicle-treated mice. Treatment with TSA and Tubacin significantly prevented the increase of gene expression levels of both ANF and BNP. The outcome of the gene expression analysis confirm our *in vitro* results, described previously (Figure 5-2).

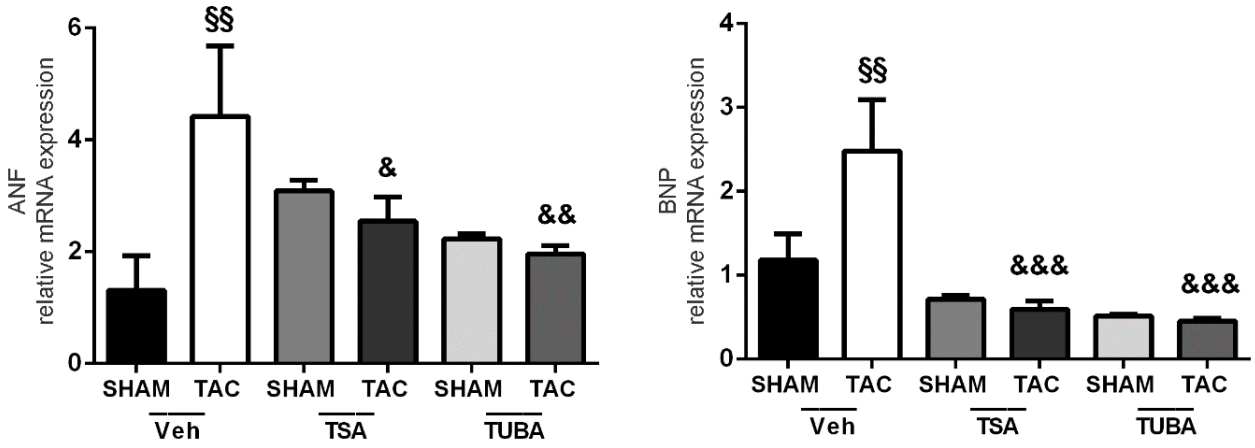

Figure 5-8: Cardiac gene expression levels from hypertrophic markers ANF and BNP (ANF: Atrial Natriuretic Factor, BNP: Brain Natriuretic Peptide). Veh: Vehicle, TSA: Trichostatin A, Tuba: Tubacin; Values are means ± SEM. §§ $p<0.01$ vs. SHAM Vehicle, & $p<0.05$ vs. TAC Vehicle, && $p<0.01$ vs. TAC Vehicle, &&& $p<0.001$ vs. TAC Vehicle; 2-way ANOVA (Bonferroni posttest).

5.3 Metabolic phenotyping of TAC/SHAM-operated mice showed no differences

Recent data indicate that TAC-intervention induces systemic metabolic dysfunction, leading to an increased lipolytic activity, inflammation of adipose tissue and marked insulin resistance and glucose intolerance (Shimizu et al., 2012). Therefore in our experiments we included also a glucose-tolerance-test (GTT) and metabolic phenotyping using the TSE-Labmaster-system. Importantly, all groups of animals showed similar body weight (BW) development, fat pads weight, and fat and lean mass (Table 5-2). In the glucose-tolerance-test were no significant changes among the different treatment groups, except in both Vehicle groups, showing significantly lower fasting blood glucose levels in the first measurement (Figure 5-9).

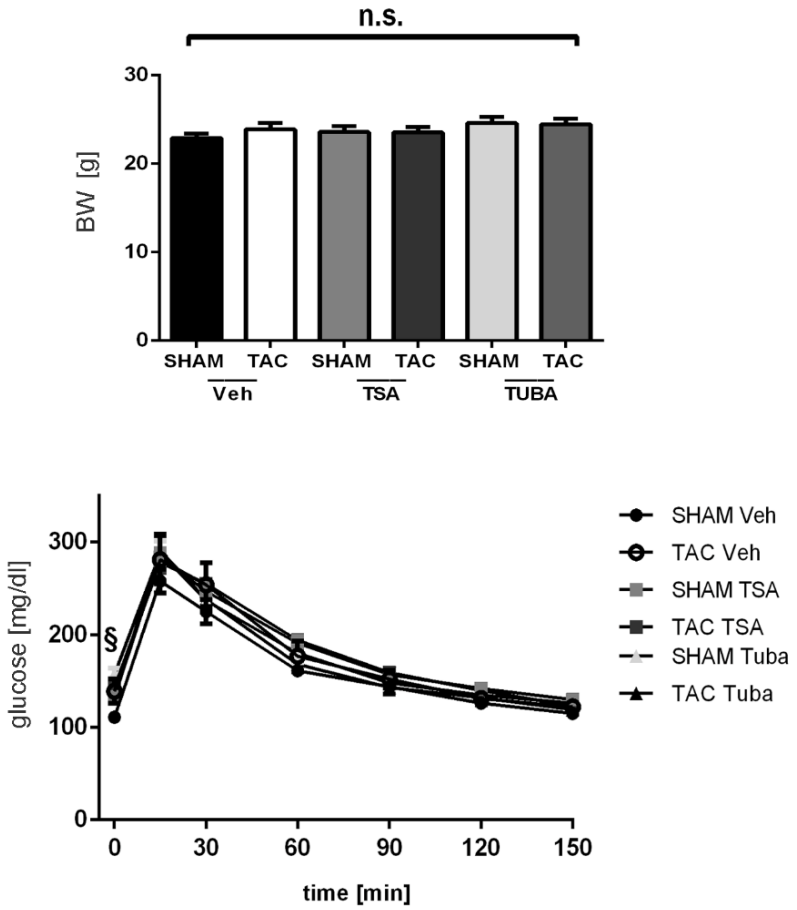

Figure 5-9: Body weight (BW) development. Veh: Vehicle, TSA: Trichostatin A, Tuba: Tubacin. Values are means ± SEM. § p<0.05 vs. SHAM Vehicle, # p<0.05 vs. SHAM Tubacin; 2-way ANOVA with repeated measurements (Bonferroni posttest). Systemic glucose tolerance test (GTT) showed no effect by the treatment or/and TAC-intervention. Values are means ± SEM. § p<0.05 vs. SHAM Vehicle, 2-way ANOVA with repeated measurements (Bonferroni posttest).

Furthermore, all animals were analyzed in metabolic cages for 24 h to determine respiratory quotient (RQ), locomotor activity and food intake. Different treated/operated animals showed no differences in RQ, locomotor activity and food intake (Figure 5-10).

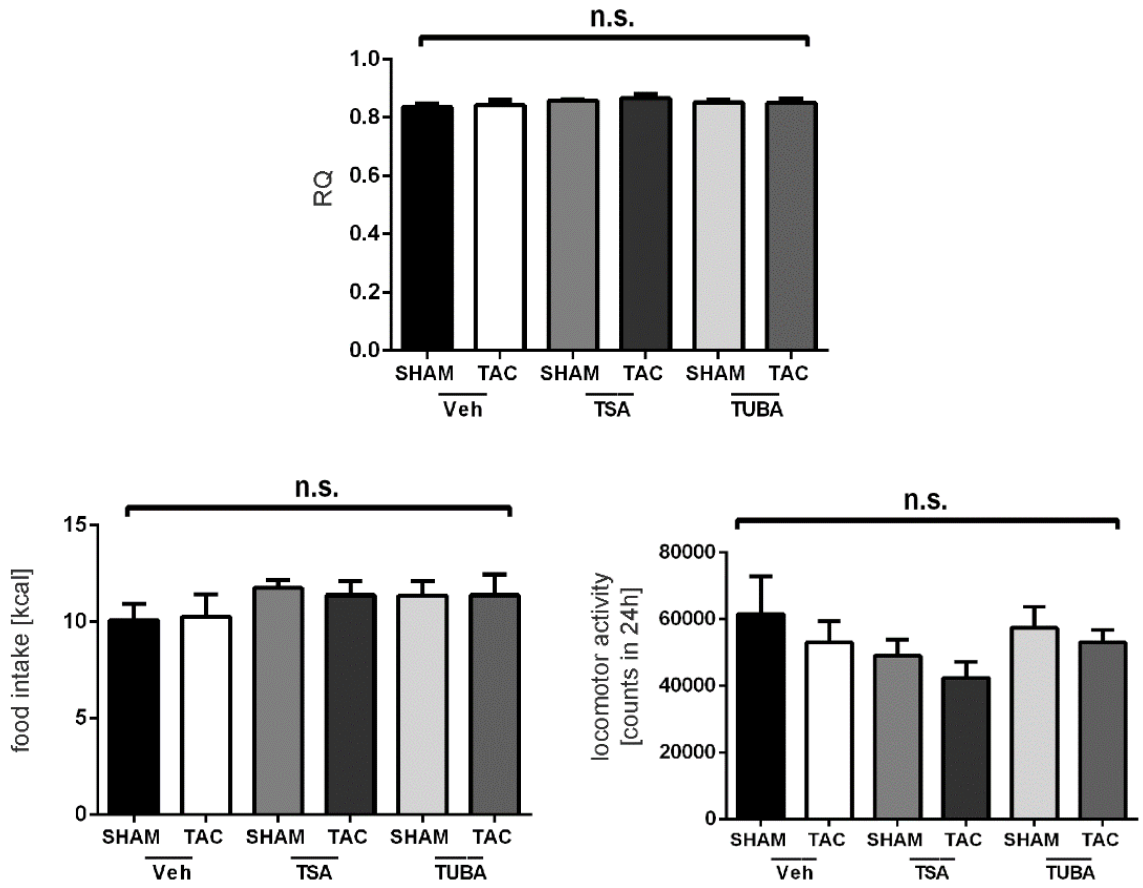

Figure 5-10: Respiratory quotient (RQ), locomotor activity and food intake analyzed in TSE-labmaster system six weeks after surgery. Veh: Vehicle, TSA: Trichostatin A, Tuba: Tubacin; 2-way ANOVA (Bonferroni posttest).

5.3.1 Metabolic key enzymes were not affected by the treatment of HDACi

Next, gene expression levels from key enzymes involved in cardiac lipid oxidation and cardiac glucose transport were investigated to analyse the effect of both HDACi on cardiac metabolism. Carnitine palmitoyltransferase 1 beta (CPT1beta), Acyl-CoA synthetase (ACSL) and Fatty acid (FA) transporter Cluster of Differentiation 36/fatty acid translocase (CD36) are enzymes mediating FA transport and β-oxidation, Glut1 and Glut4 are glucose transporters. Cardiac expression of all analysed enzymes/transporters was not significantly affected by the treatment and/or intervention. Only Glut1 transporter was significantly regulated in TAC-Tubacin-treated mice when compared to TAC-TSA-treated group (Figure 5-11, Figure 5-12).

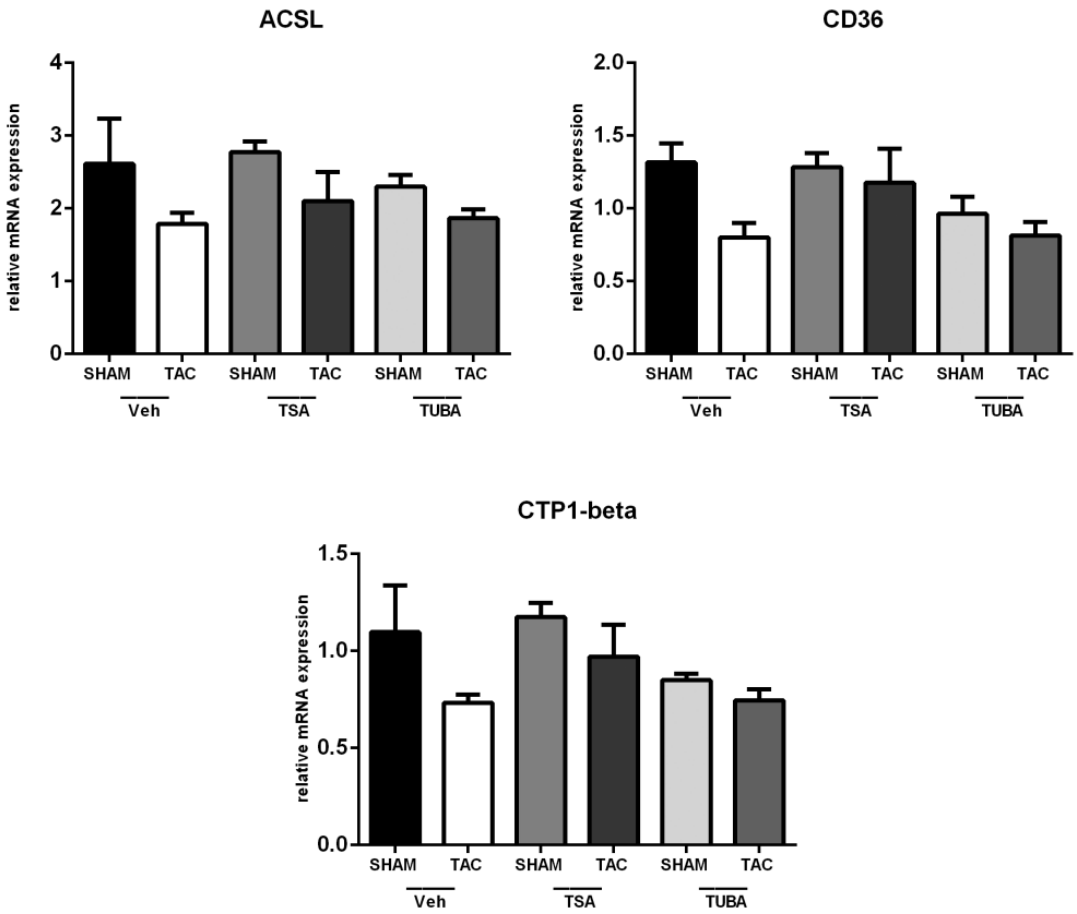

Figure 5-11: Cardiac gene expression levels of key enzymes involved in beta-oxidation; ACSL, Acyl-CoA synthetase-1; CPT1-beta, Carnitine palmitoyltransferase 1 beta; CD36, Cluster of Differentiation 36/fatty acid translocase, Veh: Vehicle, TSA: Trichostatin A, Tuba: Tubacin; 2-way ANOVA (Bonferroni posttest).

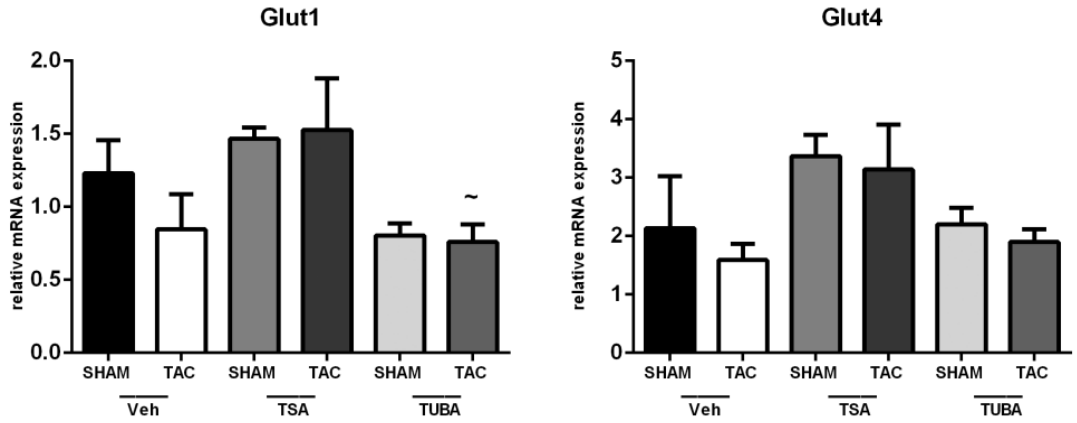

Figure 5-12: Cardiac gene expression levels of genes involved in glucose transport; Glut1 and Glut4; glucose transporter, Veh: Vehicle, TSA: Trichostatin A, Tuba: Tubacin; ~ $p<0.05$ vs. TAC TSA; 2-way ANOVA (Bonferroni posttest).

In summary key metabolic parameters are represented in Table 5-2.

Table 5-2: Metabolic characterization in TAC- and SHAM-operated mice six weeks after surgery and intervention. Represented are mean values ± SEM. WAT: white adipose tissue, TSA: Trichostatin A, Tuba: Tubacin.

	Vehicle SHAM	**Vehicle TAC**	**TSA SHAM**	**TSA TAC**	**Tuba SHAM**	**Tuba TAC**
Glucose [mg/dl]	164.80 ± 17.65	140.60 ± 9.00	163.75 ± 10.69	163.29 ± 7.99	170.00 ± 6.91	151.75 ± 9.05
BW [g]	24.48 ± 0.52	26.07 ± 0.71	25.41 ± 0.28	25.32 ± 0.42*****	26.67 ± 0.23	26.08 ± 0.71
Lean mass [NMR]	18.48 ± 0.61	19.84 ± 1.11	19.81 ± 0.20	19.73 ± 0.30	20.13 ± 0.30	20.45 ± 0.46
Fat mass [NMR]	2.10 ± 0.10	2.26 ± 0.15	1.74 ± 0.11	1.96 ± 0.14	2.36 ± 0.18	2.05 ± 0.12
WAT epididym [g]	0.28 ± 0.02	0.25 ± 0.03	0.25 ± 0.01	0.28 ± 0.02	0.32 ± 0.01	0.28 ± 0.01
WAT perirenal [g]	0.11 ± 0.01	0.10 ± 0.01	0.06 ± 0.01	0.06 ± 0.01	0.12 ± 0.01	0.10 ± 0.01

5.4 Autophagy as a possible molecular mechanism was not affected

Gene expression analyses of autophagy marker p62 and Bec-1 were done in cardiac tissue from the TAC experiment to investigate cardiac autophagy, thereby explaining a possible molecular mechanism for Tubacin action. HDAC6 seems to play an important role in the process of autophagy, a crucial intracellular protein degradation pathway (chapter 1.3.1).

Ubiquitin-binding protein p62 is an autophagosome cargo protein and Beclin-1 (Bec-1) regulates the process of autophagy. As presented in Figure 5-13, we observed no regulation of Bec-1 on mRNA and protein levels. Furthermore, p62 was not affected on mRNA level after six weeks of treatment with TSA and Tubacin.

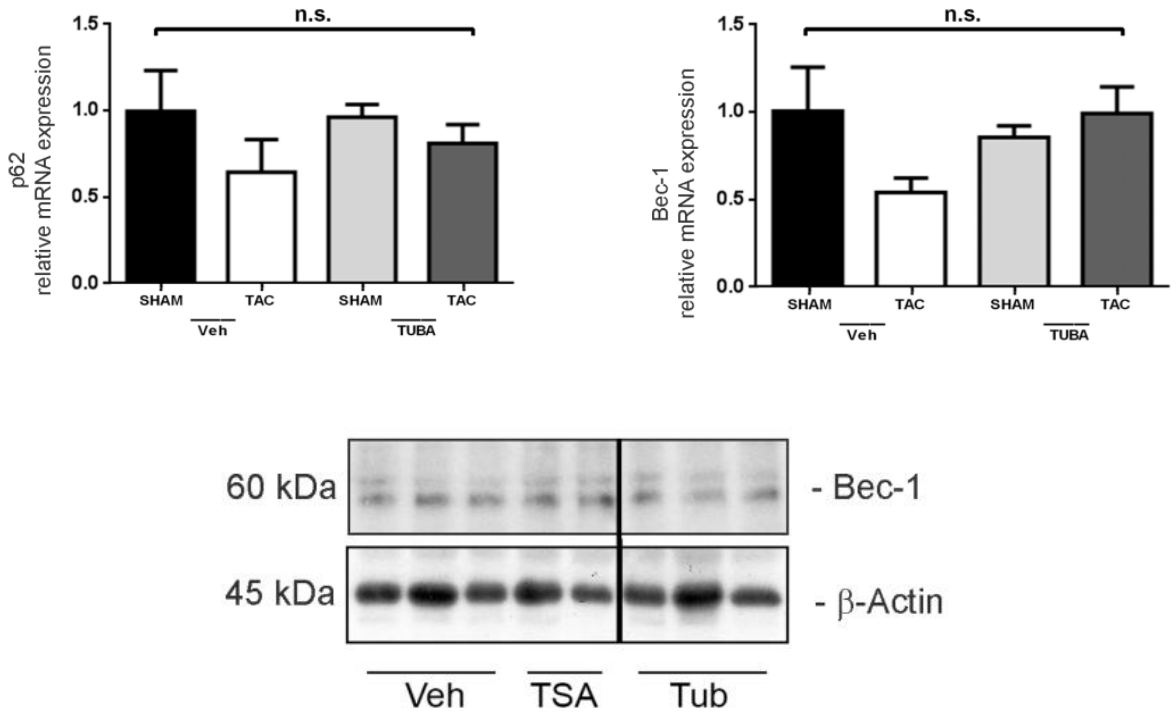

Figure 5-13: Cardiac gene expression of p62 (ubiquitin-binding protein) and beclin-1 (Bec-1), WB analysis of the expression levels of bec-1 and ß-actin in cardiac tissue samples isolated from SHAM and TAC operated Vehicle-treated mice.

5.5 HDAC6 inhibition in the Iso-induced cardiomyopathy model

Early changes during TAC intervention do not include cardiac fibrosis or cardiac inflammation. In order to study the effect of HDACi on these processes we used an additional model of Iso-induced cardiomyopathy known for extensive cardiac fibrosis and distinct cardiac inflammation. At the end of the experiment echocardiographic, histological, gene expression and protein analysis were performed.

5.5.1 Conventional echocardiography

Wall thickness analysis was performed using M-mode images from the echocardiography, similar to our TAC-study. Both LVPW and IVS values were significantly higher in Iso-Vehicle animals (Figure 5-14). IVS was attenuated in Iso-Tubacin-treated mice. LVM was strongly elevated in Iso-Vehicle mice, however these changes did not reach statistical significance.

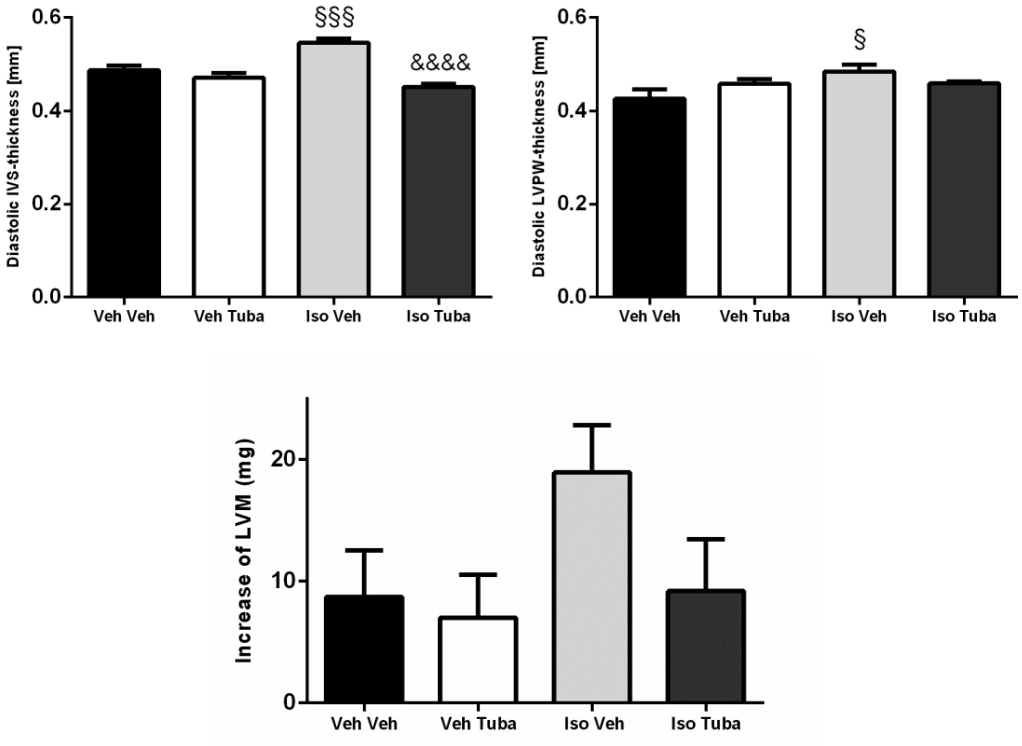

Figure 5-14: Echocardiographic analysis after 20 days of treatment with Tubacin (Tuba) or Vehicle (Veh) and treatment for four days with Isoproterenol (Iso) or Vehicle (Veh); IVS: left ventricular inter-septum, LVPW: left ventricular posterior wall, increase of left ventricular mass (LVM) from baseline to 20 days; values are means ± SEM. §§§~ $p<0.001$ vs. Vehicle Vehicle, §~ $p<0.05$ vs. Vehicle Vehicle, &&&&~ $p<0.0001$ vs. Isoproterenol Vehicle; 2-way ANOVA (Bonferroni posttest).

5.5.2 Speckle tracking echocardiography

Besides conventional echocardiography, speckle tracking echocardiography (STE)-based analysis was used to investigate longitudinal strain and longitudinal strain rate, (described in chapter 4.2.4.2). Alterations within myocardial deformation along the cardiac long axis during systole can be detected by assessment of global longitudinal peak strain (LS). Longitudinal strain was significantly reduced in the Iso-Vehicle group (Figure 5-15) compared to the Vehicle-Vehicle group. The Iso-Tubacin group showed also decreased longitudinal strain values, when compared to the Vehicle-Tubacin group. Regarding the longitudinal strain rate there were no significant changes in the differently treated groups.

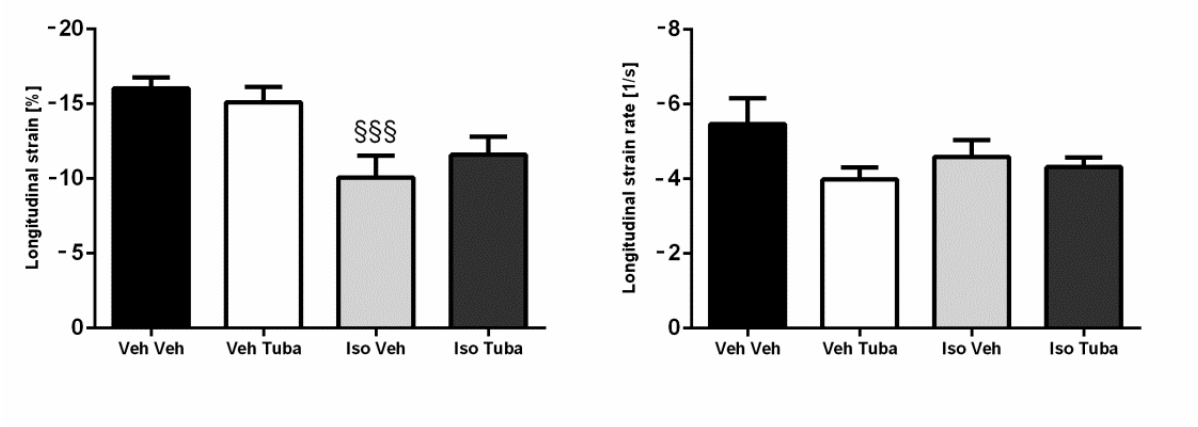

Figure 5-15: Global longitudinal strain (LS), longitudinal strain rate after Isoproterenol injection (Iso) for four days and 20 days of treatment with Vehicle (Veh) or Tubacin (Tuba); Values are means ± SEM. §§§~ $p<0.001$ vs. Vehicle Vehicle; 2-way ANOVA (Bonferroni posttest).

In summary, cardiac function parameters are represented in Table 5-3.

Table 5-3: Cardiac function parameters in Vehicle- and Isoproterenol (Iso)-treated mice 20 days after Vehicle or Tubacin treatment.

	Vehicle Vehicle	**Tubacin Vehicle**	**Vehicle Iso**	**Tubacin Iso**
IVSd [mm]	0.49 ± 0.16	0.48 ± 0.15	0.55 ± 0.18 §§§	0.45 ± 0.17 &&&&
LVPWd [mm]	0.43 ± 0.14	0.46± 0.15	0.49± 0.16 §	0.46 ± 0.17
LVM [mg]-increase	8.72 ± 3.82	7.01 ± 2.95	18.95 ± 3.67	9.19 ± 4.27
LS [%]	-17.31 ± 0.89	-16.39 ± 1.01	-12.14 ± 1.14§§§	-14.61 ± 2.09
EF [%]	50.6 ± 1.4	47.8 ± 2.4	46.6 ± 1.9	46.7 ± 3.3
FS[%]	24.3 ± 1.0	22.5 ± 1.3	23.1 ± 1.5	22.5 ± 2.1
HR [bpm]	407.5 ± 8.5	386.8 ± 8.0	396.7 ± 18.0	414.8 ± 11.2
ESV [µl]	16.60 ± 1.31	19.72 ± 2.32	20.30 ± 1.24	22.56 ± 2.09

Values are means ± SEM. §§§ $p<0.001$ vs. Vehicle-Vehicle, § $p<0.05$ vs. Vehicle-Vehicle, &&&& $p<0.0001$ vs. Iso-Vehicle. IVSd: left ventricular inter-septum during diastole, LVPWd: left ventricular posterior wall during diastole, LVM: left ventricular mass (increase of LVM: from baseline to week 6), LS: global longitudinal peak strain, EF: ejection fraction, FS: fractional shortening, HR: heart rate, ESV: end systolic volume.

5.5.3 Histological analysis showed no differences in the development of cardiac fibrosis in both Iso-treated groups

Histological analysis was performed to study the Iso-associated pro-fibrotic and pro-inflammatory processes in the heart. This was done in collaboration with Prof. Klopfleisch. Quantitative analysis of the fibrosis in percentage is shown (Figure 5-16, upper panel). The collagen content was significantly increased in Iso-Vehicle and in Iso-Tubacin treated animals when compared to the Vehicle-treated groups. There was no difference between the Iso-Vehicle and Iso-Tubacin group (Figure 5-16). In the picrosirius red-stained heart cross-sections the fibrosis content is visibly increased in the Iso-treated groups.

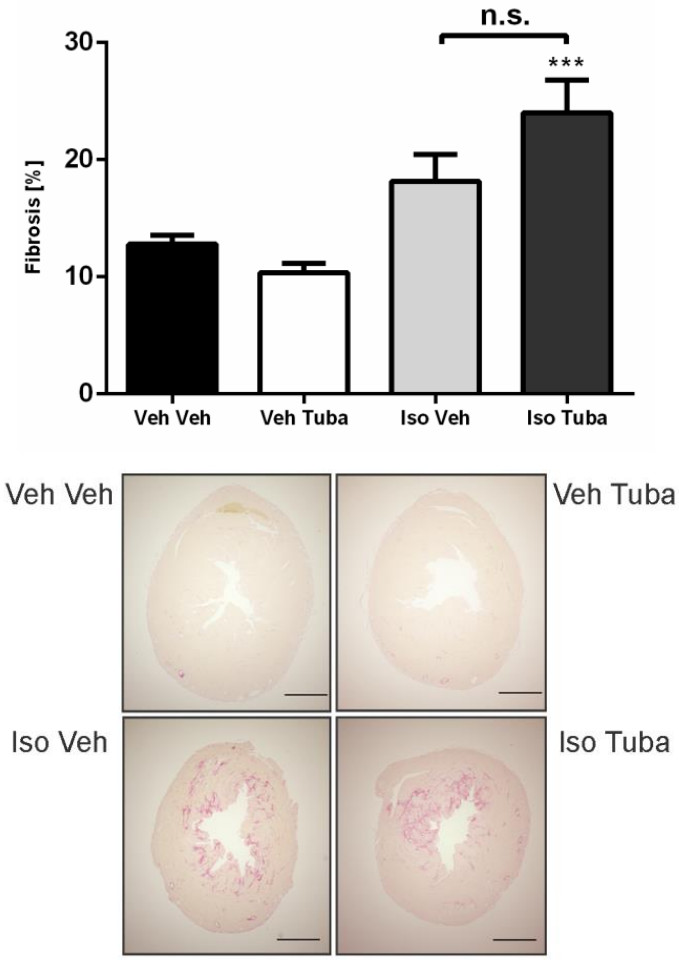

Figure 5-16: Analysis of cardiac fibrosis calculated based on microscopic sections of heart tissues stained with Picrosirius red, shown in percentage and representative images of picrosirius red-stained heart cross-sections; Veh, Vehicle; Tuba, Tubacin; Iso, Isoproterenol; values are means ± SEM. §§ $p<0.01$ vs. Vehicle-Vehicle, *** $p<0.001$ vs. Vehicle-Tubacin, Iso-Vehicle and Iso-Tubacin-treated group were n.s. (not significant); 2-way ANOVA (Bonferroni posttest).

5.5.4 Gene expression levels of pathological markers were not affected by the treatment with Tubacin after Iso-injection

Similar to the histological and echocardiographic results presented above, both Iso-treated groups of animals showed no significant differences in gene expression levels of ANF and BNP (Figure 5-17).

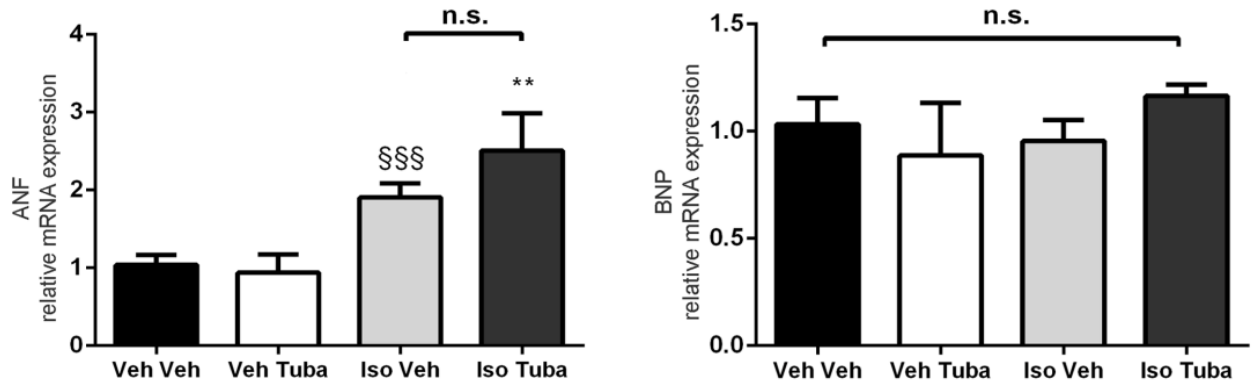

Figure 5-17: Gene expression levels of pathological markers ANF and BNP (ANF: Atrial Natriuretic Factor, BNP: Brain Natriuretic Peptide) after Iso-injection for four days and 20 days of treatment with Vehicle (Veh) or Tubacin (Tuba); Values are means ± SEM. ** $p<0.01$ vs. Vehicle-Tubacin; Iso-Vehicle and Iso-Tubacin-treated group were n.s. (not significant); 2-way ANOVA (Bonferroni posttest).

5.5.5 Gene expression levels of fibrosis and inflammation markers were not regulated by the treatment of Tubacin in the Iso groups

Collagen1 (Col1) and Collagen3 (Col3) are proteins involved in the pro-fibrotic processes in the myocardium. Cardiac gene expression levels of Col1 and Col3 were significantly upregulated in Iso-Tubacin-treated groups. There were no significant differences in Iso-Vehicle and Iso-Tubacin mice regarding gene expression levels of Col1 and Col3. Cluster of Differentiation 68 (CD68) is a marker for inflammation. Cardiac gene expression levels of CD68 were significantly increased in both Iso-treated animals. Nevertheless we observed no significant differences between Iso-Vehicle and Iso-Tubacin–treated animals. Taken together, these results indicate that Tubacin shows no anti-inflammatory and anti-fibrotic properties in our model.

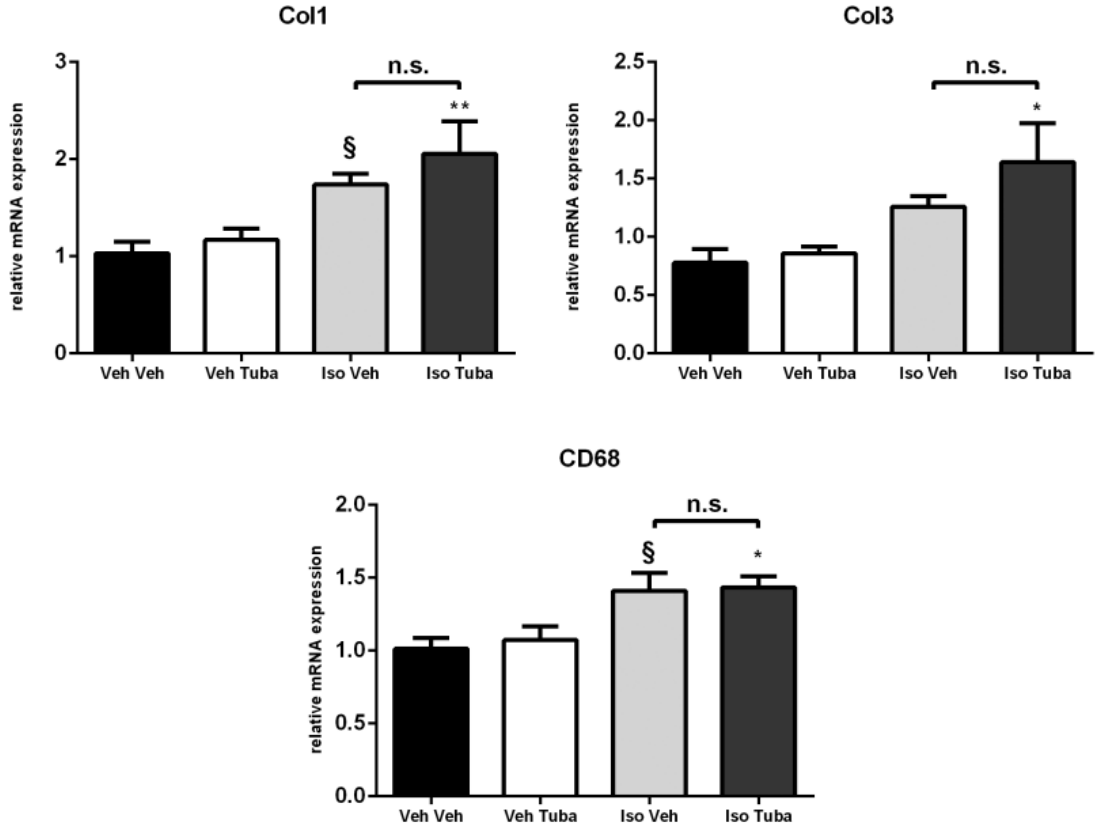

Figure 5-18: Gene expression levels of fibrosis and inflammation markers; Col1, Collagen1; Col3, Collagen3; CD68, Cluster of Differentiation 68; Veh, Vehicle; Tuba, Tubacin; Iso, Isoproterenol.Values are means ± SEM. * p<0.05 vs. Vehicle-Tubacin, ** p<0.01 vs. Vehicle-Tubacin, § p<0.05 vs. Vehicle-Vehicle; Iso-Vehicle and Iso-Tubacin-treated group were n.s. (not significant); 2-way ANOVA (Bonferroni posttest).

5.5.6 Intraperitoneal injection of Tubacin leads to altered acetylation status of α-tubulin

Cardiac HDAC6 expression was not regulated by Tubacin application in the Iso experiment, similar to the HDAC6 regulation in the TAC model (Figure 5-7). HDAC6 activity was defined by the acetylation status of α-tubulin in cardiac tissue. A slight decrease in the acetylation rate of α-tubulin was observed in Iso-treated mice (Figure 5-19). Tubacin-treated mice showed an increased acetylation status of α-tubulin which indicates less HDAC6 activity in the heart. This means that Tubacin reached the cardiac tissue by systemic application.

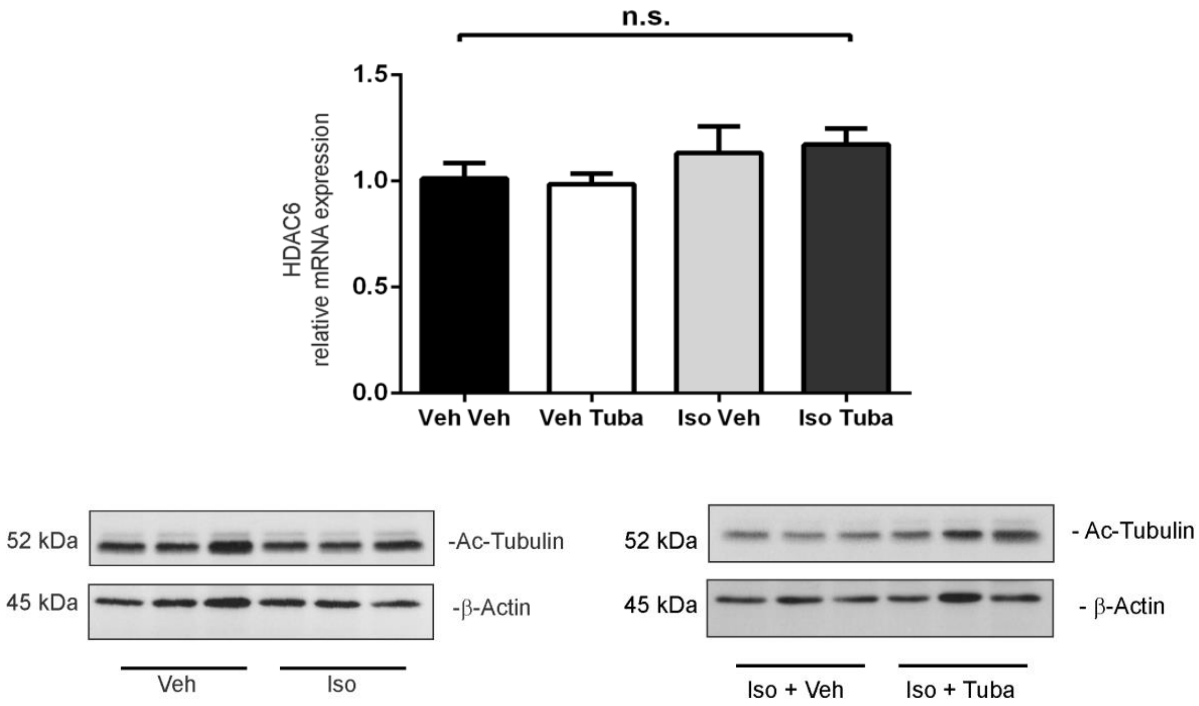

Figure 5-19: Cardiac gene expression levels of HDAC6. WB analysis of acetylated tubulin and ß-actin in cardiac tissue samples isolated from Vehicle-Vehicle and Iso-Vehicle treated mice or Iso-Vehicle and Iso-Tubacin treated mice.

6 Discussion

In this pre-clinical study, the functional importance of the specific HDAC6i Tubacin was investigated on cardiac function *in vivo* and *in vitro*.

Experiments were performed in HL-1 cells and showed anti-hypertrophic effects of both Tubacin and a general HDACi TSA. Furthermore, in a pressure overload-induced mouse model of cardiac hypertrophy, Tubacin prevented the cardiac TAC-induced hypertrophic response. Metabolic phenotyping showed no major differences among different treatment group.

In the Iso-induced cardiac fibrosis model, treatment with Tubacin does not improve cardiac function meaning Tubacin does not interfere with other pathological remodeling processes in the heart, such as fibrosis.

In summary, Tubacin might be a promising therapeutic agent for the treatment of pathological cardiac hypertrophy. However, the exact molecular mechanism remains unclear. However, the positive influence of Tubacin on the development of pathological cardiac hypertrophy coincides with its ability to regulate the cardiac tubulin-acetylation status.

6.1 HL-1 cells as a model for cardiomyoctes

In this study, we performed *in vitro* experiments with HL-1 cells analyzing the influence of the HDACi Tubacin and TSA on the hypertrophic response to ET-1.

So far, HL-1 cells originally deriving from atrial myocytes are the only available long-term cultured cardiomyocytes which contract spontaneously and proliferate. HL-1 cells are a stable cell line, not prone to external influences and show characteristics of differentiated cardiomyocytes (Bloch et al., 2016; Claycomb et al., 1998). Passaging HL-1 cells is possible but in high passages they start to change their morphology and also their molecular signaling pattern (Claycomb et al., 1998). Therefore, when cells started to change their morphology, we unfroze cells in lower passages and used them for further experiments.

In this study, the key markers for pathological cardiac hypertrophy such as ANF and ß-MHCH were investigated on mRNA expression levels in HL-1 cells. Cells treated with HDACi TSA + ET-1 or Tubacin + ET-1 showed significantly diminished gene expression levels of ANF and ß-MHCH compared to ET-1 treated cells (Figure 5-2). ET-1 is a potent vasoconstrictor and is known to induce cardiac hypertrophy (Foryst-Ludwig et al., 2015b; Nakagawa et al., 2006). ET-1 binds on G-protein receptors and blood pressure raises due to an increase peripheral resistance in the vessels.

In our study, the cell area of the HL-1 cells increased after ET-1 treatment (Figure 5-3). Previously, in a similar set of experiments we investigated the development of physiological cardiac hypertrophy also in HL-1 cells (Foryst-Ludwig et al., 2015a). In that study we identified some of the fatty acids species (FA mixture containing C14:0, C16:0, and C16:1n7) as pro-hypertrophic stimuli (Foryst-Ludwig et al., 2015a). Treatment of HL-1 cells with FAs leads to the activation of AKT-kinase and induced physiological hypertrophic response in those cells.

Considering that every cell culture system has limitations there are other possible *in vitro* models to investigate cardiac hypertrophy next to HL-1 cardiomyocytes. The limitations of HL-1 cells are that they are a very costly cell line and they originally derived from an AT-1 atrial cardiomyocyte tumor lineage originating from C57BL/6J mouse. Likewise, primary isolated embryonic and neonatal cardiomyocytes from rats or mice have similar molecular signaling pathways compared to physiological *in vivo* conditions. However, utilization of embryonic primary cardiomyocytes (PCM) is linked

to some difficulties. Primary cardiomyocytes display embryonic characteristic and are not reacting *in vitro* as adult cardiomyocytes (White et al., 2004). Main limitations of both models, the adult and embryonic PCMs, are that they are not able to proliferate. PCMs can be used for short time experiments. The adult mouse PCMs show typical adult cardiomyocyte function and structure and represent the closest model used for investigations of contractile mechanics, protein expression, electrophysiology and cellular functions (Li et al., 2014; Louch et al., 2011).

Over recent years, other possible *in vitro* models were established to investigate the morphology and function of cardiomyocytes. Studies with pluripotent stem cells (PSCs) such as murine embryonic stem cells (ESCs) and induced pluripotent stem cells (iPSCs) were performed to explore cardiac biology and are thinkable models for this present study (Masumoto et al., 2014; Rana et al., 2012). Another promising model is the utilization of human cardiomyocytes (HCM). They were previous used in our group from Jana Grune to investigate cardiac properties. However, since HCM are very expensive, and can be keeping in culture for short period of time, long-term experiments are difficult to perform because of their ability to dedifferentiate (Force and Kolaja, 2011). Furthermore, since HCM are isolated from different donor hearts there are also differ, depending on the donor (health, age and sex).

Taken together, presently no cardiomyocyte cell lines are available for studies which are derived from the ventricles (Li et al., 2014). In this study, further experiments in primary cardiomyocytes would be advantageous to repeat the HL-1 experiments and to confirm the results (Figure 5 2). Additionally, possible other *in vitro* experiments should be done regarding calcium signaling, contractility and mitochondria function to analyse the effect of the HDACi.

6.2 The model of Transverse Aortic Constriction (TAC) led to pathological cardiac hypertrophy

In the present study myocardial hypertrophy was induced by the established pressure-overload TAC model in male mice (deAlmeida et al., 2010; Rockman et al., 1991). Previously, it was shown that there are sex differences in the development of pathological cardiac hypertrophy (Fliegner et al., 2010; Kararigas et al., 2014; Skavdahl et al., 2005). In male mice the development of cardiac hypertrophy was significantly more pronounced, when compared with female littermates (Fliegner et al., 2010). Therefore, only male mice were included in this pre-clinical study.

First, the TAC model was established by Rockman and colleagues to mimic cardiac diseases induced by e.g. aortic stenosis or hypertension (Rockman et al., 1991). TAC is an approved reproducible model where the development of cardiac hypertrophy is steadily induced by a permanent increment of workload, which can lead to heart failure depending on experimental time period and tightness of banding the aorta. Heart failure is characterized by a dilatation of the LV and cardiac diastolic and systolic dysfunction (Lips et al., 2003).

After 6 weeks of surgery, cardiac hypertrophy was developed, which was confirmed by echocardiographic analysis, with regards to the parameters such as LVM, EF and FS. In our study EF and FS were not affected by TAC 6 weeks post intervention in the differently treated and operated groups. Also the chamber lumen of the LV was not influenced. In addition, a dilatation of the LV did not occur. Taken together, the significant thickening of both walls, anterior and posterior, and thereby increment of LVM in TAC-operated mice with no changes in chamber volume is characteristic for a pronounced concentric LV hypertrophy. It is well documented that pressure overload leads to concentric hypertrophy which is characterized by increased wall thickening and total cardiac mass, with no differences in the chamber volume and preserved systolic function (Bernardo et al., 2010).

Because of an intra-operative variability of banding the aorta in the mice, differences in the development of hypertrophy could occur (Lygate et al., 2006). To minimize these inter-individual alterations in our study only one operator performed the surgery. Gradient P can be determined as a tool to determine those alternations. In our study Gradient P showed in comparable values the three TAC-operated groups,

which indicate standardized TAC conditions in all groups. Furthermore, this parameter allowed the identification of other differences in the surgery process, e.g. dissolving the note. Taken together, all difficulties and variations in this model lead to a moderate standard deviation of the results and lead to variable development of cardiac hypertrophy.

One characteristic of pathological cardiac remodeling is the development of fibrosis and an inflammation response (see chapter 1.5.2) (Bernardo et al., 2010; Burchfield et al., 2013). In the TAC model, no noteworthy fibrosis and inflammation occurred six weeks after surgery, based on histological analysis and qRT-PCR results. Some studies published recently showed the development of cardiac fibrosis and inflammation few weeks after TAC- intervention in mice (Fliegner et al., 2010; Kuang et al., 2013; Westphal et al., 2012). One explanation for the lack of fibrosis development after TAC is the differences in the constriction of the aorta. In a study by Skavdahl, they used a 27-gauge needle for TAC surgery. We used a 26-gauge needle, similar to the study from Fliegner et al. (Fliegner et al., 2010; Skavdahl et al., 2005). It is possible that using a 27-gauge needle in the study could induce a more severe form of hypertrophy and therefore in later phases initiation of fibrosis and inflammation. Like previously mentioned also the mouse strain has an influence on the extent of cardiac remodeling.

Another option to investigate cardiac remodeling in this model would be an extended observation period post-TAC. The transition from cardiac hypertrophy to heart failure is linked with more matured remodeling processes. In the TAC study the mice had increased load caused by the TAC-intervention itself, echocardiography and the metabolic analyses at the end of the study. Additionally, the animals received the substances intraperitoneal every day. To avoid more stress for the mice we used a further model to investigate the effect of the specific HDAC6i Tubacin on other cardiac remodeling processes such as fibrosis.

There are various other possible models which induce pathological hypertrophy *in vivo* such as chronic infusion of Ang II or treatment with Iso (Choi et al., 2015; Demos-Davies et al., 2014; Kao et al., 2013; Kee et al., 2006).

Ang II is a peptide hormone, which increases blood pressure by direct vasoconstriction and releasement of aldosterone. Typically, chronic infusion by Ang II is performed by osmotic minipumps inserted in the animals, releasing permanent Ang

II into the organism (Demos-Davies et al., 2014). Chronic infusion with Ang II by the osmotic minipumps just allows to investigate the effects of the RAS activation. By using the TAC model, further pathways are activated and therefore can be examine. Our aim in this study was to analyze different pathways and the impact of HDACi on these pathways. Hence, we selected the TAC model for our investigations.
In summary, the pressure overload-induced TAC model is a well-established method to generate cardiac hypertrophy in mice. To investigate additional cardiac remodeling processes other models such as the Iso model are possible methods to analyze fibrosis and inflammation.

6.2.1 Treatment with HDACi Tubacin and TSA reduced cardiac hypertrophic response in the TAC model

In the field of oncology, the use of HDACi is widespread. HDACi are blocking proliferation and development of tumors (Berry et al., 2008). In various preclinical *in vivo* studies it was shown that a broad-spectrum HDACi such as TSA showed anti-hypertrophic effects and diminished pathological cardiac hypertrophy (Berry et al., 2008; Cao et al., 2011; Kao et al., 2013; Kee et al., 2006; Kong et al., 2006; Kook et al., 2003; Ooi et al., 2015).
This is the first study that analyzes the effect of the specific HDAC6i Tubacin in a pressure-overload induced cardiac hypertrophy in mice. Echocardiographic parameters and gene expression levels of pathological markers showed that both HDACi, TSA and Tubacin, reduced the development of pathological cardiac hypertrophy in TAC-operated mice.
The anti-hypertrophic effect of TSA on cardiac hypertrophy was more pronounced compared to Tubacin´s action likely because of the simultaneous inhibition of various HDACs (HDACs 1, 3, 4, 6 and 10). TSA inhibits HDACs class I and II selectively. Cao and colleagues showed that the HDAC activity is involved in the hypertrophic process of the heart. The general HDACi TSA was demonstrated to reduce or even reverse to some extend the development of cardiac pathological hypertrophy in a TAC model (Cao et al., 2011). Kee and colleagues induced cardiac hypertrophy by Ang II or aortic banding in mice and rats. Both general HDACi Trichostatin A and valproic acid decreased cardiac hypertrophy, the expression of pathological markers, α-tubulin-

acetylation and the development of interstitial fibrosis (Kee et al., 2006). Also another TAC study showed the effectivity of TSA regarding cardiac hypertrophy. TSA prevented the development of cardiac hypertrophy (Ooi et al., 2015).

In our study, TSA was used as a positive control and the potency of TSA was compared with the specific HDAC6i Tubacin.

There are just a few studies which investigated the role of specific HDAC6i on cardiac function, especially cardiac hypertrophy. One of the well investigated HDAC6i is Tubastatin A. Demos-Davies and colleagues induced cardiac remodeling by chronic Ang II-infusion pumps or TAC-intervention. Conveniently to our study, they showed that usage of a specific HDAC6i such as Tubastatin A enhanced cardiac function and reduced cardiac hypertrophy compared to control animals. Furthermore, they showed that HDAC6 null mice had improved cardiac function after TAC-intervention meaning that deletion of HDAC6 has similar cardioprotective effects such as treatment with specific HDAC6i (Demos-Davies et al., 2014). After Ang II infusion HDAC6-deficient mice had improved EF and FS compared to control animals. In contrast, in our study in both *in vivo* experiments EF and FS were not affected by TAC-intervention or Iso-treatment suggesting that in our model we mainly investigated the development of cardiac hypertrophy and not heart failure. Our study and the study from Demos-Davies and colleagues also differ regarding the used mouse strain. In our model we used C57Bl/6 mice and in the study from Demos-Davies and colleagues they used SV/129 mice for the TAC-intervention. The different study set-ups from both studies regarding mouse strain and the different investigated endpoint, may explain the discrepant results between our study and previously published data.

At the moment, more investigations are carried out with newly developed HDACi as potential agents to treat cardiac dysregulation (Lkhagva et al., 2015). For example, MPT0E014 is a very new, potent and general HDACi. Treatment with MPT0E014 reduced heart failure in a model of Iso-induced dilated cardiomyopathy (Kao et al., 2013). Kao and colleagues showed that usage of MPT0E014 reduced the development of cardiac hypertrophy. In this heart failure study they showed that the HDACi enhanced the EF combined with lower chamber sizes in the Iso-treated rats. Besides pathological cardiac hypertrophy, MPT0E014 improved cardiac contractility

and reduced the whole process of remodeling including the development of cardiac fibrosis (Kao et al., 2013).
Taken together, HDACi seem to be a potential substance in the treatment of cardiac hypertrophy.

6.3 TSA and Tubacin have no systemic influence on the metabolic phenotype in the pressure overload model

In an experiment from Shimizu and colleagues, a mechanistic link between the development of cardiac hypertrophy induced by TAC-intervention and inflammation from adipose tissue was observed (Shimizu et al., 2012). In that study, TAC induced predominant systematic metabolic dysfunction including glucose intolerance (Shimizu et al., 2012). Moreover, it was found out that in pathological cardiac hypertrophy a metabolic switch occurred where the utilization of glucose increased and fatty acid oxidation decreased (Sack et al., 1996). Therefore, in our study metabolic phenotyping of TAC-operated mice was performed to investigate the metabolic effect of Tubacin and TSA applied systemically. In a previous study in our laboratory, Winkler and colleagues showed that Tubacin interacts with glucose and fatty acid metabolism. In summary, they showed that HDAC6 is an essential regulator of hepatic glucocorticoid-stimulated gluconeogenesis (Winkler et al., 2012).
However, in our study we observed no TAC-induced disturbance of systemic glucose tolerance. Furthermore, metabolic analysis performed in metabolic cages regarding the respiratory quotient, food intake and locomotor activity showed no differences in the differently treated groups. A possible reason is the used *in vivo* model because also in the untreated TAC groups we could not confirm the metabolic disturbances described by Shimizu. Thus, we were not able to detect any metabolic actions of HDACi in our model. No differences in body weight development were observed in all tested groups. Our results indicate that both Tubacin and TSA were well tolerated and seemed to be not harmful in the applied concentrations. Gene expression levels from key enzymes, which are involved in cardiac lipid oxidation, such as Carnitine palmitoyltransferase 1 beta (CPT1beta), Acyl-CoA synthetase (ACSL), and Fatty acid (FA) transporter Cluster of Differentiation 36/fatty acid translocase (CD36) and cardiac glucose transport, Glut1 and Glut4, confirmed the previous assumption, that

TSA and Tubacin have no systemic influence on the cardiac metabolic phenotype. But these genes were not regulated by the TAC-intervention or treatment with the HDACi.

In summary, the metabolic phenotyping of the variously treated and operated mice showed no differences in systemic and cardiac metabolism. Like previously mentioned, a possible explanation for the absence of alterations in the different treated groups is the TAC model which we were used. The TAC-intervention showed no metabolic disturbance in the animals.

6.4 The model of Isoproterenol-induced cardiomyopathy led to the development of cardiac fibrosis and cardiac inflammation

In the second *in vivo* part of this study the Iso-induced cardiomyopathy model was used to investigate the impact of HDAC6-inhibiton on cardiac fibrosis and inflammation in mice. Nowadays, this model is an established model to induce fibrosis in the heart of rats and mice (Brooks and Conrad, 2009; Kao et al., 2013; Tao et al., 2016). Iso is a synthetic and potent agonist for the beta-receptors and therefore leads to positive inotropic and chronotropic effects in the heart. Chronic application induces multiple adverse cardiac effects such as hypertrophy and fibrosis. The main focus of this part of the study was the development of the cardiac fibrosis which was significantly increased in both Iso treated groups, as shown using echocardiographic-, histological- and gene expression analysis. Taken together, all results showed the induction of fibrosis and inflammation by Iso treatment (upregulated gene expression levels of collagen1, 3, CD68 and a semi quantitative histological analysis). We observed in the Iso model a mild development of LV hypertrophy but it was not as prominent as in the TAC model, probably due to the shorter time period of the experiment.

In the present study we applied Iso s.c. for 4 consecutive days in the concentration of 25mg/kg BW. The application period and dosage used in our study was adapted from the publication of Samuel and colleagues (Samuel et al., 2014). In order to reduce mortality we have restricted the Iso-application to 4 days, instead of published application over 5 days. Daily repeated infusions by Iso are necessary to increase the induction of fibrosis and inflammation over the time.

A study from George and colleagues compared the effects of Iso via serial s.c. and i.p. injections for 5 days in rats (George et al., 2010). In that study, myocardial injury was induced by both application types with no significant differences regarding morphological changes.

We decided to take the same dosage like Samuel and colleagues due to the fact that we used the same mouse strain (129 SV male mice) (Samuel et al., 2014).

However, in the literature is different information about the dosage and application time of Iso depending on the stage of pathological cardiac remodeling and the mouse strain. For example, in the study from Vergaro and colleagues, Iso was just applied for two days with a concentration of 300mg/kg to induce LV systolic dysfunction in mice (Vergaro et al., 2016). They were interested in the interaction between the protein Galectin-3 and aldosterone in HF. In another study from An and colleagues a single injection of 5mg/kg BW Iso was induced to investigate cardiac function (An et al., 2016). They compared the sensitivity of STE and the conventional echocardiography regarding the effect of the single Iso application after 3 days and 7 days in C75Bl/6 mice. STE was more sensitive than conventional echocardiography and detected changes in the cardiac function after 3 days of Iso application. Also Bauer and colleagues defined the STE as a rapid and sensitive method to investigate global and regional deformations in a myocardial infarction mouse model (Bauer et al., 2011). Regarding the results from our study, in the Iso-treated groups the global longitudinal strain was restricted after 15 days of the last Iso injection.

In comparison to the TAC model, the advantage of the used Iso-application model is that it is a noninvasive and rapid method, with lower mortality and morbidity. Also cardiac remodeling occurs much earlier than in the TAC model. In addition, different pathological mechanism can be investigated such as cardiac fibrosis vs. cardiac hypertrophy.

Altogether, the Iso model is an inexpensive and simple method to induce cardiac remodeling with enhanced fibrosis content and moderate hypertrophy in the heart. When focusing on cardiac hypertrophy, the TAC model seems to be the more efficient method to use.

6.4.1 Tubacin has no anti-fibrotic or anti-inflammatory actions in the Iso-induced cardiomyopathy model

In the present study, the specific HDAC6i Tubacin had no anti-fibrotic effects in the model of Iso-induced cardiac dysfunction. Using echocardiographic- and histological- and gene expression- analysis of fibrosis and inflammation markers, we saw no differences between both Iso treated groups (the Iso-Vehicle and the Iso-Tubacin). The longitudinal strain (GLS) and strain rate (SR) parameters showed discrete changes in systolic left ventricular function affecting the longitudinal contraction. In Iso-Tubacin and Iso-Vehicle animals, longitudinal strain and strain rate were also reduced and not affected by the treatment which may have resulted from the short application period of the HDACi. Tubacin had no beneficial effects on the development of fibrosis.

Other studies observed anti-fibrotic effects of specific HDAC6i in the heart (Kao et al., 2013; Tao et al., 2016). A study from Tao and colleagues investigated the role of HDAC6 in the development of cardiac fibrosis. They used Tubacin to regulate the order of cardiac fibroblasts *in vitro.* HDAC6 expression was increased in cardiac fibrosis tissue (Tao et al., 2016). They found out that HDAC6 prevented the expression of RAS-association domain family protein 1A (RASSF1A). Cardiac fibroblast activation might be influenced by RASSF1A which affects the ERK1/2 signal pathway (Tao et al., 2016). Moreover, another study showed anti-fibrotic effects of the specific HDAC6i MPT0E014 in failing hearts in rats (Kao et al., 2013). The authors had a possible explanation for the anti-fibrotic effect of MPT0E014 due to the downregulated expression of Ang II and TGF-ß.

Kang and colleagues found out that valproic acid, a general HDACi, reduced cardiac fibrosis and cardiac hypertrophy in spontaneously hypertensive rats. They showed that this improvement is linked to the acetylation of the mineralocorticoid receptor (Kang et al., 2015). One study showed comparable results to ours with regards to fibrosis. In that study, the fibrosis content was reduced neither in mice treated with Tubastatin A nor in HDAC6-KO mice. Demos-Davies and colleagues performed TAC-surgery and investigate the collagen fraction 4 weeks after intervention. Interstitial fibrosis was not decreased in HDAC6-KO mice and not in mice treated with Tubastatin A (Demos-Davies et al., 2014).

In summary, the published results are controversial. Some studies showed anti-fibrotic effects of HDACi, others found no significant change in the development of cardiac fibrosis. The discussed studies differ also in the experimental set-ups. In the described studies, where fibrosis was attenuated by HDACi, rats were used for the experiments or just *in vitro* experiments were performed (Kao et al., 2013; Tao et al., 2016). However, in our study mice were used. Thus, the discrepancies may result from different species sensitivities to cardiac HDACi

In their work, they showed anti-fibrotic effects of serelaxin, an artificial peptide hormone comparatively to relaxin, in the heart (Samuel et al., 2014).

Another possibility to investigate the role of HDAC6 in cardiac disease models is the use of HDAC6-KO mice. Zhang et al. showed that HDAC6 KO mice developed normally, with only slight alterations in immune response and in bone mineral density and had increased acetylation status of tubulin in most organs (Zhang et al., 2008). As discussed above, the studies from Demos-Davies and colleagues and Zhang and colleagues are the only published works which used the HDAC6-KO model to characterize cardiac function (Demos-Davies et al., 2014; Zhang et al., 2003).

6.5 Possible mechanisms of anti-hypertrophic HDACi action in the heart

It is known that HDACi alter the acetylation status of histones and non-histone proteins (McKinsey, 2012a). In both *in vivo* parts of this study, the acetylation status of α-tubulin was investigated. In our study, inhibition of HDAC6 by Tubacin eliminated deacetylation of α-tubulin. Tubacin inhibited α-tubulin deacetylation in the TAC-operated mice and in the Iso-treated mice (Figure 5-7, Figure 5-19). The α-tubulin acetylation status is regulated by the intervention (TAC surgery or Iso-treatment). A study from Zhang and colleagues showed comparable results (Zhang et al., 2014). They induced atrial fibrillation by atrial tachypacing in a canine model. Tachypacing induces deacetylation, depolimeryzation and degradation of α-tubulin. Tubastatin A, a HDAC6i, protected against cardiac remodeling in this tachypacing model by acetylation (Zhang et al., 2014). We conclude that TAC-intervention leads to deacetylation of α-tubulin and is associated with enhanced cardiac hypertrophy. Increased acetylation of α-tubulin can be the reason for the anti-hypertrophic effects of Tubacin in our *in vivo* and *in vitro* experiments.

Generally, HDAC6 deacetylates α-tubulin, a crucial component of the microtubule organizing center (MTOC) of the microtubules in the cytoskeleton. Microtubules take part in the processes of cell proliferation and cell division. Furthermore, microtubules are involved in intracellular transport and cell plasticity (Sadoul and Khochbin, 2016). Deacetylation of microtubule is linked with an enhanced destabilization of the cell by α-tubulin. Cytoskeletal alterations are linked with cardiac dysfunction. Hence, HDAC6 is an important enzyme which is involved in the development of the habitus of the cell and its inhibition may be protective.

Furthermore, we investigated cardiac autophagy in the TAC model. Autophagy activity is always present at basal levels in the cell. It guarantees the cellular homeostasis but it is unclear which amount of autophagy is beneficial or harmful. Autophagy levels increases as a reaction of stress such as starvation or cardiovascular diseases, linked with chronic ischaemia, pressure overload as in the TAC model or in heart failure (Li et al., 2016). Increment of autophagy can also be beneficial for the cells. During autophagy the energy production is elevated and preserved. But high amounts of autophagy can also lead to cell death due to self-digestion (De Meyer and Martinet, 2009).

A study from McLendon and colleagues showed that the HDAC6i SAHA increased autophagy in CryAB R129G transgenic mice which was associated with increased tubulin acetylation (McLendon et al., 2014). This was in contrary to the results from the study from Cao and colleagues, where they showed that the anti-hypertrophic effect of HDACi is associated with the inhibition of autophagy after 1 week of TAC surgery (Cao et al., 2011). Additionally, another study investigated cardiac autophagy in HDAC6-deficient mice, infused by Ang II and there the autophagy level was attenuated (Demos-Davies et al., 2014) .

In our study we showed no significant differences in the expression of autophagy markers p62 and Bec-1 due to the HDAC6i treatment after 6 weeks post TAC-intervention. Additionally, Bec-1 was not affected on protein level.

HDAC6 was reported to facilitate the fusion of autophagosomes and lysosomes (Li et al., 2011). Furthermore, other several HDACi like HDAC1 and HDAC2 are involved in the process of autophagy (Cao et al., 2011).

In summary, the exact molecular role of HDAC6 in the heart remains elusive. Because of the fluctuating autophagy activity it is not easy to detect changes in the

process of autophagy. Further investigations with different time periods should be done to analyze the exact role of HDAC6 in the process of autophagy and if an HDACi such as Tubacin influence this process. Moreover in the Iso model, autophagy marker such as Bec-1 and p62 has to be investigated on mRNA- and protein level. It seems that the cardioprotective effects of HDAC6i are probably linked with the ability to regulate cardiac tubulin-acetylation status.

Besides diseases such as cancer, neurological disorders or viral infections, HDACi has therapeutic potential in cardiovascular diseases (Zwergel et al., 2016). In clinical trials most investigated HDACi are so called pan-inhibitors working on various HDAC classes and thus, pan-HDAC-inhibitors interrupt several cellular processes (Ceccacci and Minucci, 2016). In general, pan-HDAC-inhibitors show a wide range of side effects such as fatique, diarrhea and bone marrow toxitiy. The advantage of using isoform-selective HDACi such as the HDAC6i Tubacin could be that they show more safety by decreasing side effects linked with inhibition of HDACs which are not important for the investigated pathway (Ceccacci and Minucci, 2016; McKinsey, 2012b; Thurn et al., 2011). Until now, there are various pre-clinical studies with specific HDAC6i. It is not known if the positive effects of specific HDAC6i can be translate into clinical use. Furthermore, it is a challenge to develop specific HDAC6i because of unknown three-dimensional structures for human isoforms. For this reason there are just a few selective HDAC6i available which have to be investigated in clinical trials. Another approach is a combination drug therapy with HDAC6i and other epigenetic modifiers or approved drugs.

Comprehensively, a better understanding of the molecular role of HDAC6 and the underlying mechanism will lead to a more effective aim and use of specific HDAC6i (Zwergel et al., 2016).

7 Conclusion and outlook

Taken together, we showed that HDAC6 is a central regulator of pathological cardiac hypertrophy. Inhibition of HDAC6 with Tubacin leads to anti-hypertrophic effects in the heart. This was mediated by alterations of the acetylation status of cytoplasmic mictrotubule proteins such as α-tubulin. Our results suggest that HDAC6-specific inhibitors such as Tubacin might be a promising pharmacological tool to prevent cardiac pathological hypertrophy and heart failure. Specific HDACi are more selective and safer than unselective HDACi. A protective effect of Tubacin against the development of fibrosis was not detected.

Further experiments can be performed on isolated primary cardiomyocytes to investigate cardiomyocytic contractility, calcium signaling and mitochondria function and to confirm the HL-1 experiments in primary cells.

Additionally, to investigate the molecular mechanisms of Tubacin the autophagic activity and the exact role of HDAC6 in this fluctuating process have to be analyzed. *In vivo* and *in vitro* experiments have to be done with different time points to detect important alterations in the process of autophagy.

A possible next step is to perform an acetylation screening of potential proteins which are deacetylated by HDAC6 and to identify new anti-hypertrophic mechanisms of HDAC6i.

8 Abstract

Histone Deacetylases (HDACs) are considered as central regulators of cardiac mal-adaptive hypertrophy. In particular, enzymatic activity of HDAC6 is strongly upregulated in different models of pressure-induced cardiac hypertrophy. Therefore, the effects of a general HDAC inhibitor (HDACi) Trichostatin A (TSA) and a HDAC6 specific inhibitor (HDAC6i) Tubacin were investigated in the development and progression of mal-adaptive cardiac hypertrophy *in vivo* and *in vitro*. Furthermore, we explored the effect of Tubacin in a mice model of isoproterenol (Iso)-induced cardiac dysfunction to investigate fibrosis and inflammation.

In vitro pharmacological effects of both inhibitors TSA and Tubacin were tested in HL-1 cells. The hypertrophic response of the murine HL-1 cardiomyocytes to endothelin 1 (ET-1) stimulation led to the induction of mRNA expression of pathological markers such as atrial natriuretic factor (ANF) and beta-myosin heavy chain (beta-MHCH). Treatment with Tubacin and TSA significantly reduced the hypertrophic effect of ET-1. The *in vitro* study was complemented by immunostaining experiments in HL-1 cardiomyocytes confirming the anti-hypertrophic effects of Tubacin und TSA.

Furthermore, we performed the Transverse Aortic Constriction (TAC) mouse model to investigate the functional importance of the specific HDAC6i Tubacin in the development of cardiac hypertrophy. This *in vivo* study demonstrated for the first time that treatment with the selective HDAC6i Tubacin significantly reduces cardiac hypertrophic response in the TAC mouse model. The treatment did not reduce the development of cardiac inflammation and cardiac fibrosis in model of Iso-induced cardiac dysfunction.

In summary, HDAC6 specific inhibitors may be promising pharmacological tools to prevent mal-adaptive hypertrophy in the future. Although the underlying mechanism remains elusive, beneficial anti-hypertrophic effects of Tubacin were associated with its ability to regulate the cardiac tubulin-acetylation status.

Graphical Abstract

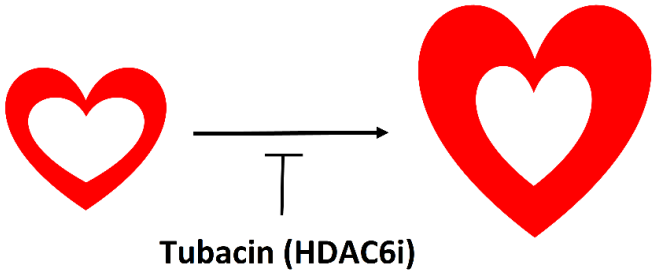

The selective HDAC6 inhibitor Tubacin prevents cardiac hypertrophy.

9 Zusammenfassung

Histondeacetylasen (HDACs) wurden als zentrale Regulatoren mal-adaptiver Hypertrophie identifiziert. Insbesondere die Aktivität von HDAC6 scheint eine wichtige Rolle bei der Entstehung kardialer Hypertrophie zu spielen. Deswegen wurde in dieser Arbeit der direkte Einfluss eines HDAC6-spezifischen Inhibitors (HDAC6i) Tubacin im direkten Vergleich mit einem generellen HDAC Inhibitor (HDACi) Trichostatin A (TSA) *in vitro* und *in vivo* untersucht.

Es wurde die hemmende Wirkung der beiden HDACi TSA und Tubacin an der Endothelin 1 (ET-1)–induzierten Hypertrophie in murinen HL1-Kardiomyozyten getestet. Das Ausmaß der mal-adaptiven Hypertrophie der HL-1 Zellen in den verschiedenen Behandlungsgruppen wurde mit pathologischen Markern auf Genexpressionsebene analysiert. Beide HDACi zeigten eine hemmende Wirkung auf die ET-1-induzierte Regulation der pathologischen Hypertrophiemarker mit einer verminderten Genexpression. Durch Immunfärbung wurde der antihypertrophe Effekt von Tubacin und TSA bestätigt.

Desweiteren wurden *in vivo* Experimente durchgeführt um die Wirkung von Tubacin in der Entwicklung kardialer Hypertrophie und kardialer Fibrose zu untersuchen. Zusammenfassend zeigen die HDACi TSA und Tubacin eine Verbesserung der kardialen pathologischen Hypertrophie. Die Behandlung mit Tubacin reduzierte jedoch nicht die Entstehung kardialer Fibrose. Der potenzielle klinische Einsatz von Tubacin könnte eine attraktive therapeutische Option zur Behandlung pathologischer Hypertrophie darstellen.

10 References

Aerni-Flessner, L., Abi-Jaoude, M., Koenig, A., Payne, M., and Hruz, P.W. (2012). GLUT4, GLUT1, and GLUT8 are the dominant GLUT transcripts expressed in the murine left ventricle. Cardiovasc Diabetol *11*, 63.

Agarwal, N., McPherson, J.P., Bailey, H., Gupta, S., Werner, T.L., Reddy, G., Bhat, G., Bailey, E.B., and Sharma, S. (2016). A phase I clinical trial of the effect of belinostat on the pharmacokinetics and pharmacodynamics of warfarin. Cancer Chemother. Pharmacol. *77*, 299–308.

Aldana-Masangkay, G.I., and Sakamoto, K.M. (2011). The role of HDAC6 in cancer. J. Biomed. Biotechnol. *2011*, 875824.

Allard, M.F. (2004). Energy substrate metabolism in cardiac hypertrophy. Curr. Hypertens. Rep. *6*, 430–435.

Allfrey, V.G., Faulkner, R., and Mirsky, A.E. (1964). ACETYLATION AND METHYLATION OF HISTONES AND THEIR POSSIBLE ROLE IN THE REGULATION OF RNA SYNTHESIS. Proc. Natl. Acad. Sci. U.S.A. *51*, 786–794.

An, X., Wang, J., Li, H., Lu, Z., Bai, Y., Xiao, H., Zhang, Y., and Song, Y. (2016). Speckle Tracking Based Strain Analysis Is Sensitive for Early Detection of Pathological Cardiac Hypertrophy. PLoS ONE *11*, e0149155.

Antos, C.L., McKinsey, T.A., Dreitz, M., Hollingsworth, L.M., Zhang, C.-L., Schreiber, K., Rindt, H., Gorczynski, R.J., and Olson, E.N. (2003). Dose-dependent blockade to cardiomyocyte hypertrophy by histone deacetylase inhibitors. J. Biol. Chem. *278*, 28930–28937.

Arai, M., Yoguchi, A., Iso, T., Takahashi, T., Imai, S., Murata, K., and Suzuki, T. (1995). Endothelin-1 and its binding sites are upregulated in pressure overload cardiac hypertrophy. Am. J. Physiol. *268*, H2084-2091.

Barbosa, J.A.A., Mota, C.C.C., Simões E Silva, A.C., Nunes, M. do C.P., and Barbosa, M.M. (2013). Assessing pre-clinical ventricular dysfunction in obese children and adolescents: the value of speckle tracking imaging. Eur Heart J Cardiovasc Imaging *14*, 882–889.

Batchu, S.N., Brijmohan, A.S., and Advani, A. (2016). The therapeutic hope for HDAC6 inhibitors in malignancy and chronic disease. Clin. Sci. *130*, 987–1003.

Bauer, M., Cheng, S., Jain, M., Ngoy, S., Theodoropoulos, C., Trujillo, A., Lin, F.-C., and Liao, R. (2011). Echocardiographic speckle-tracking based strain imaging for rapid cardiovascular phenotyping in mice. Circ. Res. *108*, 908–916.

Benjamin, I.J., Jalil, J.E., Tan, L.B., Cho, K., Weber, K.T., and Clark, W.A. (1989). Isoproterenol-induced myocardial fibrosis in relation to myocyte necrosis. Circulation Research *65*, 657–670.

Berger, S.L. (2002). Histone modifications in transcriptional regulation. Curr. Opin. Genet. Dev. *12*, 142–148.

Bernardo, B.C., Weeks, K.L., Pretorius, L., and McMullen, J.R. (2010). Molecular distinction between physiological and pathological cardiac hypertrophy: experimental findings and therapeutic strategies. Pharmacol. Ther. *128*, 191–227.

Berry, J.M., Cao, D.J., Rothermel, B.A., and Hill, J.A. (2008). Histone deacetylase inhibition in the treatment of heart disease. Expert Opin Drug Saf *7*, 53–67.

Bertos, N.R., Gilquin, B., Chan, G.K.T., Yen, T.J., Khochbin, S., and Yang, X.-J. (2004). Role of the tetradecapeptide repeat domain of human histone deacetylase 6 in cytoplasmic retention. J. Biol. Chem. *279*, 48246–48254.

Bloch, L., Ndongson-Dongmo, B., Kusch, A., Dragun, D., Heller, R., and Huber, O. (2016). Real-time monitoring of hypertrophy in HL-1 cardiomyocytes by impedance measurements reveals different modes of growth. Cytotechnology.

Boyault, C., Gilquin, B., Zhang, Y., Rybin, V., Garman, E., Meyer-Klaucke, W., Matthias, P., Müller, C.W., and Khochbin, S. (2006). HDAC6-p97/VCP controlled polyubiquitin chain turnover. EMBO J. *25*, 3357–3366.

Brooks, W.W., and Conrad, C.H. (2009). Isoproterenol-induced myocardial injury and diastolic dysfunction in mice: structural and functional correlates. Comp. Med. *59*, 339–343.

Burchfield, J.S., Xie, M., and Hill, J.A. (2013). Pathological ventricular remodeling: mechanisms: part 1 of 2. Circulation *128*, 388–400.

Cacciapuoti, F. (2011). Molecular mechanisms of left ventricular hypertrophy (LVH) in systemic hypertension (SH)-possible therapeutic perspectives. J Am Soc Hypertens *5*, 449–455.

Cao, D.J., Wang, Z.V., Battiprolu, P.K., Jiang, N., Morales, C.R., Kong, Y., Rothermel, B.A., Gillette, T.G., and Hill, J.A. (2011). Histone deacetylase (HDAC) inhibitors attenuate cardiac hypertrophy by suppressing autophagy. Proc. Natl. Acad. Sci. U.S.A. *108*, 4123–4128.

Ceccacci, E., and Minucci, S. (2016). Inhibition of histone deacetylases in cancer therapy: lessons from leukaemia. British Journal of Cancer *114*, 605–611.

Chakraborti, S., Natarajan, K., Curiel, J., Janke, C., and Liu, J. (2016). The emerging role of the tubulin code: From the tubulin molecule to neuronal function and disease. Cytoskeleton (Hoboken).

Choi, S.Y., Ryu, Y., Kee, H.J., Cho, S.-N., Kim, G.R., Cho, J.Y., Kim, H.-S., Kim, I.-K., and Jeong, M.H. (2015). Tubastatin A suppresses renal fibrosis via regulation of epigenetic histone modification and Smad3-dependent fibrotic genes. Vascul. Pharmacol. *72*, 130–140.

Claycomb, W.C., Lanson, N.A., Stallworth, B.S., Egeland, D.B., Delcarpio, J.B.,

Bahinski, A., and Izzo, N.J. (1998). HL-1 cells: a cardiac muscle cell line that contracts and retains phenotypic characteristics of the adult cardiomyocyte. Proc. Natl. Acad. Sci. U.S.A. *95*, 2979–2984.

Cohn, J.N., Bristow, M.R., Chien, K.R., Colucci, W.S., Frazier, O.H., Leinwand, L.A., Lorell, B.H., Moss, A.J., Sonnenblick, E.H., Walsh, R.A., et al. (1997). Report of the National Heart, Lung, and Blood Institute Special Emphasis Panel on Heart Failure Research. Circulation *95*, 766–770.

Collins, K.A., Korcarz, C.E., and Lang, R.M. (2003). Use of echocardiography for the phenotypic assessment of genetically altered mice. Physiol. Genomics *13*, 227–239.

Cooper, G. (1987). Cardiocyte adaptation to chronically altered load. Annu. Rev. Physiol. *49*, 501–518.

Dallavalle, S., Pisano, C., and Zunino, F. (2012). Development and therapeutic impact of HDAC6-selective inhibitors. Biochem. Pharmacol. *84*, 756–765.

deAlmeida, A.C., van Oort, R.J., and Wehrens, X.H.T. (2010). Transverse aortic constriction in mice. J Vis Exp.

De Meyer, G.R.Y., and Martinet, W. (2009). Autophagy in the cardiovascular system. Biochim. Biophys. Acta *1793*, 1485–1495.

Demos-Davies, K.M., Ferguson, B.S., Cavasin, M.A., Mahaffey, J.H., Williams, S.M., Spiltoir, J.I., Schuetze, K.B., Horn, T.R., Chen, B., Ferrara, C., et al. (2014). HDAC6 contributes to pathological responses of heart and skeletal muscle to chronic angiotensin-II signaling. Am. J. Physiol. Heart Circ. Physiol. *307*, H252-258.

Dobaczewski, M., and Frangogiannis, N.G. (2009). Chemokines and cardiac fibrosis. Front Biosci (Schol Ed) *1*, 391–405.

Dobaczewski, M., Gonzalez-Quesada, C., and Frangogiannis, N.G. (2010). The extracellular matrix as a modulator of the inflammatory and reparative response following myocardial infarction. J. Mol. Cell. Cardiol. *48*, 504–511.

Doenst, T., Nguyen, T.D., and Abel, E.D. (2013). Cardiac metabolism in heart failure: implications beyond ATP production. Circ. Res. *113*, 709–724.

Dorigo, B., Schalch, T., Bystricky, K., and Richmond, T.J. (2003). Chromatin fiber folding: requirement for the histone H4 N-terminal tail. J. Mol. Biol. *327*, 85–96.

Ferguson, B.S., and McKinsey, T.A. (2015). Non-sirtuin histone deacetylases in the control of cardiac aging. J. Mol. Cell. Cardiol. *83*, 14–20.

Finnin, M.S., Donigian, J.R., Cohen, A., Richon, V.M., Rifkind, R.A., Marks, P.A., Breslow, R., and Pavletich, N.P. (1999). Structures of a histone deacetylase homologue bound to the TSA and SAHA inhibitors. Nature *401*, 188–193.

Fliegner, D., Schubert, C., Penkalla, A., Witt, H., Kararigas, G., Kararigas, G., Dworatzek, E., Staub, E., Martus, P., Ruiz Noppinger, P., et al. (2010). Female sex

and estrogen receptor-beta attenuate cardiac remodeling and apoptosis in pressure overload. Am. J. Physiol. Regul. Integr. Comp. Physiol. *298*, R1597-1606.

Force, T., and Kolaja, K.L. (2011). Cardiotoxicity of kinase inhibitors: the prediction and translation of preclinical models to clinical outcomes. Nat Rev Drug Discov *10*, 111–126.

Foryst-Ludwig, A., Kreissl, M.C., Sprang, C., Thalke, B., Böhm, C., Benz, V., Gürgen, D., Dragun, D., Schubert, C., Mai, K., et al. (2011). Sex differences in physiological cardiac hypertrophy are associated with exercise-mediated changes in energy substrate availability. Am. J. Physiol. Heart Circ. Physiol. *301*, H115-122.

Foryst-Ludwig, A., Kreissl, M.C., Benz, V., Brix, S., Smeir, E., Ban, Z., Januszewicz, E., Salatzki, J., Grune, J., Schwanstecher, A.-K., et al. (2015). Adipose Tissue Lipolysis Promotes Exercise-induced Cardiac Hypertrophy Involving the Lipokine C16:1n7-Palmitoleate. J. Biol. Chem. *290*, 23603–23615.

Garcia-Menendez, L., Karamanlidis, G., Kolwicz, S., and Tian, R. (2013). Substrain specific response to cardiac pressure overload in C57BL/6 mice. Am. J. Physiol. Heart Circ. Physiol. *305*, H397-402.

George, J.C., Liner, A., and Hoit, B.D. (2010). Isoproterenol-Induced Myocardial Injury: A Systematic Comparison of Subcutaneous versus Intraperitoneal Delivery in a Rat Model: Subcutaneous vs Intraperitoneal Isoproterenol Injury Model. Echocardiography *27*, 716–721.

Giannandrea, M., and Parks, W.C. (2014). Diverse functions of matrix metalloproteinases during fibrosis. Disease Models & Mechanisms *7*, 193–203.

Gourdie, R.G., Dimmeler, S., and Kohl, P. (2016). Novel therapeutic strategies targeting fibroblasts and fibrosis in heart disease. Nat Rev Drug Discov.

Gregoretti, I.V., Lee, Y.-M., and Goodson, H.V. (2004). Molecular evolution of the histone deacetylase family: functional implications of phylogenetic analysis. J. Mol. Biol. *338*, 17–31.

Grozinger, C.M., Hassig, C.A., and Schreiber, S.L. (1999). Three proteins define a class of human histone deacetylases related to yeast Hda1p. Proc. Natl. Acad. Sci. U.S.A. *96*, 4868–4873.

Gryder, B.E., Sodji, Q.H., and Oyelere, A.K. (2012). Targeted cancer therapy: giving histone deacetylase inhibitors all they need to succeed. Future Medicinal Chemistry *4*, 505–524.

Haberland, M., Montgomery, R.L., and Olson, E.N. (2009). The many roles of histone deacetylases in development and physiology: implications for disease and therapy. Nat. Rev. Genet. *10*, 32–42.

Haggarty, S.J., Koeller, K.M., Wong, J.C., Grozinger, C.M., and Schreiber, S.L. (2003). Domain-selective small-molecule inhibitor of histone deacetylase 6 (HDAC6)-mediated tubulin deacetylation. Proc. Natl. Acad. Sci. U.S.A. *100*, 4389–4394.

Han, Y., Jeong, H.M., Jin, Y.-H., Kim, Y.-J., Jeong, H.G., Yeo, C.-Y., and Lee, K.-Y. (2009). Acetylation of histone deacetylase 6 by p300 attenuates its deacetylase activity. Biochem. Biophys. Res. Commun. *383*, 88–92.

Hao, R., Nanduri, P., Rao, Y., Panichelli, R.S., Ito, A., Yoshida, M., and Yao, T.-P. (2013). Proteasomes activate aggresome disassembly and clearance by producing unanchored ubiquitin chains. Mol. Cell *51*, 819–828.

Hayley, B.D., and Burwash, I.G. (2012). Heart failure with normal left ventricular ejection fraction: role of echocardiography. Curr. Opin. Cardiol. *27*, 169–180.

Heineke, J., and Molkentin, J.D. (2006). Regulation of cardiac hypertrophy by intracellular signalling pathways. Nat. Rev. Mol. Cell Biol. *7*, 589–600.

Hong, L., Schroth, G.P., Matthews, H.R., Yau, P., and Bradbury, E.M. (1993). Studies of the DNA binding properties of histone H4 amino terminus. Thermal denaturation studies reveal that acetylation markedly reduces the binding constant of the H4 “tail” to DNA. J. Biol. Chem. *268*, 305–314.

Hook, S.S., Orian, A., Cowley, S.M., and Eisenman, R.N. (2002). Histone deacetylase 6 binds polyubiquitin through its zinc finger (PAZ domain) and copurifies with deubiquitinating enzymes. Proc. Natl. Acad. Sci. U.S.A. *99*, 13425–13430.

Hubbert, C., Guardiola, A., Shao, R., Kawaguchi, Y., Ito, A., Nixon, A., Yoshida, M., Wang, X.-F., and Yao, T.-P. (2002). HDAC6 is a microtubule-associated deacetylase. Nature *417*, 455–458.

Iyer, A., Fenning, A., Lim, J., Le, G.T., Reid, R.C., Halili, M.A., Fairlie, D.P., and Brown, L. (2010). Antifibrotic activity of an inhibitor of histone deacetylases in DOCA-salt hypertensive rats. Br. J. Pharmacol. *159*, 1408–1417.

Jenuwein, T., and Allis, C.D. (2001). Translating the histone code. Science *293*, 1074–1080.

Jonker, S.S., Giraud, M.K., Giraud, G.D., Chattergoon, N.N., Louey, S., Davis, L.E., Faber, J.J., and Thornburg, K.L. (2010). Cardiomyocyte enlargement, proliferation and maturation during chronic fetal anaemia in sheep: Cardiomyocyte growth during fetal anaemia. Experimental Physiology *95*, 131–139.

Jugdutt, B.I. (2003). Ventricular remodeling after infarction and the extracellular collagen matrix: when is enough enough? Circulation *108*, 1395–1403.

Kameshima, S., Okada, M., and Yamawaki, H. (2016). Expression and localization of calmodulin-related proteins in brain, heart and kidney from spontaneously hypertensive rats. Biochem. Biophys. Res. Commun. *469*, 654–658.

Kang, S.-H., Seok, Y.M., Song, M., Lee, H.-A., Kurz, T., and Kim, I. (2015). Histone deacetylase inhibition attenuates cardiac hypertrophy and fibrosis through acetylation of mineralocorticoid receptor in spontaneously hypertensive rats. Mol. Pharmacol. *87*, 782–791.

Kao, H.-Y., Lee, C.-H., Komarov, A., Han, C.C., and Evans, R.M. (2002). Isolation and characterization of mammalian HDAC10, a novel histone deacetylase. J. Biol. Chem. *277*, 187–193.

Kao, Y.-H., Liou, J.-P., Chung, C.-C., Lien, G.-S., Kuo, C.-C., Chen, S.-A., and Chen, Y.-J. (2013). Histone deacetylase inhibition improved cardiac functions with direct antifibrotic activity in heart failure. International Journal of Cardiology *168*, 4178–4183.

Kararigas, G., Fliegner, D., Forler, S., Klein, O., Schubert, C., Gustafsson, J.-Å., Klose, J., and Regitz-Zagrosek, V. (2014). Comparative proteomic analysis reveals sex and estrogen receptor β effects in the pressure overloaded heart. J. Proteome Res. *13*, 5829–5836.

Kawaguchi, Y., Kovacs, J.J., McLaurin, A., Vance, J.M., Ito, A., and Yao, T.P. (2003). The deacetylase HDAC6 regulates aggresome formation and cell viability in response to misfolded protein stress. Cell *115*, 727–738.

Kee, H.J., Sohn, I.S., Nam, K.I., Park, J.E., Qian, Y.R., Yin, Z., Ahn, Y., Jeong, M.H., Bang, Y.-J., Kim, N., et al. (2006). Inhibition of histone deacetylation blocks cardiac hypertrophy induced by angiotensin II infusion and aortic banding. Circulation *113*, 51–59.

Khorasanizadeh, S. (2004). The nucleosome: from genomic organization to genomic regulation. Cell *116*, 259–272.

Klopfleisch, R., Lenze, D., Hummel, M., and Gruber, A.D. (2011). The metastatic cascade is reflected in the transcriptome of metastatic canine mammary carcinomas. Vet. J. *190*, 236–243.

Kong, P., Christia, P., and Frangogiannis, N.G. (2014). The pathogenesis of cardiac fibrosis. Cell. Mol. Life Sci. *71*, 549–574.

Kong, Y., Tannous, P., Lu, G., Berenji, K., Rothermel, B.A., Olson, E.N., and Hill, J.A. (2006). Suppression of class I and II histone deacetylases blunts pressure-overload cardiac hypertrophy. Circulation *113*, 2579–2588.

Kook, H., Lepore, J.J., Gitler, A.D., Lu, M.M., Wing-Man Yung, W., Mackay, J., Zhou, R., Ferrari, V., Gruber, P., and Epstein, J.A. (2003). Cardiac hypertrophy and histone deacetylase-dependent transcriptional repression mediated by the atypical homeodomain protein Hop. J. Clin. Invest. *112*, 863–871.

Kornberg, R.D. (1977). Structure of chromatin. Annu. Rev. Biochem. *46*, 931–954.

Kovacs, J.J., Murphy, P.J.M., Gaillard, S., Zhao, X., Wu, J.-T., Nicchitta, C.V., Yoshida, M., Toft, D.O., Pratt, W.B., and Yao, T.-P. (2005). HDAC6 regulates Hsp90 acetylation and chaperone-dependent activation of glucocorticoid receptor. Mol. Cell *18*, 601–607.

Kuang, S.-Q., Geng, L., Prakash, S.K., Cao, J.-M., Guo, S., Villamizar, C., Kwartler, C.S., Peters, A.M., Brasier, A.R., and Milewicz, D.M. (2013). Aortic remodeling after

transverse aortic constriction in mice is attenuated with AT1 receptor blockade. Arterioscler. Thromb. Vasc. Biol. *33*, 2172–2179.

Kuo, M.H., and Allis, C.D. (1998). Roles of histone acetyltransferases and deacetylases in gene regulation. Bioessays *20*, 615–626.

Lai, Y.-H., Lo, C.-I., Wu, Y.-J., Hung, C.-L., and Yeh, H.-I. (2013). Cardiac Remodeling, Adaptations and Associated Myocardial Mechanics in Hypertensive Heart Diseases. Zhonghua Minguo Xin Zang Xue Hui Za Zhi *29*, 64–70.

Lavandero, S., Chiong, M., Rothermel, B.A., and Hill, J.A. (2015). Autophagy in cardiovascular biology. Journal of Clinical Investigation *125*, 55–64.

Lee, J.-Y., Koga, H., Kawaguchi, Y., Tang, W., Wong, E., Gao, Y.-S., Pandey, U.B., Kaushik, S., Tresse, E., Lu, J., et al. (2010). HDAC6 controls autophagosome maturation essential for ubiquitin-selective quality-control autophagy. EMBO J. *29*, 969–980.

Lemon, D.D., Horn, T.R., Cavasin, M.A., Jeong, M.Y., Haubold, K.W., Long, C.S., Irwin, D.C., McCune, S.A., Chung, E., Leinwand, L.A., et al. (2011). Cardiac HDAC6 catalytic activity is induced in response to chronic hypertension. J. Mol. Cell. Cardiol. *51*, 41–50.

Levy, D., Garrison, R.J., Savage, D.D., Kannel, W.B., and Castelli, W.P. (1990). Prognostic implications of echocardiographically determined left ventricular mass in the Framingham Heart Study. N. Engl. J. Med. *322*, 1561–1566.

Li, D., Wu, J., Bai, Y., Zhao, X., and Liu, L. (2014). Isolation and culture of adult mouse cardiomyocytes for cell signaling and in vitro cardiac hypertrophy. J Vis Exp.

Li, G., Jiang, H., Chang, M., Xie, H., and Hu, L. (2011). HDAC6 α-tubulin deacetylase: a potential therapeutic target in neurodegenerative diseases. J. Neurol. Sci. *304*, 1–8.

Li, S., Liu, C., Gu, L., Wang, L., Shang, Y., Liu, Q., Wan, J., Shi, J., Wang, F., Xu, Z., et al. (2016). Autophagy protects cardiomyocytes from the myocardial ischaemia-reperfusion injury through the clearance of CLP36. Open Biol *6*.

Li, Y., Shin, D., and Kwon, S.H. (2013). Histone deacetylase 6 plays a role as a distinct regulator of diverse cellular processes. FEBS J. *280*, 775–793.

Lips, D.J., deWindt, L.J., van Kraaij, D.J.W., and Doevendans, P.A. (2003). Molecular determinants of myocardial hypertrophy and failure: alternative pathways for beneficial and maladaptive hypertrophy. Eur. Heart J. *24*, 883–896.

Livak, K.J., and Schmittgen, T.D. (2001). Analysis of Relative Gene Expression Data Using Real-Time Quantitative PCR and the $2^{-\Delta\Delta CT}$ Method. Methods *25*, 402–408.

Lkhagva, B., Lin, Y.-K., Kao, Y.-H., Chazo, T.-F., Chung, C.-C., Chen, S.-A., and Chen, Y.-J. (2015). Novel Histone Deacetylase Inhibitor Modulates Cardiac Peroxisome Proliferator-Activated Receptors and Inflammatory Cytokines in Heart

Failure. Pharmacology *96*, 184–191.

Louch, W.E., Sheehan, K.A., and Wolska, B.M. (2011). Methods in cardiomyocyte isolation, culture, and gene transfer. J. Mol. Cell. Cardiol. *51*, 288–298.

Luger, K. (2003). Structure and dynamic behavior of nucleosomes. Curr. Opin. Genet. Dev. *13*, 127–135.

Luger, K., and Richmond, T.J. (1998). The histone tails of the nucleosome. Curr. Opin. Genet. Dev. *8*, 140–146.

Luger, K., Mäder, A.W., Richmond, R.K., Sargent, D.F., and Richmond, T.J. (1997). Crystal structure of the nucleosome core particle at 2.8 A resolution. Nature *389*, 251–260.

Lundby, A., Lage, K., Weinert, B.T., Bekker-Jensen, D.B., Secher, A., Skovgaard, T., Kelstrup, C.D., Dmytriyev, A., Choudhary, C., Lundby, C., et al. (2012). Proteomic analysis of lysine acetylation sites in rat tissues reveals organ specificity and subcellular patterns. Cell Rep *2*, 419–431.

Lygate, C.A., Schneider, J.E., Hulbert, K., ten Hove, M., Sebag-Montefiore, L.M., Cassidy, P.J., Clarke, K., and Neubauer, S. (2006). Serial high resolution 3D-MRI after aortic banding in mice: band internalization is a source of variability in the hypertrophic response. Basic Res. Cardiol. *101*, 8–16.

Maeder, M.T., and Rickli, H. (2013). [Heart failure with preserved left ventricular ejection fraction]. Praxis (Bern 1994) *102*, 1299–1307.

Mahlknecht, U., Schnittger, S., Landgraf, F., Schoch, C., Ottmann, O.G., Hiddemann, W., and Hoelzer, D. (2001). Assignment of the human histone deacetylase 6 gene (HDAC6) to X chromosome p11.23 by in situ hybridization. Cytogenet. Cell Genet. *93*, 135–136.

Majumdar, G., Rooney, R.J., Johnson, I.M., and Raghow, R. (2011). Panhistone deacetylase inhibitors inhibit proinflammatory signaling pathways to ameliorate interleukin-18-induced cardiac hypertrophy. Physiol. Genomics *43*, 1319–1333.

Masumoto, H., Ikuno, T., Takeda, M., Fukushima, H., Marui, A., Katayama, S., Shimizu, T., Ikeda, T., Okano, T., Sakata, R., et al. (2014). Human iPS cell-engineered cardiac tissue sheets with cardiomyocytes and vascular cells for cardiac regeneration. Sci Rep *4*, 6716.

Mathiyalagan, P., Keating, S.T., Du, X.-J., and El-Osta, A. (2014). Chromatin modifications remodel cardiac gene expression. Cardiovasc. Res. *103*, 7–16.

Matsuyama, A., Shimazu, T., Sumida, Y., Saito, A., Yoshimatsu, Y., Seigneurin-Berny, D., Osada, H., Komatsu, Y., Nishino, N., Khochbin, S., et al. (2002). In vivo destabilization of dynamic microtubules by HDAC6-mediated deacetylation. EMBO J. *21*, 6820–6831.

McKinsey, T.A. (2012). Therapeutic potential for HDAC inhibitors in the heart. Annu.

Rev. Pharmacol. Toxicol. *52*, 303–319.

McKinsey, T.A., Zhang, C.L., and Olson, E.N. (2002). MEF2: a calcium-dependent regulator of cell division, differentiation and death. Trends Biochem. Sci. *27*, 40–47.

McLendon, P.M., Ferguson, B.S., Osinska, H., Bhuiyan, M.S., James, J., McKinsey, T.A., and Robbins, J. (2014). Tubulin hyperacetylation is adaptive in cardiac proteotoxicity by promoting autophagy. Proc. Natl. Acad. Sci. U.S.A. *111*, E5178-5186.

Miljkovik, L.V., and Spiroska, V. (2015). Heart Failure with Preserved Ejection Fraction - Concept, Pathophysiology, Diagnosis and Challenges for Treatment. Open Access Maced J Med Sci *3*, 521–527.

Miyata, S., Minobe, W., Bristow, M.R., and Leinwand, L.A. (2000). Myosin heavy chain isoform expression in the failing and nonfailing human heart. Circ. Res. *86*, 386–390.

Montgomery, R.L., Potthoff, M.J., Haberland, M., Qi, X., Matsuzaki, S., Humphries, K.M., Richardson, J.A., Bassel-Duby, R., and Olson, E.N. (2008). Maintenance of cardiac energy metabolism by histone deacetylase 3 in mice. J. Clin. Invest. *118*, 3588–3597.

Nabeebaccus, A., Zheng, S., and Shah, A.M. (2016). Heart failure-potential new targets for therapy. Br. Med. Bull.

Nakagawa, Y., Kuwahara, K., Harada, M., Takahashi, N., Yasuno, S., Adachi, Y., Kawakami, R., Nakanishi, M., Tanimoto, K., and Usami, S. (2006). Class II HDACs mediate CaMK-dependent signaling to NRSF in ventricular myocytes. Journal of Molecular and Cellular Cardiology *41*, 1010–1022.

Nemer, M., Lavigne, J.P., Drouin, J., Thibault, G., Gannon, M., and Antakly, T. (1986). Expression of atrial natriuretic factor gene in heart ventricular tissue. Peptides *7*, 1147–1152.

Norton, V.G., Imai, B.S., Yau, P., and Bradbury, E.M. (1989). Histone acetylation reduces nucleosome core particle linking number change. Cell *57*, 449–457.

Ooi, J.Y.Y., Tuano, N.K., Rafehi, H., Gao, X.-M., Ziemann, M., Du, X.-J., and El-Osta, A. (2015). HDAC inhibition attenuates cardiac hypertrophy by acetylation and deacetylation of target genes. Epigenetics *10*, 418–430.

Ouyang, H., Ali, Y.O., Ravichandran, M., Dong, A., Qiu, W., MacKenzie, F., Dhe-Paganon, S., Arrowsmith, C.H., and Zhai, R.G. (2012). Protein aggregates are recruited to aggresome by histone deacetylase 6 via unanchored ubiquitin C termini. J. Biol. Chem. *287*, 2317–2327.

Ouzounian, M., Lee, D.S., and Liu, P.P. (2008). Diastolic heart failure: mechanisms and controversies. Nat Clin Pract Cardiovasc Med *5*, 375–386.

Pandey, U.B., Nie, Z., Batlevi, Y., McCray, B.A., Ritson, G.P., Nedelsky, N.B.,

Schwartz, S.L., DiProspero, N.A., Knight, M.A., Schuldiner, O., et al. (2007). HDAC6 rescues neurodegeneration and provides an essential link between autophagy and the UPS. Nature *447*, 859–863.

Pereira, R.O., Wende, A.R., Olsen, C., Soto, J., Rawlings, T., Zhu, Y., Riehle, C., and Abel, E.D. (2014). GLUT1 deficiency in cardiomyocytes does not accelerate the transition from compensated hypertrophy to heart failure. J. Mol. Cell. Cardiol. *72*, 95–103.

Piperno, G., LeDizet, M., and Chang, X.J. (1987). Microtubules containing acetylated alpha-tubulin in mammalian cells in culture. J. Cell Biol. *104*, 289–302.

Ponikowski, P., Voors, A.A., Anker, S.D., Bueno, H., Cleland, J.G.F., Coats, A.J.S., Falk, V., González-Juanatey, J.R., Harjola, V.-P., Jankowska, E.A., et al. (2016). 2016 ESC Guidelines for the diagnosis and treatment of acute and chronic heart failure: The Task Force for the diagnosis and treatment of acute and chronic heart failure of the European Society of Cardiology (ESC). Developed with the special contribution of the Heart Failure Association (HFA) of the ESC. Eur. J. Heart Fail. *18*, 891–975.

Rana, P., Anson, B., Engle, S., and Will, Y. (2012). Characterization of human-induced pluripotent stem cell-derived cardiomyocytes: bioenergetics and utilization in safety screening. Toxicol. Sci. *130*, 117–131.

Razeghi, P., Young, M.E., Alcorn, J.L., Moravec, C.S., Frazier, O.H., and Taegtmeyer, H. (2001). Metabolic gene expression in fetal and failing human heart. Circulation *104*, 2923–2931.

Reddy, Y.N.V., and Borlaug, B.A. (2016). Heart Failure With Preserved Ejection Fraction. Curr Probl Cardiol *41*, 145–188.

Robert, C., and Rassool, F.V. (2012). HDAC inhibitors: roles of DNA damage and repair. Adv. Cancer Res. *116*, 87–129.

Robert, S., Gicquel, T., Victoni, T., Valenca, S., Barreto, E., Bailly-Maitre, B., Boichot, E., and Lagente, V. (2016). Involvement of matrix metalloproteinases (MMPs) and inflammasome pathway in molecular mechanisms of fibrosis. Bioscience Reports *36*, e00360–e00360.

Roche, J., and Bertrand, P. (2016). Inside HDACs with more selective HDAC inhibitors. Eur J Med Chem *121*, 451–483.

Rockman, H.A., Ross, R.S., Harris, A.N., Knowlton, K.U., Steinhelper, M.E., Field, L.J., Ross, J., and Chien, K.R. (1991). Segregation of atrial-specific and inducible expression of an atrial natriuretic factor transgene in an in vivo murine model of cardiac hypertrophy. Proc. Natl. Acad. Sci. U.S.A. *88*, 8277–8281.

Sack, M.N., Rader, T.A., Park, S., Bastin, J., McCune, S.A., and Kelly, D.P. (1996). Fatty acid oxidation enzyme gene expression is downregulated in the failing heart. Circulation *94*, 2837–2842.

Sadoul, K., and Khochbin, S. (2016). The growing landscape of tubulin acetylation: lysine 40 and many more. Biochem. J. *473*, 1859–1868.

Samuel, C.S., Bodaragama, H., Chew, J.Y., Widdop, R.E., Royce, S.G., and Hewitson, T.D. (2014). Serelaxin is a more efficacious antifibrotic than enalapril in an experimental model of heart disease. Hypertension *64*, 315–322.

Schmoldt, A., Benthe, H.F., and Haberland, G. (1975). Digitoxin metabolism by rat liver microsomes. Biochem. Pharmacol. *24*, 1639–1641.

Seto, E., and Yoshida, M. (2014). Erasers of histone acetylation: the histone deacetylase enzymes. Cold Spring Harb Perspect Biol *6*, a018713.

Shah, A.M., and Solomon, S.D. (2012). Myocardial deformation imaging: current status and future directions. Circulation *125*, e244-248.

Shahbazian, M.D., and Grunstein, M. (2007). Functions of site-specific histone acetylation and deacetylation. Annu. Rev. Biochem. *76*, 75–100.

Shimizu, I., and Minamino, T. (2016). Physiological and pathological cardiac hypertrophy. J. Mol. Cell. Cardiol. *97*, 245–262.

Shimizu, I., Yoshida, Y., Katsuno, T., Tateno, K., Okada, S., Moriya, J., Yokoyama, M., Nojima, A., Ito, T., Zechner, R., et al. (2012). p53-induced adipose tissue inflammation is critically involved in the development of insulin resistance in heart failure. Cell Metab. *15*, 51–64.

Simms-Waldrip, T., Rodriguez-Gonzalez, A., Lin, T., Ikeda, A.K., Fu, C., and Sakamoto, K.M. (2008). The aggresome pathway as a target for therapy in hematologic malignancies. Mol. Genet. Metab. *94*, 283–286.

Skavdahl, M., Steenbergen, C., Clark, J., Myers, P., Demianenko, T., Mao, L., Rockman, H.A., Korach, K.S., and Murphy, E. (2005). Estrogen receptor-beta mediates male-female differences in the development of pressure overload hypertrophy. Am. J. Physiol. Heart Circ. Physiol. *288*, H469-476.

Soonpaa, M.H., Kim, K.K., Pajak, L., Franklin, M., and Field, L.J. (1996). Cardiomyocyte DNA synthesis and binucleation during murine development. Am. J. Physiol. *271*, H2183-2189.

Stanley, W.C., Recchia, F.A., and Lopaschuk, G.D. (2005). Myocardial substrate metabolism in the normal and failing heart. Physiol. Rev. *85*, 1093–1129.

Struhl, K. (1998). Histone acetylation and transcriptional regulatory mechanisms. Genes Dev. *12*, 599–606.

Studelska, D.R., Campbell, C., Pang, S., Rodnick, K.J., and James, D.E. (1992). Developmental expression of insulin-regulatable glucose transporter GLUT-4. Am. J. Physiol. *263*, E102-106.

Taegtmeyer, H., Sen, S., and Vela, D. (2010). Return to the fetal gene program: a

suggested metabolic link to gene expression in the heart. Ann. N. Y. Acad. Sci. *1188*, 191–198.

Tao, H., Yang, J.-J., Hu, W., Shi, K.-H., and Li, J. (2016). HDAC6 Promotes Cardiac Fibrosis Progression through Suppressing RASSF1A Expression. Cardiology *133*, 18–26.

Thomas, S., Aggarwal, R., Jahan, T., Ryan, C., Troung, T., Cripps, A.M., Raha, P., Thurn, K.T., Chen, S., Grabowsky, J.A., et al. (2016). A phase I trial of panobinostat and epirubicin in solid tumors with a dose expansion in patients with sarcoma. Ann. Oncol. *27*, 947–952.

Thurn, K.T., Thomas, S., Moore, A., and Munster, P.N. (2011). Rational therapeutic combinations with histone deacetylase inhibitors for the treatment of cancer. Future Oncology *7*, 263–283.

Travers, J.G., Kamal, F.A., Robbins, J., Yutzey, K.E., and Blaxall, B.C. (2016). Cardiac Fibrosis: The Fibroblast Awakens. Circ. Res. *118*, 1021–1040.

Valenzuela-Fernández, A., Cabrero, J.R., Serrador, J.M., and Sánchez-Madrid, F. (2008). HDAC6: a key regulator of cytoskeleton, cell migration and cell-cell interactions. Trends Cell Biol. *18*, 291–297.

Van Dyke, M.W. (2014). Lysine deacetylase (KDAC) regulatory pathways: an alternative approach to selective modulation. ChemMedChem *9*, 511–522.

Verdel, A., Curtet, S., Brocard, M.P., Rousseaux, S., Lemercier, C., Yoshida, M., and Khochbin, S. (2000). Active maintenance of mHDA2/mHDAC6 histone-deacetylase in the cytoplasm. Curr. Biol. *10*, 747–749.

Vergaro, G., Prud'homme, M., Fazal, L., Merval, R., Passino, C., Emdin, M., Samuel, J.-L., Cohen Solal, A., and Delcayre, C. (2016). Inhibition of Galectin-3 Pathway Prevents Isoproterenol-Induced Left Ventricular Dysfunction and Fibrosis in Mice. Hypertension *67*, 606–612.

Voigt, J.-U., Pedrizzetti, G., Lysyansky, P., Marwick, T.H., Houle, H., Baumann, R., Pedri, S., Ito, Y., Abe, Y., Metz, S., et al. (2015). Definitions for a common standard for 2D speckle tracking echocardiography: consensus document of the EACVI/ASE/Industry Task Force to standardize deformation imaging. J Am Soc Echocardiogr *28*, 183–193.

Volpe, M., Rubattu, S., and Burnett, J. (2014). Natriuretic peptides in cardiovascular diseases: current use and perspectives. Eur. Heart J. *35*, 419–425.

Wang, H., and Dymock, B.W. (2009). New patented histone deacetylase inhibitors. Expert Opin Ther Pat *19*, 1727–1757.

Weeks, K.L., and McMullen, J.R. (2011). The athlete's heart vs. the failing heart: can signaling explain the two distinct outcomes? Physiology (Bethesda) *26*, 97–105.

Westphal, C., Schubert, C., Prelle, K., Penkalla, A., Fliegner, D., Petrov, G., and

Regitz-Zagrosek, V. (2012). Effects of estrogen, an ERα agonist and raloxifene on pressure overload induced cardiac hypertrophy. PLoS ONE *7*, e50802.

White, S.M., Constantin, P.E., and Claycomb, W.C. (2004). Cardiac physiology at the cellular level: use of cultured HL-1 cardiomyocytes for studies of cardiac muscle cell structure and function. Am. J. Physiol. Heart Circ. Physiol. *286*, H823-829.

Winkler, R., Benz, V., Clemenz, M., Bloch, M., Foryst-Ludwig, A., Wardat, S., Witte, N., Trappiel, M., Namsolleck, P., Mai, K., et al. (2012). Histone deacetylase 6 (HDAC6) is an essential modifier of glucocorticoid-induced hepatic gluconeogenesis. Diabetes *61*, 513–523.

Woods, R.L. (2004). Cardioprotective functions of atrial natriuretic peptide and B-type natriuretic peptide: a brief review. Clin. Exp. Pharmacol. Physiol. *31*, 791–794.

Writing Group Members, Mozaffarian, D., Benjamin, E.J., Go, A.S., Arnett, D.K., Blaha, M.J., Cushman, M., Das, S.R., de Ferranti, S., Després, J.-P., et al. (2016). Heart Disease and Stroke Statistics-2016 Update: A Report From the American Heart Association. Circulation *133*, e38-60.

Wynn, T.A. (2008). Cellular and molecular mechanisms of fibrosis. J. Pathol. *214*, 199–210.

Yan, J. (2014). Interplay between HDAC6 and its interacting partners: essential roles in the aggresome-autophagy pathway and neurodegenerative diseases. DNA Cell Biol. *33*, 567–580.

Yancy, C.W., Jessup, M., Bozkurt, B., Butler, J., Casey, D.E., Drazner, M.H., Fonarow, G.C., Geraci, S.A., Horwich, T., Januzzi, J.L., et al. (2013). 2013 ACCF/AHA guideline for the management of heart failure: a report of the American College of Cardiology Foundation/American Heart Association Task Force on Practice Guidelines. J. Am. Coll. Cardiol. *62*, e147-239.

Yang, X.-J. (2004). Lysine acetylation and the bromodomain: a new partnership for signaling. Bioessays *26*, 1076–1087.

Yoon, S., and Eom, G.H. (2016). HDAC and HDAC Inhibitor: From Cancer to Cardiovascular Diseases. Chonnam Med J *52*, 1–11.

Zhang, D., Wu, C.-T., Qi, X., Meijering, R.A.M., Hoogstra-Berends, F., Tadevosyan, A., Cubukcuoglu Deniz, G., Durdu, S., Akar, A.R., Sibon, O.C.M., et al. (2014). Activation of histone deacetylase-6 induces contractile dysfunction through derailment of α-tubulin proteostasis in experimental and human atrial fibrillation. Circulation *129*, 346–358.

Zhang, X., Yuan, Z., Zhang, Y., Yong, S., Salas-Burgos, A., Koomen, J., Olashaw, N., Parsons, J.T., Yang, X.-J., Dent, S.R., et al. (2007). HDAC6 modulates cell motility by altering the acetylation level of cortactin. Mol. Cell *27*, 197–213.

Zhang, Y., Li, N., Caron, C., Matthias, G., Hess, D., Khochbin, S., and Matthias, P. (2003). HDAC-6 interacts with and deacetylates tubulin and microtubules in vivo.

EMBO J. *22*, 1168–1179.

Zhang, Y., Gilquin, B., Khochbin, S., and Matthias, P. (2006). Two catalytic domains are required for protein deacetylation. J. Biol. Chem. *281*, 2401–2404.

Zhang, Y., Kwon, S., Yamaguchi, T., Cubizolles, F., Rousseaux, S., Kneissel, M., Cao, C., Li, N., Cheng, H.-L., Chua, K., et al. (2008). Mice lacking histone deacetylase 6 have hyperacetylated tubulin but are viable and develop normally. Mol. Cell. Biol. *28*, 1688–1701.

Zheng, Q., and Wang, X. (2010). Autophagy and the ubiquitin-proteasome system in cardiac dysfunction. Panminerva Med *52*, 9–25.

Zwergel, 1, , Giulia, Stazi, 1, , Sergio Valente, 1, and, and Antonello Mai (2016). Histone Deacetylase Inhibitors: Updated Studies in Various Epigenetic-Related Diseases.

Structure of Chromatin - annurev.bi.46.070177.004435.

11 Publication list

Grune, J., Benz, V., **Brix, S.**, Salatzki, J., Blumrich, A., Höft, B., Klopfleisch, R., Foryst-Ludwig, A., Kolkhof, P., and Kintscher, U. (2016).
Steroidal and Nonsteroidal Mineralocorticoid Receptor Antagonists Cause Differential Cardiac Gene Expression in Pressure Overload-induced Cardiac Hypertrophy. Journal of Cardiovascular Pharmacology. 2016 May; *67*, 402–411. doi:10.1097/FJC.0000000000000366

Foryst-Ludwig A, Kreissl MC, Benz V, **Brix S**, Smeir E, Ban Z, Januszewicz E, Salatzki J, Grune J, Schwanstecher AK, Blumrich A, Schirbel A, Klopfleisch R, Rothe M, Blume K, Halle M, Wolfarth B, Kershaw EE, Kintscher U.
Adipose Tissue Lipolysis Promotes Exercise-induced Cardiac Hypertrophy Involving the Lipokine C16:1n7-Palmitoleate. Journal of Biological Chemistry. 2015 Sep; *290*, 23603–23615. doi:10.1074/jbc.M115.645341

Horna, V., Schuldt, B., **Brix, S.**, Leuschner, C.
Environment and tree size controlling stem sap flux in a perhumid tropical forest of Central Sulawesi, Indonesia. Annals of Forest Science. 2011 July; 68, 1027. doi:10.1007/s13595-011-0110-2

Zach, A., Schuldt, B., **Brix, S.**, Horna,V., Culmsee, H., Leuschner,C.
Vessel diameter and xylem hydraulic conductivity increase with tree height in tropical rainforest trees in Sulawesi, Indonesia. Flora – Morphology, Distribution, Functional Ecology of Plants. 2010 Jan; 205, 506-512.
doi:10.1016/j.flora.2009.12.008